



## JRC TECHNICAL REPORT

iRESIST+

Innovative seismic and energy retrofitting  
of the existing building stock

*Numerical simulations and  
impact assessment*

Pohoryles, D.A.; Bournas, D.A.

2021



*This publication is a Technical report by the Joint Research Centre (JRC), the European Commission's science and knowledge service. It aims to provide evidence-based scientific support to the European policymaking process. The scientific output expressed does not imply a policy position of the European Commission. Neither the European Commission nor any person acting on behalf of the Commission is responsible for the use that might be made of this publication. For information on the methodology and quality underlying the data used in this publication for which the source is neither Eurostat nor other Commission services, users should contact the referenced source. The designations employed and the presentation of material on the maps do not imply the expression of any opinion whatsoever on the part of the European Union concerning the legal status of any country, territory, city or area or of its authorities, or concerning the delimitation of its frontiers or boundaries.*

Contact information

Name: Dionysios BOURNAS

Address: via E. Fermi 2749

Email: [Dionysios.BOURNAS@ec.europa.eu](mailto:Dionysios.BOURNAS@ec.europa.eu)

Tel: +39 033278-5321

EU Science Hub

<https://ec.europa.eu/jrc>

<https://ec.europa.eu/jrc/en/research-topic/improving-safe-construction/i-resist-plus>

JRC123638

EUR 30583 EN

Print ISBN 978-92-76-29686-7 ISSN 1018-5593 doi:10.2760/496388

PDF ISBN 978-92-76-29687-4 ISSN 1831-9424 doi:10.2760/768985

Luxembourg: Publications Office of the European Union, 2021

© European Union, 2021

*The reuse policy of the European Commission is implemented by Commission Decision 2011/833/EU of 12 December 2011 on the reuse of Commission documents (OJ L 330, 14.12.2011, p. 39). Reuse is authorised, provided the source of the document is acknowledged and its original meaning or message is not distorted. The European Commission shall not be liable for any consequence stemming from the reuse. For any use or reproduction of photos or other material that is not owned by the EU, permission must be sought directly from the copyright holders.*

All content © European Union 2021 (unless otherwise specified)

*How to cite this report: Pohoryles, D. A. and Bournas, D. A., iRESIST+ Innovative seismic and energy retrofitting of the existing building stock, EUR 30583 EN, Publications Office of the European Union, Luxembourg, 2021, ISBN 978-92-76-29687-4, doi:10.2760/768985, JRC123638.*

## Contents

Abstract .....	1
Acknowledgements .....	2
1 Introduction .....	3
2 Relevance to EU Policies .....	5
2.1 Building energy efficiency.....	5
2.2 Circular economy .....	6
2.3 Disaster risk reduction .....	6
2.4 Safeguard cultural heritage.....	6
2.5 Contributions of iRESIST+ .....	6
3 Review on retrofitting materials.....	8
3.1 Seismic retrofitting of existing structures with composites.....	8
3.2 Combined retrofitting with TRM .....	13
3.3 Materials for thermal insulation.....	14
4 Modelling the seismic performance of TRM retrofitted infills .....	16
4.1 Simplified tie-model calibration (Pohoryles and Boumas, 2020c) .....	16
4.2 Unified strut and tie model for composite retrofits (Pohoryles and Bournas, 2020a).....	17
5 Numerical analyses on the iRESIST+ prototype structure .....	20
5.1 Experimental prototype .....	20
5.2 Proposed iRESIST+ retrofit scheme .....	23
5.3 Numerical evaluation .....	23
6 Fragility curves of mid-rise RC buildings strengthened with TRM .....	27
6.1 Building design and material characteristics .....	27
6.2 Seismic assessments to Eurocode 8 – Part 3 .....	28
6.3 Incremental dynamic analysis .....	29
6.4 Fragility functions.....	31
6.5 Seismic loss assessment.....	32
7 Analysis of combined seismic and energy retrofitting for twenty case study locations .....	34
7.1 Case study locations .....	34
7.2 Building stock.....	36
7.3 Retrofit targets .....	38
7.3.1 Energy retrofit target.....	38
7.3.2 Seismic retrofit target .....	39
7.4 Modelling .....	40
7.4.1 Building energy modelling .....	40
7.4.2 Seismic loss assessment .....	41

7.4.3	Combined losses and retrofit costs .....	44
7.5	Results.....	45
7.5.1	Energy performance evaluation.....	45
7.5.1.1	Energy demand of existing and retrofitted buildings.....	45
7.5.1.2	Foresight study on renovation impact .....	49
7.5.2	Seismic performance .....	50
7.5.3	Combined assessment of integrated retrofitting.....	52
7.5.3.1	Disaggregation of seismic and energy loss reductions.....	52
7.5.3.2	Combined seismic and energy classification .....	53
7.5.3.3	Payback periods of combined energy retrofits .....	54
8	Conclusions .....	56
9	References.....	58
	List of abbreviations and definitions.....	66
	List of figures .....	67
	List of tables .....	68

## **Abstract**

The European building stock is ageing and requires significant renovation efforts to improve its energy performance and ensure structural safety and resilience. Within the European Green Deal, the Renovation Wave initiative promotes increases in building renovation rates to ensure that ambitious EU energy saving targets for 2030 and beyond can be achieved. To incentivise renovation further, integrating energy retrofitting with seismic strengthening is explored in the Exploratory Research project iRESIST+ by investigating a novel seismic-plus-energy retrofit. The research conducted in iRESIST+ is of high timeliness and has relevance for the policy areas related to the energy efficiency of buildings, circular-economy principles, as well as resilience.

In iRESIST+, the combination of inorganic textile reinforced mortar (TRM) composites with thermal insulation materials is explored. A review of the experimental studies on TRM highlighted their potential for seismic strengthening, but also their suitability for combined seismic and energy retrofitting. Based on the gathered scientific literature, a new macro-modelling approach for TRM-strengthened infilled reinforced concrete (RC) buildings was developed, and then used to quantify the effectiveness of the retrofit in increasing the in-plane capacity of the iRESIST+ prototype structure. By conducting a series of incremental dynamic analyses, the results were expanded, showing improvements in the dynamic behaviour of mid-rise RC buildings, with reduced damage at higher earthquake intensities. Fragility curves of existing mid-rise RC buildings, typical for the EU building stock, as well as a TRM-retrofitted building were then constructed, showing that the losses of a building with low seismic design level can be reduced to those of a modern, high-code structure.

A broader study on combined energy and seismic retrofitting was then conducted across twenty European cities in five different seismic and four climatic zones, in order to assess the retrofit for all possible combinations of seismic hazard and climatic conditions. Typical masonry and RC buildings were defined in terms of their energy and structural characteristics and were associated with the building population of each city. By means of building energy modelling and seismic fragility assessments, the potential reductions in losses, after applying the iRESIST+ integrated retrofitting concept, for each building type were modelled. The results were extended to the entire building stock of the case study cities to assess different renovation scenarios. In the case of non-action, i.e. keeping the current annual renovation rate of around 1%, the ambitious targets of the EU Green Deal in terms of energy use reductions cannot be achieved. Instead, if renovation rates are tripled to 3%, the energy use for heating and cooling may be reduced by up to 32.5%. This would lead to reductions of around 30% in CO<sub>2</sub> emissions across all cities by 2030 for the residential sector. In terms of seismic performance, the assessments of different building typologies showed high seismic loss reductions particularly for older and mid-rise structures in moderate to high seismic hazard zones. A combined monetary metric based on expected annual losses was established considering energy costs and costs related to structural damage. It was found that combined retrofitting can reduce investment payback periods substantially in moderate to high seismicity regions.

Overall, this report highlights the potential of combined retrofitting with TRM and thermal insulation for the EU building stock. The proposed retrofit is cost-effective and lends itself to large-scale applications due to its easy application and reduced building down-time compared to traditional retrofitting. Finally, the validity of the proposed approach will be evaluated experimentally on the iRESIST+ prototype structure at the European Commission's Joint Research Centre (JRC) ELSA laboratory in Ispra.

## **Acknowledgements**

The work of this study was carried out under the European Commission, Joint Research Centre (JRC) Exploratory Research project iRESIST+ (Innovative seismic and energy retrofitting of the existing building stock).

The support received from Carmen Maduta and Leonidas Alexandros S. Kouris is gratefully acknowledged by the authors.

## ***Authors***

Daniel A. Pohoryles, Dionysios A. Bournas

## 1 Introduction

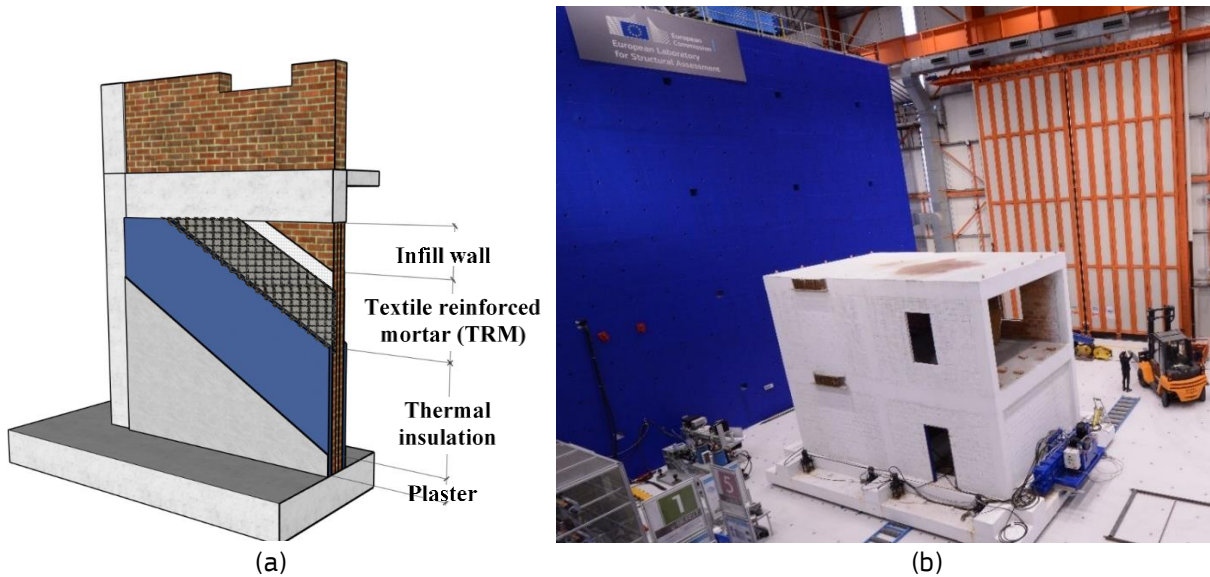
Of the current EU building stock, 80% was built before the 1990's when modern seismic and energy provisions were put in practice, and a third of buildings is over 50 years old (Economidou et al., 2011). As a consequence of their age of construction, degradation of materials and non-compliance with modern standards, the energy performance of older buildings is often inadequate. In fact, buildings are responsible for 36% of CO<sub>2</sub> emissions in the EU and 40% of the total energy consumption (European Commission, 2020b). Similarly, their performance under seismic loading is often also poor, as highlighted by the observed heavy damage and collapses of existing buildings in recent earthquakes (Ricci, De Luca, and Verderame, 2011; De Luca et al., 2014; Indirli et al., 2013; Bournas, Negro, and Taucer, 2014), resulting not only in significant economic losses, but also severe injuries and loss of human lives.

Since replacing the existing buildings with new is prohibitively expensive and has a significant environmental and social impact, these buildings require upgrading to meet modern standards and extend their lifetime. Renovating the existing building stock, can achieve significant reductions in energy consumption and CO<sub>2</sub> emissions (Salvalai, Sesana, and Iannaccone, 2017; Corrado and Ballarini, 2016), however, on average, less than 1% of the national building stock is currently being renovated annually, with Member State rates varying from 0.4% to 1.2% (European Commission, 2020c). Recognising the importance of building renovation, the ambitious European Green Deal (Communication 2019/640), emphasises the need for the EU and its Member States to engage in a 'renovation wave' of public and private buildings (European Commission, 2019). The objective of the Renovation Wave (Communication 2020/662) is to 'at least double the annual energy renovation rate of residential and non-residential buildings by 2030' (European Commission, 2020b).

The implementation of the recently amended Energy Performance of Buildings Directive (EPBD) (European Parliament and Council of the European Union, 2018) is a key strategy to increase current renovation rates. The EPBD states that 'renovation would be needed at an average rate of 3 % annually to accomplish the Union's energy efficiency ambitions in a cost-effective manner'. Within the EPBD, it was recognised that next to reducing greenhouse gas emissions, fire safety and seismic risks, which affect the lifetime of buildings, should be addressed by Member States when planning their long-term renovation strategies (LTRS). Including these aspects will help preventing significant human and economic losses from earthquakes and fires, as well as reducing the emissions from the building sector. At the same time, combining the application of seismic and energy retrofitting can achieve cost effectiveness, and hence incentivise renovation.

An innovative approach to achieve combined retrofitting was explored in the [iRESIST+](#) project. The project aimed to explore a novel retrofit system, combining inorganic textile-based composites with thermal insulation to achieve simultaneous improvements in the energy efficiency and seismic performance of the European building stock. In particular, based on pilot background studies (Bournas, 2018a; Bournas, 2018b), a new combined retrofit scheme was proposed in iRESIST+, consisting of textile-reinforced mortars (TRM) applied at the same time with thermal insulation materials, as illustrated in Figure 1a. The impact of the proposed approach was evaluated through numerical simulations and will be validated experimentally on a full-scale prototype building, representing a typical pre-1970's infilled reinforced concrete (RC) structure, at the JRC's ELSA reaction wall facility (see Figure 1b).

**Figure 1.** (a) iRESIST+ combined retrofitting with TRM and thermal insulation. (b) Prototype structure at ELSA, Joint Research Centre (JRC), European Commission



In this report, the EU policy framework surrounding the project will be presented first in **Section 2**. To explore the potential of textile-based composites for combined retrofitting, a state-of-the-art review of seismic retrofitting of infilled RC buildings with TRM was conducted, exploring also recent research on their integration with thermal insulation, presented in **Section 3**. The review of experimental literature led to the creation of a database of experimental results, which was used to develop new analytical models for TRM and composite strengthened infill walls (**Section 4**). Using the analytical model, numerical simulations of the behaviour of the iRESIST+ experimental prototype structure were conducted with and without retrofitting under cyclic loading in **Section 5**. The results will help inform the experimental study, but also allow to evaluate the impact of the suggested retrofit scheme on a typical European pre-1970's building. The model was then used to develop seismic fragility curves of mid-rise RC buildings with different level of seismic design and retrofitted with TRM. These fragility curves, presented in **Section 6**, serve to further generalise the results of TRM-strengthening of infilled RC buildings and allow to compare the performance of the retrofit for structures with a low level of seismic design to that of modern structure. Finally, in **Section 7**, an analysis of the effect of combined seismic and energy retrofitting using the iRESIST+ retrofit scheme was evaluated for twenty case study cities across different seismic and climatic zones in Europe. A foresight study up to 2030 investigating the impact of different building renovation rates is provided, where the effect of retrofitting was assessed in terms of energy consumption reduction, reductions in carbon emissions, as well as seismic losses.

## 2 Relevance to EU Policies

The combined retrofitting of buildings, as investigated in iRESIST+, can be seen as the nexus between policies encouraging the energy renovation of buildings, promoting circularity principles within the construction sector, improving the resilience of our EU building stock to natural disasters, as well as protecting our built heritage (Figure 2). Different EU policies in these four domains were identified as being mutually beneficial when taking a holistic approach to building renovation.

**Figure 2.** Combined retrofitting at the nexus of relevant policy domains.



### 2.1 Building energy efficiency

In terms of implementing sustainability in the built environment sector, the ambitious plans of the European Green Deal (Communication 2019/640) emphasise the need for the EU and its Member States to engage in a “**renovation wave**” of public and private buildings (European Commission, 2019). To support this renovation wave and make further develop circular economy principles, the Commission recently announced The New European Bauhaus initiative (STATEMENT/20/1902), aiming to combine good design with sustainability.

Until recently, the renovation of existing buildings was focusing either on addressing structural safety problems or on increasing the energy efficiency. The Energy Performance of Buildings Directive (EPBD) was set-up as a framework for building energy performance strategies and measures for reducing greenhouse gas emissions from the built environment to be implemented by the EU Member States. In its 2018 amendment, Directive 2018/844 (European Parliament and Council of the European Union, 2018) additionally encourages measures related to fire safety and seismic risks, which affect the lifetime of buildings, for planning long-term renovation strategies by the Member States. Here, combined seismic and energy retrofit strategies can provide synergistic technical solutions encompassing these aspects and hence be beneficial for the long-term renovation strategies. Finally, improving the energy performance of historical buildings is also encouraged by the EPBD, while simultaneously safeguarding and preserving cultural heritage.

## **2.2 Circular economy**

In the context of the European Green Deal, a New Circular Economy Action Plan (Communication 2020/98) was also brought forward, encouraging **life cycle thinking** approaches, i.e. from production and consumption to waste management, in all major sectors (European Commission, 2020a). In the building and construction sector, this regards improvements of the energy performance of buildings, but encourages the lifetime-extension of buildings by means of maintenance, repair and upgrading. A combined retrofit strategy, such as the one investigated in iRESIST+, can be instrumental in promoting circular economy principles, as improvements in energy performance are combined with reducing repair works, demolitions and rebuilding associated with seismic damage.

## **2.3 Disaster risk reduction**

With respect to **resilience** from man-made and natural hazards, the Union Civil Protection Mechanism (Decision 2019/420) promotes and facilitates cooperation between MS in the fields of risk mitigation, management and preparedness (European Parliament and Council of the European Union, 2019). The UCPM addresses primarily the protection of people, but also includes the environment and property, comprising our built heritage, against man-made and natural disasters, such as earthquakes. Moreover, investments in disaster risk reduction are encouraged within the Action Plan on the Sendai network (SWD 2016/205), which promotes "Build Back Better" principles for a more resilient built environment (European Commission, 2016a). Finally, the Sendai Priority (iv) also encourages the integration of safeguarding cultural heritage in the national disaster risk reduction strategies.

## **2.4 Safeguard cultural heritage**

The [European framework for action on cultural heritage](#) SWD 2018/491 (DG EAC, European Commission, 2019) was a key outcome of the European Year of Cultural Heritage (EYCH) 2018 (Decision 2017/864/EU) and also highlights the importance of **safeguarding the built heritage**. Our built heritage is crucial to be preserved and may be instrumental in "Promoting our European way of life", one of the six European Commission's priorities for 2019–2024. "Cultural heritage" encompasses a wide range of the EU's built heritage that goes beyond monuments, castles or museums, and includes the architectural heritage of a country (e.g. Brutalist concrete architecture of the 1950s and 60s), historic masonry town centres (e.g. in Portugal, Greece, Italy). Combined seismic and energy retrofitting of cultural heritage buildings is also explicitly addressed by the Urban Agenda Partnership on Culture and Cultural Heritage (formed in 2019). The Partnership includes Commission DGs (REGIO, EAC, RTD, DEVCO, AGRI, CLIMA, JRC, SG), EU Governmental Bodies, Member States, Regional and supra-municipal bodies, Cities and other members, such as the European Committee of the Regions and the European Investment Bank.

## **2.5 Contributions of iRESIST+**

The relevance of iRESIST+ is particularly highlighted within the context of promoting combined seismic and energy retrofitting as part of safeguarding cultural heritage. iRESIST+ contributed in terms of participation at workshops and events, as well as by being included in key documents of the EU's cultural heritage agenda.

**iRESIST+** was invited to present at one of the major events of the EYCH, namely the Fair of innovators in Cultural Heritage, which took place in Brussels, 15–16<sup>th</sup> November 2018, and

also marked the launch of the European framework for action on cultural heritage (DG EAC, European Commission, 2019). The event brought together policy makers at EU and national level, with researchers and industry working in the broad field of Cultural Heritage. The contribution of iRESIST+ was presented within the topic of safeguarding cultural heritage against natural disasters and climate change.

Moreover, an Expert Group on Cultural Heritage (E03650) was formed by the Commission to advise on issues related to the European framework for action on cultural heritage. The Expert Group's first meeting was organised by DG EAC and took place in Brussels, 15-16<sup>th</sup> October 2019. The JRC was invited to present the **iRESIST+** project at the Expert Group meeting.

In terms of the European framework for action on cultural heritage, **iRESIST+** was explicitly referred to in SWD 2018/491 (DG EAC, European Commission, 2019) within the CLUSTER OF ACTIONS 9: Protecting cultural heritage against natural disasters and climate change. Upgrading the European built heritage from a seismic capacity point of view, but also making heritage buildings more energy efficient, is acknowledged specifically as part of the set of actions required to protect cultural heritage.

The Urban Agenda Partnership on Culture and Cultural Heritage sees preserving the quality of landscapes and built environment heritage as a powerful tool to achieve social, ecological and economic goals. In its [Orientation Paper](#) (Urban Agenda for the EU, 2019), it states specifically in Section 2.1.2, that the preservation and further development of existing building stock is the starting point for future-proof urban development. Recently, the Partnership developed an "[Urban Agenda Action Plan](#)", published in November 2020<sup>1</sup>, consisting of concrete proposals for improvements in EU legislation, funding and knowledge, in the overall theme of culture and cultural heritage. In this Action Plan, "*exploring the need for incorporating structural safety within climate change adaptation measures, while preserving the values and character of Cultural Heritage assets based on results from JRC's **iRESIST+** project*" is explicitly mentioned as part of ACTION N° 09 – Observatory on Culture/Cultural Heritage and climate change in the urban framework, as well as mentioned in ACTION N° 08 – Guiding Principles for Resilience and Integrated Approaches in Risk and Heritage Management in European Cities.

---

<sup>1</sup> Final Action Plan of the Partnership on Culture/Cultural Heritage : <https://ec.europa.eu/futurium/en/culturecultural-heritage/final-action-plan-partnership-culturecultural-heritage>

### 3 Review on retrofitting materials

#### 3.1 Seismic retrofitting of existing structures with composites

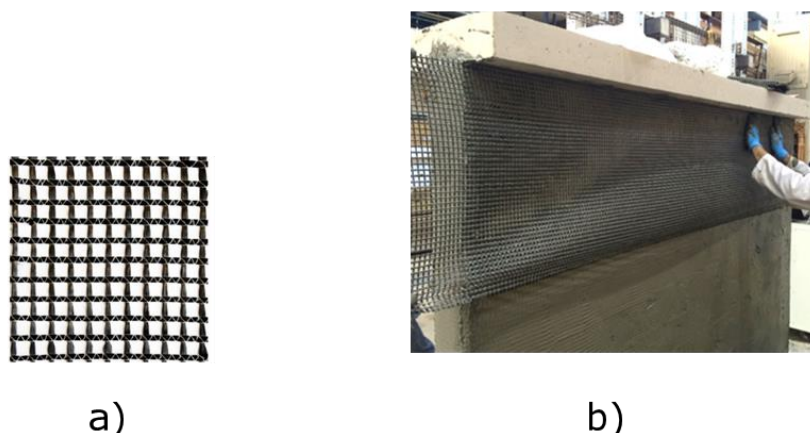
Significant damage to existing reinforced concrete (RC) frame structures during recent earthquakes has highlighted the potential detrimental effect of non-structural masonry infills and hence the vulnerability of infilled RC structures (De Luca et al., 2014; Fikri et al., 2018; Kouris, Borg, and Indirli, 2010; Ricci, De Luca, and Verderame, 2011). Moreover high costs are associated with losses even at low intensity earthquakes due to damage in non-structural infills (De Luca et al., 2014). Vulnerable infilled RC structures hence require fast, reliable, and effective retrofit strategies.

Conventional techniques such as RC jacketing (Varum, 2003) are generally seen to be labour intensive, use large quantities of materials and lead to a significant increase in wall thickness. Several experimental studies have hence investigated the use of composite materials for in-plane retrofitting of infills to reduce the risk of brittle collapse.

A state-of-the-art on strengthening infilled RC frames with composite materials, with an emphasis on textile-reinforced mortars (TRM) was conducted (Pohoryles and Bournas, 2020c) and a database of experimental results was compiled. A summary of different strengthening applications for infilled RC frames using composites can be found in Table 1.

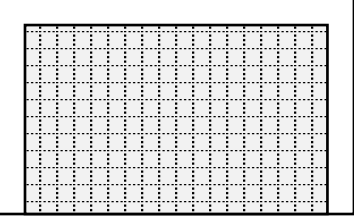
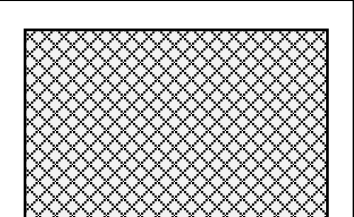
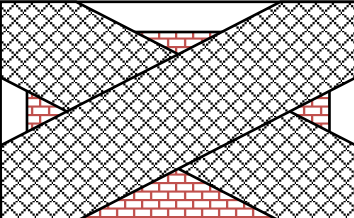
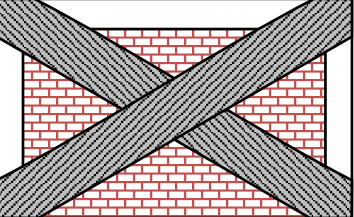
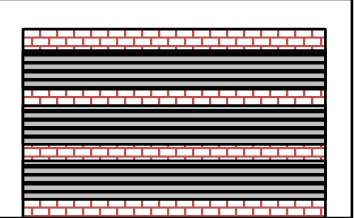
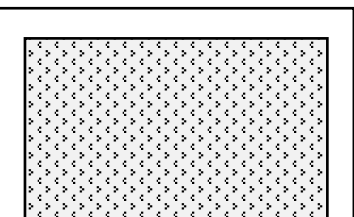
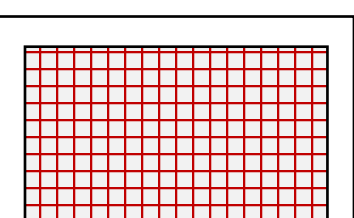
TRM constitutes a relatively new composite material for seismic retrofitting of existing concrete structures (Koutas et al., 2019) consisting of open-mesh textiles embedded in a cementitious matrix, as illustrated in Figure 3. Strengthening masonry infilled frames with TRM aims to achieve a reliable building response, utilising the strength and stiffness of the infills. As shown in Table 1, TRM forms part of a family of composite materials that have been tested in the literature. Composites can be applied as bands or strips or over the full surface of the infill. The orientation of the fibres can be orthogonal, with fibres in the vertical and horizontal directions, at  $\pm 45^\circ$  or in the diagonal angle of the infill. A variety of composite strengthening materials can be used, ranging from fibre-based textile meshes embedded in mortar (TRM), unidirectional fibre-sheets bonded using epoxy resins (FRP) and short fibres randomly orientated and embedded in mortar (ECCs), to steel meshes for reinforcing thin layers of plaster.

**Figure 3.** (a) Carbon based textile (b) Application of textile with inorganic matrix on masonry infill walls.



Source: (Koutas and Bournas, 2019) (CC BY 4.0).

Table 1. Summary of composite retrofit applications in the literature.

Type	Layout	Strengthening material	Fibre direction	Examples
Orthogonal TRM		Fibre-textile	2	(Akhoundi, Vasconcelos, Lourenço, Silva, et al., 2018; Koutas, Bousias, and Triantafillou, 2015; da Porto et al., 2015; Sagar, Singhal, and Rai, 2019; Selim et al., 2015)
TRM at 45°		Fibre-textile	2	(Sagar, Singhal, and Rai, 2019)
Diagonal TRM bands		Fibre-textile	2	(Ismail, El-Maaddawy, and Khattak, 2018)
Diagonal FRP strips		Fibre-sheet	1	(Erol and Karadogan, 2016; Yuksel et al., 2010; Ozkaynak et al., 2011)
Horizontal FRP strips		Fibre-sheet	1	(Almusallam and Al-Salloum, 2007)
ECCs		Lose fibres	$\infty$	(Ayatar, Canbay, and Binici, 2018; Dehghani, Nateghi-Alahi, and Fischer, 2015; Koutromanos et al., 2013; Kyriakides and Billington, 2014; Li, Zhu, and Wang, 2019; Yaman and Canbay, 2014)
Reinforced Plasters		Steel bars	2	(Altin, Anil, and Kara, 2008; Korkmaz et al., 2010)

Source: (Pohoryles and Bourmas, 2020c)

The use of epoxy-based composites, such as fibre-reinforced polymer (FRP) sheets for retrofitting has grown significantly in popularity due to their small thickness increase, important for architectural reasons, and corrosion resistance. FRP can be applied in the diagonal of the infill wall, leading to considerable strength increase (Erol and Karadogan, 2016; Yuksel et al., 2010; Ozkaynak et al., 2011). This strength increase was however not found to be proportional to the strip width (Altin et al., 2008). Strengthening by means of horizontal FRP strips, in turn, did not lead to significant increase in lateral capacity (Almusallam and Al-Salloum, 2007).

While high increases in strength and ductility can be achieved with FRPs, their application is also associated with some drawbacks, as the use of epoxy leads to higher costs and the need for the use of protective equipment. Moreover, the behaviour of FRPs at high temperature and difficulty of application at low temperatures, as well as on wet surfaces are practical constraints, that may be remediated by using inorganic matrices, such as cementitious mortars or plasters, as alternative to epoxy-based resins as binder.

Cement-based composites include (sprayable) engineered cementitious composites (ECC) for masonry infills (Ayatar, Canbay, and Binici, 2018; Dehghani, Nateghi-Alahi, and Fischer, 2015; Koutromanos et al., 2013; Kyriakides and Billington, 2014; Li, Zhu, and Wang, 2019; Yaman and Canbay, 2014). The disadvantage of ECCs is however the non-directionality and uncertainty of equal distribution of fibres, which make predicting the strength increase more challenging. Reinforced plasters, on the other hand, consist of mesh reinforcement with two orthogonal directions embedded in a thin layer of plaster for strengthening infills (Altin, Anil, and Kara, 2008; Korkmaz et al., 2010). This kind of retrofit is analogous to the orthogonal TRM strengthening method, but instead of fibres woven into a textile mesh, a steel reinforcement mesh is used, which can be associated with similar durability concerns regarding corrosion as RC jacketing.

Finally, in terms of retrofitting infills with TRM, a variety of fibre materials has been used in the experimental campaigns, including Carbon (C), Basalt (B), Glass (G) and Steel (S) fibres, as shown in Table 2. The retrofit applications were made with a range of orthogonal mesh sizes between 8 and 25 mm, the thickness per layer of TRM (textile + mortar) is between 4 and 20 mm and the elastic moduli range from 13.8 GPa for softer glass textiles to 252 GPa for stiffer Carbon textiles.

Table 2. Typical TRM properties from the literature.

<b>Study</b>	<b>Fibre Material</b>	<b>Mesh size <math>m</math> (mm)</b>	<b>Thickness/layer <math>t</math> (mm)</b>	<b>Elastic modulus <math>E_f</math> (GPa)</b>
Koutas et al. (2015)	G	25	4	73
Selim et al. (2015)	G	25	5	72
Da Porto et al. (2015)	B+S	10	15	90
Akhoundi et al. (2018)	G	25	20	72
Ismail et al. (2018) - G	G	20	7.5	32
Ismail et al. (2018) - C	C	20	7.5	252
Ismail et al. (2018) - B	B	8	7.5	89
Sagar et al. (2019)	G	25	6	114

Inorganic textile-based composites have advantages over FRP systems in terms of fire resistance (Kapsalis et al., 2019; Triantafillou et al., 2017) and behaviour at high temperatures (Tetta and Bournas, 2016; Raoof and Bournas, 2017b; Raoof and Bournas, 2017a; Cerniauskas et al., 2020), better bond and strain compatibility with masonry, as well as their applicability at low temperatures or on wet surfaces and lower costs. Moreover, unidirectional FRP as a retrofit material can rupture in the weaker orthogonal direction, which can be avoided when using randomly arranged fibres or orthogonal meshes.

Initial work by Koutas et al. (2015) consisted of cyclic tests up to failure of a 2/3-scale three-storey fully infilled RC frame retrofitted with TRM. The aim of the retrofit was to achieve a more ductile failure mechanism with a regular displacement demand along the height of the structure. The scheme consisted of applying two layers of glass TRM (G-TRM) in the first storey and one in the second and third storeys, using previously tested textile anchors at the perimeter of the infills. Moreover, the column-ends were wrapped with TRM to prevent shear failure observed in the control specimen.

The as-built specimen failed in a brittle single-storey mechanism, with damage concentrated in the ground storey. For the ground storey, diagonal cracking along the infill surface was observed, with spalling of the bricks closer to the corners, and finally shearing of the columns at the top corner. The retrofitted structure instead presented a behaviour characterised by a regular distribution of lateral storey displacements along the height of the structure, which led to an enhanced deformation capacity (+52%). Shear damage to the columns was successfully prevented by the local TRM jacketing. The use of anchors at the infill perimeter successfully delayed debonding of TRM and hence ensured an adequate lateral load resisting system with a good infill-frame connection up to localised rupture of the TRM fibres at the interface. An increased lateral strength (+54%) and initial stiffness (twofold) were observed for the retrofitted structure. The cracking pattern on the TRM surface indicated horizontal sliding of the bricks. After removal of the retrofitting material, significant corner crushing was observed in the underlying infill. The observed damage appears to indicate that the TRM retrofit successfully confined the infill wall and allowed it to ultimately reach crushing of the bricks, without losing full integrity of the wall up to large levels of lateral displacement. The test on a three-storey specimen also highlighted that a non-uniform distribution of lateral displacements, leading to soft-storey failure, can be successfully prevented by a well-designed TRM retrofit with different numbers of layers along the height of the structure. Recently, the use of TRM has been successfully demonstrated for the out-of-plane strengthening (Koutas and Bournas, 2019) of masonry-infilled RC frames.

Selim et al. (2015) tested two non-seismically designed 1/3-scale infilled RC frames, of which one was retrofitted with G-TRM. The retrofit consisted of two layers of TRM on each face of the infill wall, extended onto the columns and using five fabric anchors applied through the infill. Due to inadequate detailing and high localised forces in the corners of the infilled frame, the control specimen failed by a beam-column joint shear failure mechanism, combined with extensive corner crushing observed in the infill wall. A brittle failure at 1% drift with 79.2 kN lateral force was observed. The TRM retrofit ensured the corner crushing and joint shear mechanisms were prevented. TRM jacketing of the infill ensured crushing of the bricks was prevented, despite the higher sustained lateral loads of 131.7 kN (+66.3%). TRM contribution in tension was demonstrated by increased diagonal cracking and an improved ductility. While damage to the RC frame was generally reduced by the retrofit, ultimately, failure due to column bar buckling at the foundation was observed.

Da Porto et al. (2013; 2015) studied the effect of TRM strengthening on eight full-scale RC frames infilled with light clay masonry walls. After in-plane cycling testing up to 1.2% drift, the out-of-plane residual capacity of the specimens was assessed in this study. Two test series were conducted, using stronger masonry mortar for the first four specimens (two control and two retrofitted) and a weaker mortar to bind the bricks in the latter four. As shown in Table 2, for the textile, a combined glass and steel fibre mesh was used for one specimen, while a basalt and steel fibre mesh was used for the other three. The influence of the inorganic binder used for the TRM was also investigated with high strength mortar ( $f_{m,f} = 5.4$  MPa) used for two retrofitted specimens (3-GC-NR and 4-GC-FN), while for two other specimens (6-BG-NR and 8-BC-NR), low strength gypsum plaster or natural hydraulic lime plasters, respectively, were used ( $f_{m,f} = 1.1$  MPa). The gypsum plaster has the benefit of being more environmentally friendly and able to capture volatile organic pollutants. Finally, anchorage of the mesh to the upper beams using steel-ties was provided for one specimen (4-GC-FN).

During the in-plane tests, the control specimens experienced heavy damage, including spalling and crushing of masonry units at the corners. This was not observed for any of the retrofitted units, for which damage was delayed significantly, with no cracking up to 0.5% drift. For the specimens retrofitted using low strength mortar, a higher level of damage was observed, with visible cracking initiating at 0.5% drift, compared to 1.2% for the higher strength mortar. For the specimen with weaker masonry mortar, horizontal sliding was observed for the control and retrofitted specimens. For the three unanchored specimens, limited local detachment of the TRM was observed. This ultimately led to localised crushing at the corners of the infills in two specimens, which was prevented in the specimen with steel tie anchorage. Despite the reduction in damage, the recorded results indicate that in-plane strength and stiffness were not affected by the retrofit. Still, prevention of brittle failure in the retrofitted specimens resulted in considerably improved ductility and reduced post-peak strength degradation. This allowed the retrofitted walls to behave better in the subsequent out-of-plane tests, with higher residual strength recorded compared to the control specimens.

More recently, Akhoundi et al. (2018; 2018) tested two G-TRM retrofitted frames, using a commercial and a custom-made braided textile, respectively. The braided textile, previously tested on masonry [45], was specifically designed to maximise the mechanical interlock between textile mesh and mortar. To enhance the effectiveness of the retrofit, twelve glass fibre connectors through the infill and four connectors at the interfaces to each RC member were used for anchorage. Next to a significant increase in initial stiffness, strength increases of 25% and 30% were obtained for the commercial and braided TRM. The commercial TRM surface was fully cracked along the diagonal after testing, while the braided TRM specimen only presented infill detachment cracks at the interfaces. After removal of the jacket post-testing, crushing of the infill corners was observed for both specimens, but more extensively for the specimen using a commercial TRM. No diagonal cracks in the infill were observed. Overall, the use of a braided textile achieved the same global behaviour as the commercial material but reduced the amount of visible damage.

The use of TRM applied as diagonal strips was also found to be very effective, and the stiffness of the fibres was found to affect this strength increase more than the increase in width of the diagonal TRM layers (Ismail, El-Maaddawy, and Khattak, 2018). Ismail et al. performed cyclic tests on infilled 2/3-scaled frames with three different TRM layouts, including an orthogonal full-surface application and two diagonal band configurations with varying width (one-sixth and one-third of the diagonal length of the infill). The latter

diagonal band application is similar to the application of FRP strips for infill strengthening. For the diagonal application, the effect of three different fibre materials was evaluated (carbon, basalt and glass), while the orthogonal application employed B-TRM only. Low extend of damage was observed for all retrofitted specimens. Some infill-frame separation was observed in all cases and for the diagonal application of TRM, cracks perpendicular to the strips were observed to form at drift levels above 0.3%. For the full-face TRM retrofit, only minor cracks appeared in the bottom interface and a small extend of diagonal cracks was observed on the TRM surface, with limited debonding. The initial stiffness of the specimens was not found to be affected the retrofit, with differences between 5% up to 24% observed. Interestingly, the stiffness was found to be higher for the specimens with the thinner TRM strips. In terms of lateral load capacity, large increases in capacity were observed for all specimens. The increase in width of the diagonal TRM layers was not found to significantly affect this strength increase and the behaviour of the full-surface retrofit was similar to the diagonal strengthening layout. Interestingly, despite the carbon textile had the highest strength of the three fibre materials, the highest strength increase was obtained with the basalt TRM (+ 99%). For the carbon TRM the peak was reached at a load 40% higher than the control specimen, while the glass TRM retrofit achieved a slightly lower increase of up to 32%.

Finally, Sagar et al. (2019) looked at the interaction of in- and out-of-plane damage in masonry infilled RC frames with TRM retrofitting. Six single-storey half-scale frames were tested under cyclic in-plane loading, with out-of-plane testing on a shake table carried out at different levels of in-plane drift. The TRM was applied in a single layer to the outer face of the infills only. The investigated parameters were the angle of the fabric mesh (orthogonal vs  $\pm 45^\circ$ ), the contribution of mechanical anchors, as well as the sequence of fabric placement. In direct bond tests, the latter was found to affect bond strength, with a direct application of the textile on the wall having a higher bond strength (0.83 MPa) compared to 0.63 MPa obtained for the conventional “sandwich application”, with a base layer of mortar applied on the infill. In three specimens, mechanical anchors (steel bolts), were installed and a tighter mesh size of the fabric (8 mm instead of 25 mm) was used at the frame-infill interface, to improve transfer of forces to the anchors, but also to strengthen the interface. The experimental results focused on the interaction of in-plane damage and out-of-plane behaviour, with a reduction in connection between frame and infill observed due to out-of-plane plane damage. For the anchored specimens, a better out-of-plane behaviour was observed, however without anchorage, the connection between frame and infill was significantly reduced. This also meant that the in-plane behaviour displayed a more gradual strength degradation for the specimens with anchorage. The specimens with orthogonal TRM application presented a more ductile and dissipative behaviour. In general, strength increase was very similar for all retrofitted specimens, with values close to +30%.

### **3.2 Combined retrofitting with TRM**

The use of TRM with energy retrofitting technologies is a very recent, but emerging research field, offering the possibility for the concurrent seismic and energy retrofitting of RC and masonry building envelopes (Bournas, 2018b; Gkournelos, Triantafillou, and Bournas, 2020; Kouris et al., 2021; Triantafillou et al., 2017; Triantafillou et al., 2018).

Bournas (2018) explored the avenues of TRM for hybrid structural-plus-energy retrofitting solutions, proposing the combination of TRM with different thermal insulation materials (e.g. TRM+PUR, TRM+XPS, TRM+Aerogels, TRM+NIM), or the integration of capillary tube

heating systems within the TRM. Triantafillou et al. (2017, 2018) tested different configurations of TRM and thermal insulation (foamed polystyrene and foamed cement insulation) as integrated seismic and energy retrofitting systems for masonry wall panels under in-plane and out-of-plane, as well as evaluating their fire behaviour. High effectiveness of the retrofit was observed, and the effect of applying the TRM above or below the insulation layer was not found to be critical. Moreover, a single-sided application, which would have benefits of reducing the impact on building occupancy during retrofitting, was not found to significantly reduce the effectiveness of the retrofit. As part of the same effort, the out-of-plane capacity of masonry walls retrofitted with TRM and foamed polystyrene were tested by Gkournelos et al. (2020) after initial in-plane damage. Next to an improved in-plane behaviour, the out-of-plane capacity of the retrofitted specimens was significantly improved. It is of particular interest, that the combined seismic and energy retrofitted specimens (TRM+polystyrene) presented a better behaviour than the TRM retrofit alone due to the increased lever arm.

Borri et al. (2016) investigated the mechanical and thermal properties of different insulating mortars with embedded glass fibre grids as strengthening system for masonry wall panels, i.e. a system analogous to TRM. Mortars made of natural materials (hydraulic lime, aerial lime, limestone sand and lightweight mineral aggregates) were tested, finding that the addition of the fibre grid improves the thermal properties of the mortar layer by 12-15% due to additional air trapped in the mortar layer. While the mortars with the best thermal properties achieve a significant reduction in U-values of a masonry wall (up to 45%), the shear behaviour of the retrofitted wall specimens is not improved. However, results for a mortar with moderate strength and thermal properties, shows potential, but it remains to be evaluated for its use in combined thermal retrofit and seismic strengthening.

In terms of developments in mortars, a recent work by Coppola et al. (2019) investigated the use of lightweight cement-free alkali-activated slag plaster for the structural retrofit and energy upgrading of low quality masonry walls, in which mortars at different lightweight aggregate content were combined with a GFRP mesh and characterised in terms of mechanical and thermal properties. Similarly, Longo et al. have explored the use of different lightweight geopolymers-based mortars for their use with GFRP meshes for their use in concurrent structural and energy retrofitting (Longo, Lassandro, et al., 2020; Longo, Cascardi, et al., 2020), creating analogous materials to TRM. Similar strength and a 50% increase in thermal resistance was obtained compared to normal hydraulic lime mortars.

None of the solutions integrating fibre grids into thermal mortars can however be used alone to achieve the desired strength and thermal properties for combined seismic and energy retrofitting, hence leaving the need for addition of thermal insulation materials.

### **3.3 Materials for thermal insulation**

An important aspect to develop combined seismic and energy retrofitting systems with TRM is hence to define thermal insulation compatible with the seismic strengthening material. Different types or systems exist, including (1) the most typical rolls of soft blanket insulation, (2) more rigid foam or fibre boards, e.g., made from mineral wool or fiberglass, (3) liquid foam insulation materials, that can be poured, injected, or sprayed, (4) structural insulation panels, such as vacuum insulation panels, or (5) active systems, such as capillary tubes, that heat the walls actively.

Typical thermal retrofits nowadays use mineral wool or polystyrene as insulation material, which have  $\lambda$ -values around 35 mW/mK (Schiavoni et al., 2016). A variety of other

materials exist and are applied in real buildings for thermal insulation, good reviews of these materials are available in the literature (e.g.: Aditya et al., 2017; Jelle, 2011; Papadopoulos, 2005; Schiavoni et al., 2016). A summary of materials based on these reviews is offered below and typical thermal conductivity values ( $\lambda$ -values) given in Table 3.

- Traditional materials like mineral wools include glass wool (e.g. glass fibre) or rock wool (made from melted basalt, diabase or dolerite), normally produced as mats and boards. Typical  $\lambda$ -values for can be between 30 and 40 mW/mK. Another material is expanded polystyrene (EPS), which consists of small spheres of polystyrene containing an expansion agent, hence creating a porous material usually casted as boards. Using instead melted polystyrene and adding an expansion gas, extruded polystyrene (XPS) can be produced. Continuous lengths of XPS can be obtained by extrusion with pressure through a nozzle. For both these materials, typical  $\lambda$ -values also vary between 30 and 40 mW/mK. Polyurethane (PUR) is another closed porous material obtained from an expansion process using an expansion gas. Boards of PUR are available, but the material can also be used as expanding foam, achieving very good thermal performance with  $\lambda$ -values between 20 and 40 mW/mK. An issue with PUR is however the release of toxic hazards in case of a fire. Natural materials, such as cellulose obtained from recycled paper or wood fibre mass can also be used as insulation material. It has similar consistence to wool and can be found as filler material or as insulation boards and mats with thermal conductivity values around 40 mW/mK. Slightly higher values up to 50 mW/mK are typically obtained for insulation boards made from cork.
- More advanced materials for thermal insulation include Vacuum insulation panels (VIP), which consist of a core of porous material of low thermal conductivity (e.g. fumed silica) protected by an envelope of good mechanical strength. This includes metal foils, metallized films and polymer films. Very low thermal conductivity values of 3.5 to 8 mW/mK can be obtained for VIPs. Another type of advanced panels are Gas filled panels (GFP), which instead contain a gas (such as air, argon or krypton) protected from the external environment. Values between 10 mW/mK for Krypton and 40 mW/mK for air have been reported. Finally, aerogels are a class of material gaining increasing attention in the last years. The material is characterised by a very high porosity produced by drying a silica foam, leading to porosities up to 99.8% and hence very low densities and thermal conductivities. The material can be used as granular aerogel within window cavities, as full panels or as additive to stone wool. While the thermal conductivities of aerogels can be extremely low, materials available for construction have typically higher  $\lambda$ -values between 10 and 15 mW/mK. Aerogel have also been used as additives to finishing plasters in lower volume percentages (ca. 2%) achieving improved thermal performance compared to normal plasters (Berardi, 2017; Kim et al., 2013).

Table 3. Thermal insulation performance of different insulation products.

	<b>Thermal conductivity</b> $\lambda$ (mW/mK)	<b>Density</b> $\rho$ (kg/m <sup>3</sup> )	<b>Fire class</b>	<b>Form</b>
<b>Traditional materials</b>				
Stone wool	33-44	40-200	A1-A2-Ba	rolls, boards
Glass wool	31-37	15-75	A1-A2	rolls, boards
Expanded Polystyrene (EPS)	31-38	15-35	E	boards
Extruded Polystyrene (XPS)	32-37	32-40	E	boards
Polyurethane (PUR)	22-40	15-45	E	boards, foams
Cellulose	37-42	30-80	B-C-E	rolls, boards, loose
Cork	37-50	110-170	E	boards, loose, plaster additive
<b>Advanced materials</b>				
Vacuum insulation panels (VIP)	3.5-8	160-230	A1c	boards
Gas filled panels (GFP)	10-40	N.A.	N.A.	boards
Aerogel	13-15	70-150	C	rolls, boards, plaster additive

Sources: Aditya et al., 2017; Jelle, 2011; Papadopoulos, 2005; Schiavoni et al., 2016

## 4 Modelling the seismic performance of TRM retrofitted infills.

Despite increasing experimental evidence, research on simplified modelling is still needed to facilitate the use of TRM and other composite materials for strengthening masonry-infilled RC frames. Next to the experimental investigation in the iRESIST+ project, significant advances have hence been made on developing macro-models for TRM-retrofitted infilled RC frames (Pohoryles and Bournas, 2020a; Pohoryles and Bournas, 2020c).

Macro-models using compressive struts are commonly used for simplified modelling of infilled frames (Asteris et al., 2011) and the aim of the current research efforts is to propose a unified macro-modelling approach for composite strengthened infilled frames. Based on the gathered experimental data from the literature, an analytical model for composite-strengthened infilled RC frames was developed. The effect of different parameters on the effectiveness of the retrofitting applications was assessed, including the stiffness of the fibre material, as well as the angle of the retrofit application.

### 4.1 Simplified tie-model calibration (Pohoryles and Bournas, 2020c)

First, a simplified tensile tie to account for the TRM based on the work of (Koutas, Triantafillou, and Bousias, 2015) was calibrated with extended experimental data gathered from the literature. The correlation between experimental parameters and the obtained effective strain was assessed and an empirical formulation of effective strain in terms of fibre stiffness and retrofit amount is finally proposed. Details of the modelling and calibration can be found in (Pohoryles and Bournas, 2020c).

In the model of Koutas et al. (2015b), the force developed in the tie depends on the relative orientation of the tie angle  $\theta$ , angle of the fibres,  $a$ , and the angles  $\theta_{cr,j}$  of an assumed multilinear stepped-crack pattern, i.e. an inclined crack ( $j=1$ ) and a horizontal crack ( $j=2$ ). The total force mobilised in the two axes  $i$  of the TRM fibres is then transformed geometrically into the direction of the diagonal tie as in Eq. (1) from (Koutas, Triantafillou, and Bousias, 2015):

$$F_{tie} = \sum_{i=1}^2 \sum_{j=1}^2 \frac{A_{t,i}}{s_i} (\varepsilon_{te,i} \cdot E_{t,i}) \cdot d_j \cdot [\cot \theta_{cr,j} + (2i - 3) \cdot \cot \beta_i] \cdot \sin \beta_i \quad (1)$$

Where,  $A_t$  is the area of TRM and  $E_t$  the elastic modulus from TRM coupon tests,  $\beta_i$  the angle of the fibres to the level normal to the tie-axis,  $s_i$  is the textile mesh spacing and  $d_j$  the crack lengths, both projected to the normal to the tie-axis. To predict the shear force of the strengthened specimen, Koutas et al. (2015b) suggested that the effective strain developed in the textile at maximum load,  $\varepsilon_{te}$ , is the main parameter. Based on a single experiment, Koutas calculated an effective strain of 0.8% for one layer of TRM for matching their experimental results. For multi-layered TRM, the effective strain was to a value of 0.57 % strain for double-layer TRM.

In the presented study (Pohoryles and Bournas, 2020c), instead a database of 16 experimental results from the literature was taken to calibrate an expression for the effective strain developed in the textile at maximum load,  $\varepsilon_{te}$ . The equation was expressed in terms of the area ratio of TRM ( $\rho_t$  in %) and the square root of textile elastic modulus ( $E_f$  in MPa), giving rise to the empirical Eq. (2):

$$\varepsilon_{eff} = \frac{1.40 \cdot \rho_t}{\sqrt{E_f}} \quad (2)$$

Where  $\rho_t$  is the cross-sectional area of TRM ( $A_t$ ) given in Eq. (3) as a fraction of the infill wall surface, determined from the height and length ( $h_w \cdot l_w$ ):

$$\rho_t = \frac{A_t \cdot \cos \theta}{h_w \cdot l_w} \quad (3)$$

The calibrated values for effective strain was found to average at 0.24%, with maximum and minimum values of 0.66% (with G-TRM) and 0.03% (with C-TRM), respectively.

#### **4.2 Unified strut and tie model for composite retrofits (Pohoryles and Bournas, 2020a)**

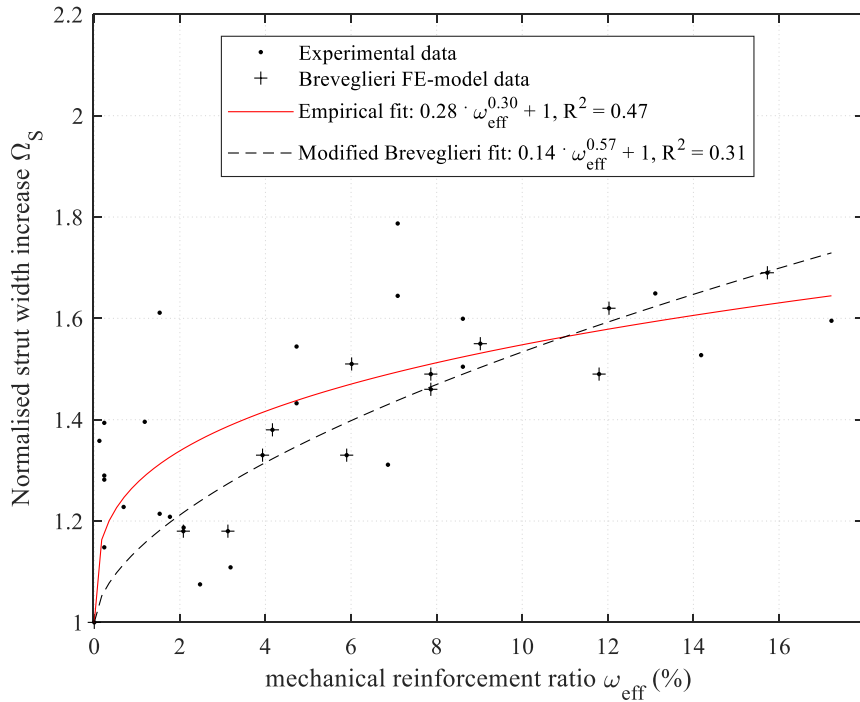
It is important to note that with the initial simplified model above, the secant stiffness of the retrofitted specimens does not significantly change, as the effect of the retrofit on the strut width is ignored. Similarly, post-peak softening increases significantly for the retrofitted specimens after the peak force in the tensile tie is reached. In reality, due to improved confinement and connection of the infill with the frame, softening is expected to be reduced and the initial stiffness would be larger, this is however not captured by the model used. This aspect may be improved when considering an increase in compressive strut width due to jacketing, and to improve the initial model, a more detailed approach was taken in (Pohoryles and Bournas, 2020a).

In addition to the tensile tie calibration, an empirical equation was proposed to increase the strut width based on the increase in secant stiffness for experimentally tested specimens. Based on this new strut width equation, a tensile tie was re-defined based on the remaining strength increase for the experimental specimens. The equations for strut-width increase and the tie strength were defined in terms of the effective mechanical reinforcement ratio ( $\omega_{eff}$ ).

The increase in strut width due to composite retrofitting of the infilled RC frame is defined from the ratio of the experimentally obtained secant stiffness of retrofitted specimens to the secant stiffness of the non-retrofitted control specimens. It is plotted against the mechanical reinforcement ratio in Figure 4. The secant stiffness increase is equivalent to the increase in strut width if all other parameters remain unchanged between the retrofitted and control specimen. The proposed model is also compared to a previously defined equation for FRP retrofitted infills modified from Breveglieri et al. and their data obtained from FE-modelling (Breveglieri, Camata, and Spacone, 2018). As can be seen, the modified Breveglieri equation fits the data points obtained from FE-modelling very well, however, the fit with the experimentally obtained values is poor ( $R^2 = 0.31$ ). Instead a new empirical equation is proposed for the strut width increase ( $\Omega_{s,emp}$ ) based on the experimental data alone:

$$\Omega_{s,emp} = 0.28 \cdot \omega_{eff}^{0.30} + 1 \quad (R^2 = 0.47) \quad (4)$$

**Figure 4.** Increase in secant stiffness against  $\omega_{\text{eff}}$  for the experiments on composite strengthened frames.



Source: (Pohoryles and Bourias, 2020a) (CC BY 4.0).

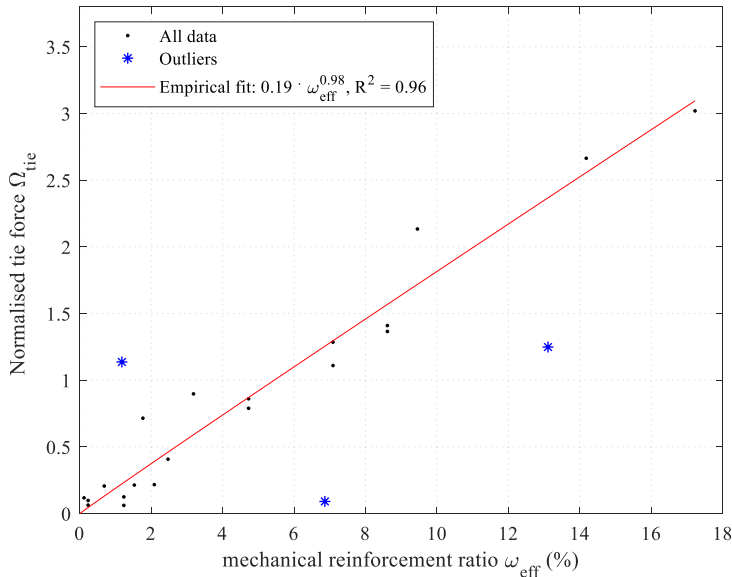
The empirical fit equation is obtained by least square fitting. The calibration includes a large range of mechanical strengthening ratios and is based on a range of different experiments. The reasons for the low  $R^2$ -value (0.47) may be related to the stiffness of the retrofitted frames being affected significantly by potential pre-damage in the frames, by the different types of anchorage used, as well as by the application of composite retrofit (full-face or diagonal strip), i.e. factors that cannot be considered in the empirical equation.

For the re-defined tie model, now a quasi-linear empirical equation of the normalised tie strength is expressed in relation to the effective mechanical ratio ( $\omega_{\text{eff}}$ ), similarly to the calibrated strut width increase equation (4). The proposed equation is obtained by least square fitting excluding the outliers defined based on a difference of 1.65 times the standard deviation based on the model, i.e. corresponding to a 90 % confidence interval.

$$\Omega_{\text{tie}} = 0.19 \cdot \omega_{\text{eff}}^{0.98} \quad (R^2 = 0.96) \quad (5)$$

For the sake of completeness, Figure 5 displays the gathered experimental, highlighting the outliers, and the empirical fit equation considering said outliers. The goodness of fit for the equation is very high, however further empirical data, particularly for higher mechanical reinforcement ratios is still needed for a more adequate equation.

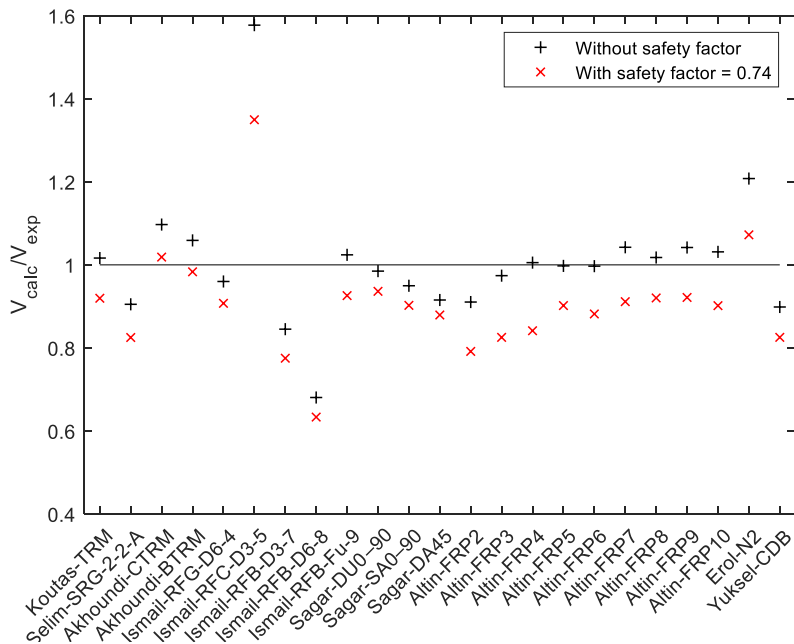
**Figure 5.** Normalised tie force against  $\omega_{\text{eff}}$  for the experiments on composite strengthened frames.



Source: (Pohoryles and Bournas, 2020a) (CC BY 4.0).

Using the proposed empirical equations, the ratio of calculated strength due to the combined strut and tie strength increases against the experimental base shear is shown in Figure 6. As expected, the mean value of the ratio is very close to unity (1.01), however the standard deviation is relatively large (0.16). To ensure a safe conservative design, a safety factor is hence proposed based on 1.65 standard deviations of the results (i.e. 90% confidence interval). This safety factor could be used for design purposes, by multiplying it with the calculated shear capacity ( $V_{\text{calc}}$ ) to ensure a more conservative estimation of the expected capacity. Applying a multiplication safety factor of 0.74 ensures 90% of predicted values fall on the conservative side, as illustrated by the red-crosses in Figure 6.

**Figure 6.** Ratio of calculated and experimental base shear for all specimens (including outliers).



Source: (Pohoryles and Bournas, 2020a) (CC BY 4.0)..

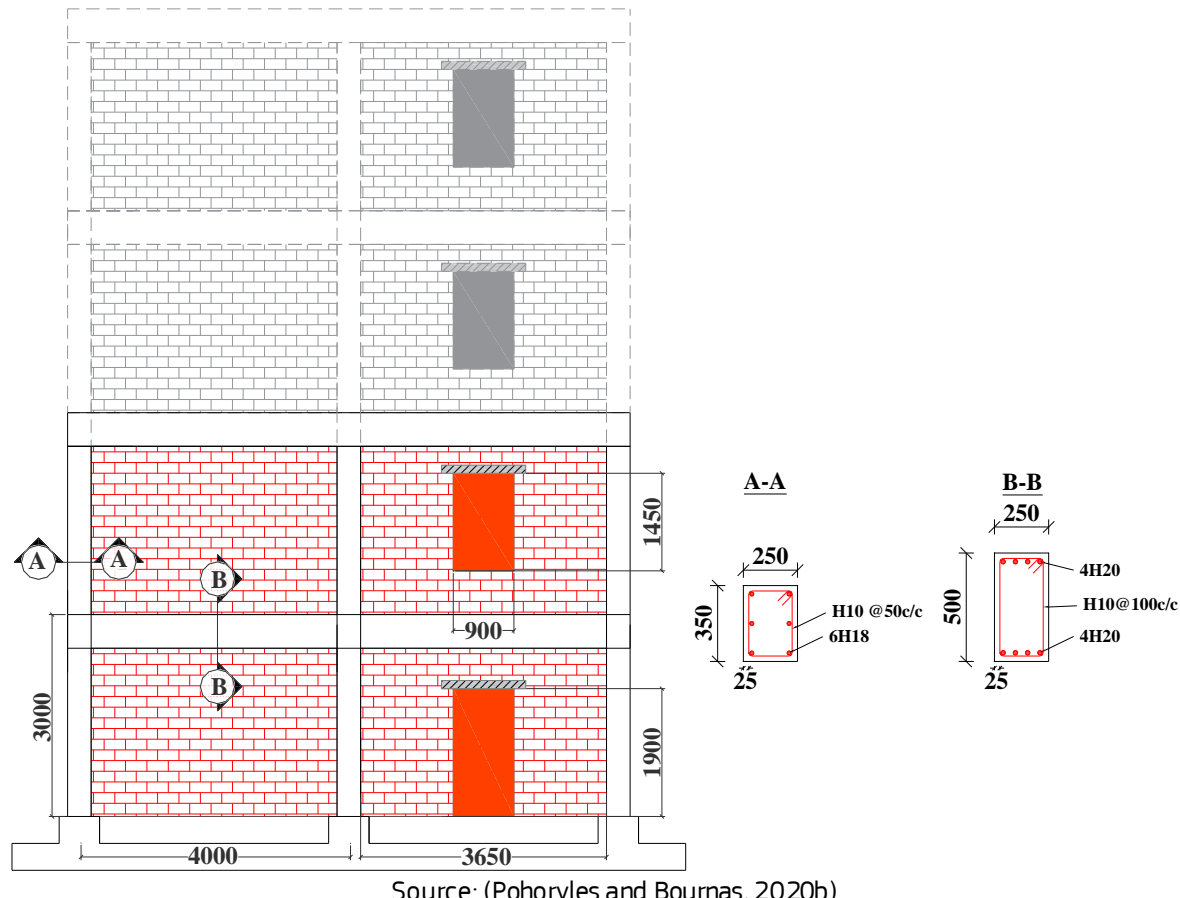
## 5 Numerical analyses on the iRESIST+ prototype structure

In order to assess the iRESIST+ prototype structure before experimental testing and evaluate the effectiveness of TRM retrofitting, a numerical analysis was conducted (Pohoryles and Bournas, 2020b). The prototype four-storey structure presented in Figure 7 was modelled with and without TRM retrofitting, using the TRM macro-model developed in the iRESIST+ project (Section 4.1).

### 5.1 Experimental prototype

The prototype building represents a typical European pre-1970s masonry-infilled RC building. The structure, shown in Figure 7, has four storeys with storey heights of 3 m and two 4m-wide bays in the direction of testing. Only a segment of a full building is taken, with the external frames of structure in the perpendicular directions represented by the prototype, simulating the weak direction of the building. The bays in the perpendicular direction in the modelled sub-structure are 6 m wide. Note that the first two storeys are present physically, while the upper two storeys are a numerical sub-structure during the pseudo-dynamic test.

**Figure 7.** Dimensions of building prototype in direction of loading and reinforcement detailing. Note: the modelled substructure is indicated in grey colour and dashed lines.



Source: (Pohoryles and Bournas, 2020b).

The cross-sectional dimensions and reinforcement detailing for the main structural elements are detailed in Figure 7. The dimensions of all columns are 250x350 mm and the beams are 500 mm deep, while the slab thickness is 150mm. The steel reinforcement of the RC frame is over-designed in order to concentrate damage on the infills and allow for re-testing of the frame after retrofitting.

Perforated clay bricks (60 x 140 x 300 mm) are used to build the double-leaf infill wall of a total thickness equal to 120 mm (2x60 mm). The opening percentage is 14.3% for the infills with windows and 18.6% for the infills with door.

The dimensions for the two-storey physical sub-structure are detailed and illustrated in Figure 8, Figure 9 and Figure 10. There are 2 bays of 4 m in the x-direction and 1 bay of 4 m in the y-direction, the total floor area in each storey is hence 32 m<sup>2</sup>.

**Figure 8.** Dimensions of the physical structure for testing: plan view.

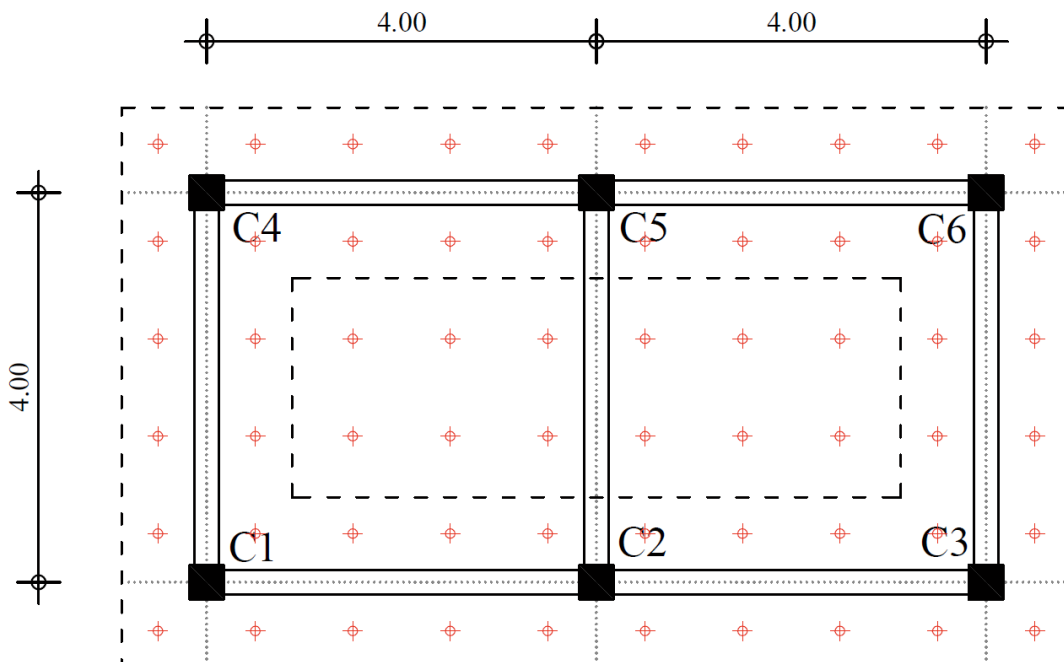


**Figure 9.** Dimensions of the physical structure for testing: side view in X-direction.

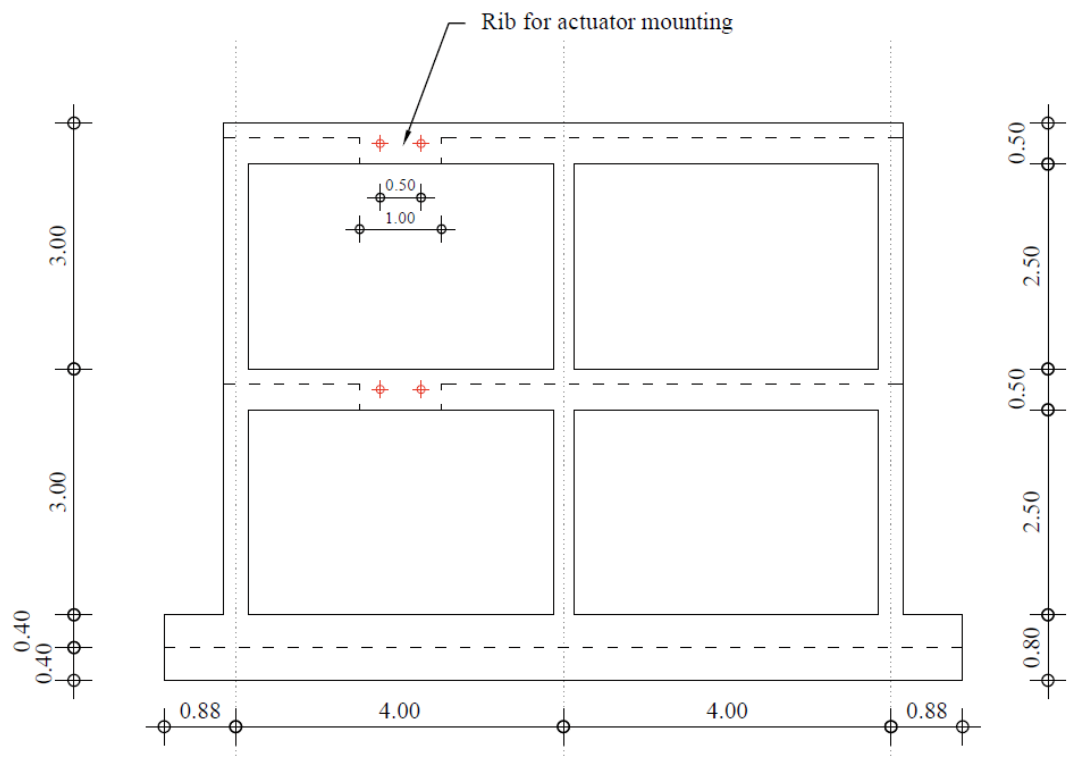
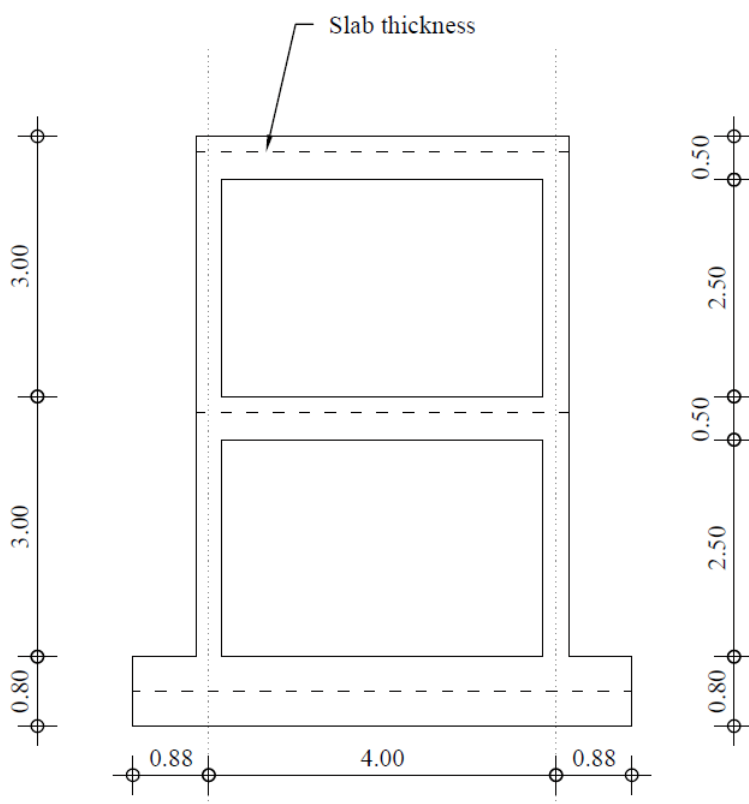


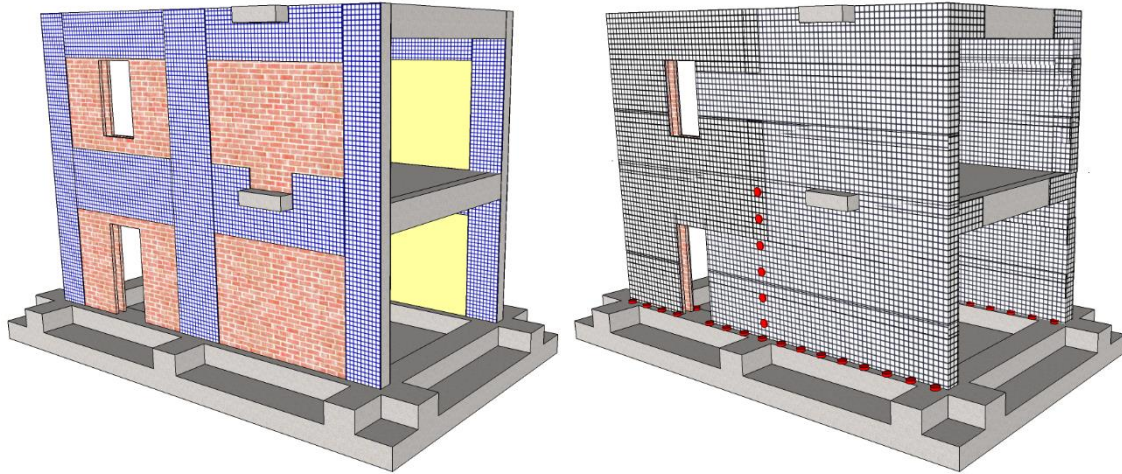
**Figure 10.** Dimensions of the physical structure for testing: side view in Y-direction.



## 5.2 Proposed iRESIST+ retrofit scheme

The proposed combined retrofit scheme in iRESIST+, which consists of TRM and thermal insulation materials, applied to the iRESIST+ prototype structure, is shown in Figure 11. The basalt textile material used for the TRM retrofitting is displayed in blue and black, while the thermal insulation is represented in yellow.

**Figure 11.** Full retrofit scheme of the iRESIST+ prototype building (thermal insulation in yellow).



## 5.3 Numerical evaluation

The effect of a seismic retrofitting using TRM was investigated numerically by means of cyclic analyses (Pohoryles and Bournas, 2020b). For this preliminary analysis, the use of Glass TRM was assumed, based on the properties of (Koutas, Bousias, and Triantafillou, 2015) due to the availability of material tests. The material properties assumed for the modelling are summarised in Table 4. Next to the mean compressive concrete strength ( $f_{cm}$ ) and the main steel reinforcement yield strength ( $f_y$ ), the brick ( $f_b$ ) and mortar ( $f_m$ ) compressive strengths are given and used to estimate the infill wall strength ( $f_{m,inf}$ ) using eq. 3.1 of Eurocode 6 (CEN, 2005). For the seismic retrofit material, the TRM is assumed to consist of a textile of polymer coated E-glass fibres with a mesh size of  $25 \times 25$  mm and a weight of  $405 \text{ g/m}^2$  embedded in a strengthening mortar. The textile elastic modulus and TRM elastic moduli in both directions of the textile are also given in Table 4.

Table 4. Material properties

$f_{cm}$	$f_y$	$f_m$	$f_b$	$f_{m,inf}$	$E_f$	$E_{t1}$	$E_{t2}$
[MPa]	35	520	12.5	11.0	3.57	73,000	520

In terms of the modelling of the RC frame, the rectangular reinforced concrete sections were modelled as inelastic fibre elements with plastic hinge lengths of 16.7% of the element. The confined concrete model by Mander et al. (Mander, Priestley, and Park, 1988) and the Menegotto-Pinto model (Menegotto and Pinto, 1973) were used for the concrete and steel reinforcement, respectively, while the masonry infills were modelled as diagonal compressive struts with the cyclic behaviour of the material defined using the nonlinear hysteresis rule proposed in (Crisafulli, 1997). To obtain the maximum sustained shear force, the maximum compressive stress carried by an area of infill defined from the equivalent

strut width,  $w$ , and the actual infill thickness,  $t$ , is calculated. The strut properties were defined using the empirical equations by (Mainstone, 1974). To account for the openings, the strut width reduction factor developed by Asteris et al. (Asteris et al., 2016) is considered. The maximum compressive stress due to corner crushing in the infills is defined by the empirical equation of Decanini et al. (Decanini and Fantin, 1986) based on the vertical infill compressive strength  $f_{m,inf}$ , the strut angle  $\theta$  and the relative panel-to-frame stiffness  $\lambda$ , as given by Eq. (6):

$$f_{m\theta} = \frac{1.12 \cdot f_{m,inf} \cdot \sin \theta \cdot \cos \theta}{K1 \cdot (\lambda \cdot H)^{-0.12} + K2 \cdot (\lambda \cdot H)^{0.88}} \quad (6)$$

Where  $H$  is the storey height and  $K1$  and  $K2$  are empirical parameters defined based on the values of  $\lambda$  (Decanini and Fantin, 1986).

For the TRM-retrofitted masonry-infilled frames, the simple strut-and-tie approach presented in Section 4.1 was used (Pohoryles and Bournas, 2020c). To implement the tie in the finite-element programme Seismostruct (Seismosoft Ltd, 2018), a simple truss element with elastic material properties up to a maximum tensile force in the diagonal tie of the infill was implemented.

The values of the modelling parameters for the strut and tie are shown in Table 5 and Table 6, respectively. For the tie, the strength is given for the application of 1, 2 and 3 layers of TRM. Note that the maximum axial strain in the strut,  $\varepsilon_m$ , is determined to be obtained at the inter-storey drift (ISD) corresponding to an extensive damage state (DS3), using the definition of damage states for infilled RC frames in (Cardone, Rossino, and Gesualdi, 2018).

Table 5. Modelling parameters for the compressive strut.

Parameter	Description	Equation	Value
$f_{m,inf}$	Compressive strength of the infill	$f_{m,inf} = 0.4 \cdot f_b^{0.65} \cdot f_m^{0.25}$ (CEN, 2005)	3.57 MPa
$f_{m,\theta}$	Compressive strength of the strut	Eq. (6) (Decanini and Fantin, 1986)	2.88 MPa
$\varepsilon_m$	Axial strain at maximum (masonry)	$\varepsilon_m = \frac{l_w}{h_w} \cdot \sin \theta \cdot ISD(DS3) \cdot H$	0.36%
$\varepsilon_u$	Ultimate axial strain (masonry)	$\varepsilon_u = 5 \cdot \varepsilon_m$	1.81%
$w$	Strut width	$w = 0.56(\lambda \cdot H)^{-0.875} \cdot d_m$ (Mainstone, 1974)	0.95 m
$w_{op}$	Strut width (opening)	$w_{op} = w(1 - 2\alpha_w^{0.54} + 2\alpha_w^{14})$ (Asteris et al., 2013)	0.38 m (window) 0.32 m (door)
$\alpha_w$	Infill wall opening percentage	$\alpha_w = \frac{A_{opening}}{h_w \cdot l_w}$	14.3% (window) 18.6% (door)
$\theta$	Strut and tie angle	$\tan^{-1} \frac{h_w}{l_w}$	34.5°

Source: (Pohoryles and Bournas, 2020b).

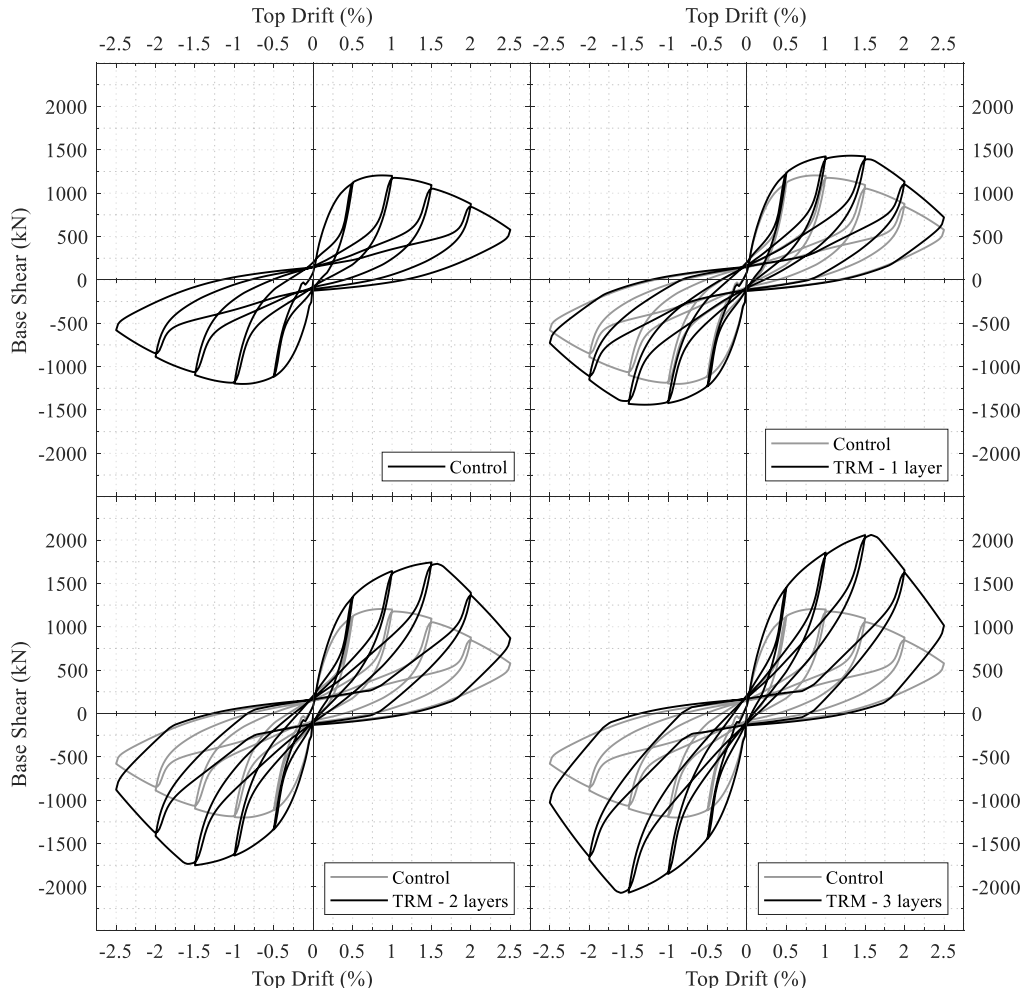
Table 6. Modelling parameters for the tensile tie.

Parameter	Description	Equation	TRM layers		
			1 layer	2 layers	3 layers
$\rho_t$	Area ratio of TRM	$\rho_t = \frac{A_t \cdot \cos\theta}{h_w \cdot l_w}$	1.05%	2.10%	3.15%
	Effective diagonal strain in TRM	$\varepsilon_{eff} = \frac{1.40 \cdot \rho_t}{\sqrt{E_f}}$ (Pohoryles and Bournas, 2020c)	0.17%	0.34%	0.50%
$F_{tie}$	Tie strength	Eq. (1) (Koutas, Triantafillou, and Bousias, 2015)	35.7 kN	142.6 kN	321.0 kN

Source: (Pohoryles and Bournas, 2020b).

The four-storey structure shown in Figure 7 was analysed under cyclic loading with a cyclic displacement protocol consisting of five cycles increasing by 0.5% top-drift up to a top-drift of 2.5%. The displacement is applied at each storey following a triangular displacement pattern. Next to the as-built control building, the use of one, two and three TRM-retrofitting layers per side was investigated. The hysteresis for the control and TRM-strengthened models are presented in Figure 12. The hysteresis curve of the control specimen is included in all curves for ease of comparison with the respective retrofit specimen. The peak base shear of 1204.9 kN for the control specimen is reached at a top drift of 0.87%.

**Figure 12.** Hysteresis curves from the cyclic analysis for the control and retrofitted buildings.



Source: (Pohoryles and Bournas, 2020b).

As shown in Table 7, in the case of the buildings retrofitted with three different TRM reinforcement ratios, an increase in base shear capacity from 19.5% for one layer of TRM up to 71.7% for the three layers can be obtained. The drift at which the peak load is reached also increases significantly between the control specimen and the retrofitted specimens. With top drifts at peak between 1.3% and 1.6% for one to three layers of TRM, respectively.

Table 7. Peak response parameters for the four specimens under cyclic loading

<b>Specimen</b>	<b>Peak Base Shear (kN)</b>	<b>Top drift at peak (%)</b>
Control	1204.9	0.87 %
TRM – 1 layer	1439.5 (+19.5%)	1.30 %
TRM – 2 layers	1750.3 (+45.3%)	1.50 %
TRM – 3 layers	2068.6 (+71.7%)	1.60 %

Through the modelling, it was demonstrated that TRM strengthening has a high effectiveness in increasing the in-plane capacity of the prototype structure. This is combined with increases in drift at the peak load, i.e. reduced damage progression for the same displacement demand. Combined with the increase in residual capacity determined in the cyclic analysis, the improvement in building safety due to the TRM retrofit is hence established.

## 6 Fragility curves of mid-rise RC buildings strengthened with TRM

In order to further generalise the results of TRM strengthening of infilled RC buildings, fragility curves for typical mid-rise RC buildings were developed. For this purpose, different levels of seismic design (Low-Code, Mid-Code and High-Code) were established based on the geometry of the iRESIST+ prototype structure.

The topic of fragility curves for the existing European building stock has been addressed in depth in (Maio and Tsionis, 2015). For retrofitted buildings, only few works assess their performance in a probabilistic framework. Such efforts include using modification factors based on experiments (e.g.: Cardone, Gesualdi, and Perrone, 2019), assuming performance levels of modern structures (Kappos and Dimitrakopoulos, 2008), or carrying out incremental dynamic analysis (e.g.: Güneyisi and Altay, 2008; O'Reilly and Sullivan, 2018; Özel and Güneyisi, 2011). Here the fragility curves were constructed by means of a series of Incremental Dynamic Analyses (IDA) (Vamvatsikos and Cornell, 2002).

### 6.1 Building design and material characteristics

The building geometry of the mid-rise masonry infilled RC buildings is the same as the prototype structure of the iRESIST+ experiment presented in Section 5.1. To account for differences in seismic design from low-code (LC), mid-code (MC) and high-code (HC), the steel reinforcement and material properties were changed to the values in Table 8. The reinforcement detailing is in line with previous works in the literature (e.g.: Kappos, Stylianidis, and Ptilakis, 1998; Masi and Vona, 2012). The masonry infill characteristics are equivalent to the double-leaf infill (2x60 mm) of the iRESIST+ structure. The opening percentage is 14.3% for the infills with windows and 18.6% for the infills with door.

Table 8. Materials and reinforcement details for the different design levels.

Design	Concrete $f_y$ [MPa]	Column reinforcement			Beam reinforcement		
		Longitudinal	$\rho_l$ (%)	Shear <sup>1</sup>	Longitudinal <sup>2</sup>	$\rho_l$ (%)	Shear <sup>1</sup>
LC	C12/15	250	4 Φ16	0.9%	Φ6 at 250 c/c	3 Φ16	0.5% Φ6 at 150 c/c
MC	C20/25	440	6 Φ16	1.4%	Φ6 at 150 c/c	3 Φ16	0.5% Φ6 at 150 c/c
HC	C25/30	520	6 Φ28	4.2%	Φ10 at 50 c/c	2 Φ14	0.2% Φ10 at 100 c/c

<sup>1</sup>The stirrups of the LC and MC were modelled with open hooks (90°), while for the HC, the hooks are closed at 135°. <sup>2</sup>Bottom layer.

The reinforcement design of the LC building, in particular, leads to a number of seismic deficiencies typical of pre-1970's reinforced concrete residential buildings in Southern Europe. These deficiencies lead to brittle failure mechanisms due to an inappropriate hierarchy of strengths with a lower flexural capacity of the columns than the beams (weak-column/strong-beam mechanism) and a lack of shear capacity and confinement in the columns with inadequate transverse reinforcement spacing.

The TRM retrofit of the LC, hence consists of confinement wrapping of the column ends, together with TRM strengthening of the infill walls. Three layers of C-TRM applied in the first two floors (confinement factor of 1.46), reduced to two layers in the third and fourth floor for the four-storey building. This is analogous to the retrofit applied by Koutas et al. (2015). Moreover, TRM U-jackets are applied in the shear-deficient beams to achieve a strength increase of 30%. Finally, the masonry-infills are strengthened with three layers of B-TRM jackets in the first two levels only. The bi-directional textiles are applied in the vertical and horizontal direction (0/90°). The materials properties of the textiles,

summarised in Table 9, were assumed from previous works for C-TRM (Koutas et al. 2015a) and B-TRM (Tetta, Koutas, and Bournas, 2018). To model the TRM retrofit of the infills, the TRM macro-model developed in (Pohoryles and Bournas, 2020a) and presented in Section 4.2, was used.

Table 9. TRM material properties used for the retrofit of the LC building.

<b>Material</b>	<b><math>t_f</math></b>	<b><math>f_{fu}</math></b>	<b><math>E_f</math></b>	<b><math>\epsilon_u</math></b>	<b>weight</b>	<b>density</b>	<b>biaxial</b>
	mm	MPa	GPa	%	g/m <sup>2</sup>	kg/dm <sup>3</sup>	
B-TRM (Tetta et al 2018)	0.037	1628.7	89	1.80%	220	2.67	yes
C-TRM (Koutas et al. 2015a)	0.193	3375	225	1.50%	348	1.8	yes

## 6.2 Seismic assessments to Eurocode 8 – Part 3

To evaluate the design levels of the existing structures (LC, MC, HC) and design the retrofit intervention, a displacement-based assessment according to Eurocode 8 – Part 3 (EC8-3) (CEN, 2006) was carried out using non-linear adaptive push-over analyses in the weak direction of the structure. The applied displacement at each storey is based on the modal characteristics and the spectral shape of the structure in order to be able to capture irregular response features (e.g. soft storey).

For the sake of consistency, the assessment of the HC building and the design of the retrofit were carried out assuming soil type C and a peak ground acceleration (pga) of 0.36g for the return period of 475 years (e.g. highest seismic zone III in Greece). The MC structure was designed to have an inadequate performance for this pga, while the LC structure was designed to not comply with the assessment for an even lower zone (pga = 0.24g, Zone II in Greece).

The performance of the buildings was evaluated at the target displacements, defined according to cl. 4.3.3.4.2.6(1) Eurocode 8 – Part 1 (EC8-1), assuming the respective design spectrum. Following the procedure in EC8-3 for the assessment of structures, the safety verifications for the limit states of Damage Limitation (for an event with 20% probability of exceedance in 50 years) and Near Collapse (2% in 50 years), were carried out. The verifications are defined in terms of the chord rotation  $\theta_E$  in the RC members, verified against the yield chord rotation  $\theta_y$  capacity for DL and against the ultimate chord rotation capacity chord rotation  $\theta_{um}$  at NC, respectively. Moreover, the shear forces  $V_E$  were checked against the design shear capacity  $V_{Rd}$  for both limit states.

The target roof displacements ( $\Delta$ ) at 0.24g and 0.36g for soil type C for the existing LC, MC and HC, as well as the TRM-retrofitted mid-rise buildings are shown in Table 10 together with the roof displacements at which the limit state criteria are reached ( $\Delta_{DL}$  and  $\Delta_{NC}$  for DL and NC, respectively) Compliance (✓) and non-compliance (✗) are indicated by checkmarks to aid the reader. Note that due to the changing eigen-properties for different structural design or different retrofit schemes, the target displacements are changing between the different buildings.

As can be seen, non-compliance is obtained for the LC and MC buildings, at the target displacements calculated for 0.24g and 0.36g, respectively. The amount of TRM retrofitting of the LC building was designed to achieve compliance with the verification checks at DL and NC for 0.36g.

Table 10. Eurocode 8 target displacements in m (and roof drifts in %) for the buildings for reference pgas of 0.24 and 0.36 g.

Building	Damage Limitation (DL)			Near Collapse (NC)		
	$\Delta_{DL}$	Target $\Delta$ (0.24g)	Target $\Delta$ (0.36g)	$\Delta_{NC}$	Target $\Delta$ (0.24g)	Target $\Delta$ (0.36g)
	(m)	(m)	(m)	(m)	(m)	(m)
LC	0.030 (0.25%)	0.029 (0.24%) ✓	0.044 (0.36%) ✗	0.032 (0.27%)	0.077 (0.64%) ✗	0.111 (0.92%) ✗
MC	0.030 (0.25%)	0.026 (0.22%) ✓	0.045 (0.38%) ✗	0.073 (0.61%)	0.072 (0.60%) ✓	0.115 (0.96%) ✗
HC	0.063 (0.53%)	0.029 (0.25%) ✓	0.049 (0.41%) ✓	0.140 (1.17%)	0.080 (0.67%) ✓	0.127 (1.06%) ✓
TRM	0.035 (0.29%)	0.019 (0.16%) ✓	0.035 (0.29%) ✓	0.136 (1.13%)	0.060 (0.50%) ✓	0.099 (0.82%) ✓

### 6.3 Incremental dynamic analysis

A set of 14 natural earthquake records from Europe, summarised in Table 11, were selected for the incremental dynamic analyses using the REXEL record selection tool (Iervolino, Galasso, and Cosenza, 2010) to match the Eurocode 8 (EC8) spectrum for ground type B. Figure 13 shows the individual record spectra, as well as their mean spectrum together with the EC8 target spectrum (soil type B) and the selected upper and lower bound limits. In accordance with Eurocode 8 – Part 1 (CEN, 2004), in the range of 0.2·T1 and 2·T1, where T1 is the natural period of the as-built LC structure obtained from analysis (0.23s), the criteria for the record selection were set with a lower bound tolerance of 10% and an upper bound tolerance of 30% for the resulting mean elastic spectrum from records with regards to the code design spectrum. The 14 records were then scaled for values of pga of 0.025-0.8g for the incremental dynamic analysis.

**Figure 13.** Target and mean spectra for the selected ground motion records, normalised by pga.

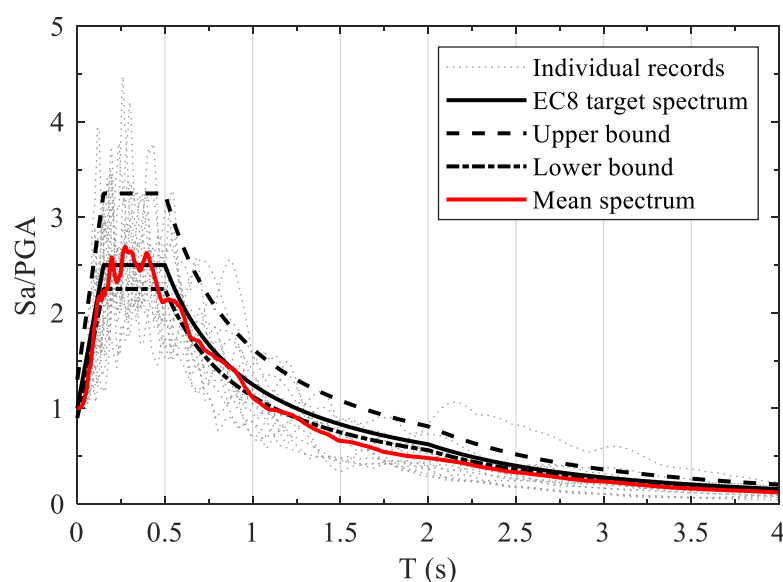


Table 11. List of selected earthquake records for the incremental dynamic analysis

<b>Event ID</b>	<b>Event Name</b>	<b>Country</b>	<b>Date</b>	<b>Station code</b>
IT-1976-0027	Friuli (2 <sup>nd</sup> shock)	Italy	15/09/1976	BUIA
ME-1979-0012	North-western Balkan	Montenegro	24/05/1979	KOTN
IT-1980-0012	Irpinia	Italy	23/11/1980	RNR
IT-1984-0004	Lazio-Abruzzo	Italy	07/05/1984	CSNO
GR-1993-0007	Kallithea	Greece	18/03/1993	PAT2
GR-1995-0047	Greece	Greece	15/06/1995	PATA
GR-1997-0019	Ionian Sea	Greece	18/11/1997	PYR1
TK-1998-0063	Turkey	Turkey	27/06/1998	0105
TK-1999-0415	Duzce	Turkey	12/11/1999	1401
IT-2009-0009	L'Aquila	Italy	06/04/2009	MMP
IT-2012-0008	Emilia (1 <sup>st</sup> shock)	Italy	20/05/2012	SRP
EMSC-20160824_0000006	Central Italy	Italy	24/08/2016	FEMA
EMSC-20161026_0000095	Central Italy	Italy	26/10/2016	NOR
EMSC-20191126_0000013	Albania	Albania	26/11/2019	TIR1

For the definition of fragility curves in this study, the four damage state limits in terms of inter-storey drift (ISD) from Cardone and Perrone (Cardone and Perrone, 2015; Cardone and Perrone, 2017) for infills with openings are used, as summarised in Table 12.

Table 12. Median inter-storey drift values for the four damage states for infilled frames with openings

<b>Damage state</b>	<b>ISD (%)</b>
DS1 - light	0.10 %
DS2 - moderate	0.30 %
DS3 - extensive	0.75 %
DS4 - partial collapse	1.75 %

Source: (Cardone and Perrone, 2015; Cardone and Perrone, 2017)

Next to the damage state definitions of the infilled frames, an adaptation of the damage states to account for the infill retrofitting is required, as experimental evidence for infills retrofitted with TRM has shown not only improvements in the shear capacity, but also changes in the damage progression, with increases in the drifts related to attainment of peak lateral load and the ultimate displacement capacity. Due to the limited number of experiments, it is not possible to define new damage states for retrofitted specimens, instead, the approach of (Cardone, Gesualdi, and Perrone, 2019) was taken. This consisted of applying a correction factor to the median ISD limits in Table 12, defined as the ratios of inter-storey drift for the attainment of the respective DS in previous experiments summarised in Table 13. Note that only specimens tested up to maximum load and specimens in which the TRM retrofit application had a fibre orientation of 0/90° with respect to the building axis (i.e. no diagonal applications) and over the full face of the infill (i.e. no strips) were selected.

Table 13. Full-face orthogonal TRM-strengthened infilled RC frame specimens tested in the literature

Study	Specimen name	Type	Inter-storey drift (%)				Ratio			
			DS1	DS2	DS3	DS4	DS1	DS2	DS3	DS4
Koutas et al. 2015a	Specimen #1	C	0.19%	0.60%	1.81%	2.50%				
	Specimen #2	R	0.22%	1.00%	2.43%	3.00%	1.16	1.67	1.34	1.20
Selim et al. 2015	C2	C		0.5%	1.0%	2.00%				
	SRG-2-2-A	R	0.30%	1.00%	2.50%	3.50%		2.00	2.50	1.75
Sagar et al 2019	CS	C	0.80%	1.05%	1.83%	0.80%				
	DAO-90	R	0.80%	1.51%	2.64%	0.80%		1.00	1.44	1.44
	SAO-90	R	1.00%	1.53%	2.68%	1.00%		1.25	1.46	1.46
Average							1.16	1.46	1.45	1.45

For type: C = Control, R = Retrofit; For geometry: H and W are height and width of the infill wall, respectively. Note, the physical DS definition from Cardone and Perrone (Cardone and Perrone, 2015; Cardone and Perrone, 2017) was followed for consistency.

#### 6.4 Fragility functions

The fragility curves for the existing and retrofitted buildings were constructed at each damage state DS<sub>i</sub> based on the common assumption of a lognormal cumulative distribution function (e.g.: Kappos and Panagopoulos, 2010). The fragility curves for the mid-rise RC buildings (MR) in terms of peak ground acceleration (pga) are displayed in Figure 14. The parameters of the obtained fragility curves are summarised in Table 14, providing the mean value ( $\theta_i$ ) of the intensity measure at which the building reaches the inter-storey drift threshold of damage state DS<sub>i</sub> (see Table 12) and the standard deviation ( $\beta_i$ ) of the natural logarithm of the intensity measure for damage state DS<sub>i</sub>. These two quantities were derived using the algorithm developed by Baker (Baker, 2015), which is based on the method of maximum likelihood fitting.

As can be observed, the attainment of all damage states, is moved to higher values of pga with increasing level of seismic design. While the differences between LC and MC are only modest, the HC structure presents the strongest shift to higher pga values, with the mean pga at collapse increased by over 50%. Similarly, the retrofit achieves a significant improvement of the seismic fragility of the LC structure, coming close to the performance of the HC structure.

It is important to note however that the results are relevant in terms of economic losses based on damage state definitions focussed on the infills and their interaction with the surrounding frame. For the high design code structure, results are to be seen as indicative, as in modern buildings, infills can be designed not to interfere with the frame. This will have an important impact on the life safety and structural collapse, which is only delayed in the retrofitted structure.

**Figure 14.** Fragility curves for the different mid-rise RC buildings: (a) Low Code; (b) Mid Code; (c) High Code; (d) TRM-Retrofit.

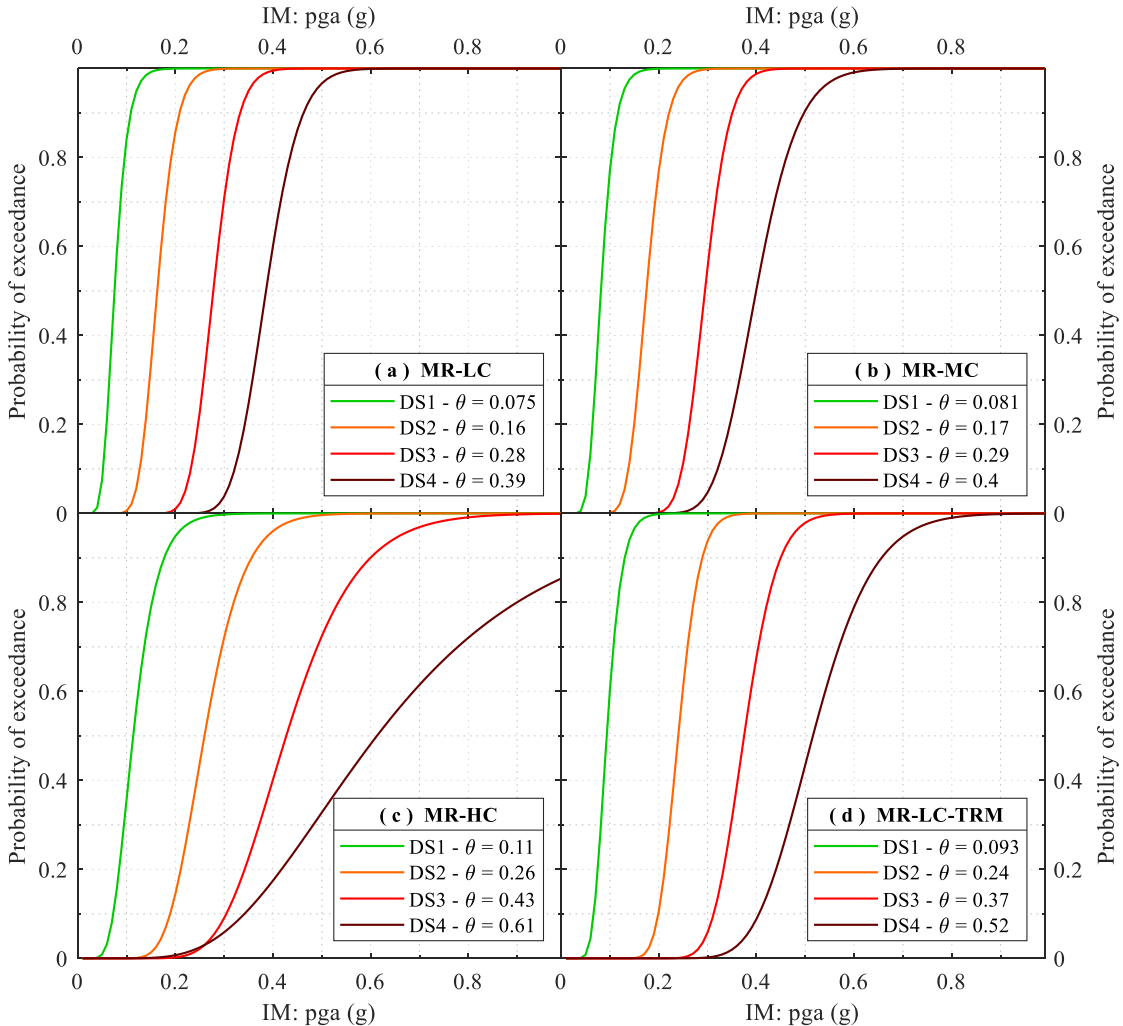


Table 14. Mean pga (standard deviation) for the fragility curves of the as-built and retrofitted buildings

<b>Damage state</b>		<b>LC</b>	<b>MC</b>	<b>HC</b>	<b>TRM retrofit</b>
Light	DS1	0.075 (0.28)	0.081 (0.28)	0.114 (0.35)	0.093 (0.26)
Moderate	DS2	0.163 (0.19)	0.175 (0.18)	0.260 (0.25)	0.240 (0.15)
Extensive	DS3	0.278 (0.14)	0.295 (0.14)	0.427 (0.26)	0.375 (0.14)
Near Collapse/collapse	DS4	0.386 (0.14)	0.399 (0.17)	0.613 (0.46)	0.516 (0.19)

## 6.5 Seismic loss assessment

To compare the performance of the retrofitted mid-rise LC building with the three existing building buildings, the expected annual loss due to seismic events ( $EAL_s$ ) are evaluated using the PEER performance based earthquake engineering (PBEE) methodology was used (Porter, 2003). To do so, the vulnerability of the structures were first obtained by the combination of the respective fragility curve with the damage-to-loss function for infilled RC buildings from (Kappos et al., 2006), shown in Table 15.

Table 15. Damage-to-loss function for infilled RC buildings.

DS	Loss (%)
DS1	0.5%
DS2	5.0%
DS3	20.0%
DS4	45.0%
DS5	80.0%

Source: (Kappos et al., 2006)

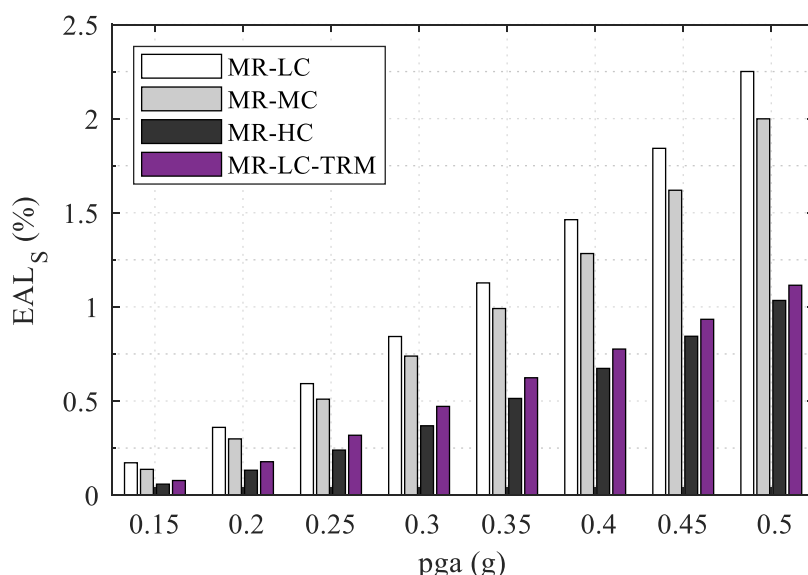
Different hazard curves are then defined based on Eurocode 8 – Part 1 (CEN, 2004), in which the annual rate of exceedance  $H(a_{gR})$  of a reference pga ( $a_{gR}$ ) can be assumed to vary with  $a_{gR}$  according to Eq. (7):

$$H(a_{gR}) \cong k_0 \cdot a_{gR}^{-k} \quad (7)$$

Where  $k$  is typically taken as 3 and  $k_0$  is computed by evaluating the annual rate of exceedance is the ratio,  $r^*/50$ , where  $r^* = r(1+0.5r)$  and  $r$  is the probability of exceedance in 50 years (USGS, 2020). This can be calculated for a reference pga with a probability of exceedance of 10% in 50 years.

By combining the hazard curve with the vulnerability curve, the annual probability of exceedance of loss (in % of building value) is calculated. Finally, the expected annual seismic loss ( $EAL_S$ ) is the integral of this curve. The results of this procedure repeated for an increasing level of seismic hazard (in terms of pga with a probability of exceedance of 10% in 50 years) is shown in Figure 15. It can be observed that the seismic losses for the mid-rise low-code and medium-code buildings are similar, with the LC building presenting about 10% higher losses. The high-code structure presents the lowest losses; however, the retrofitted building achieves a very similar performance throughout. Most crucially, the retrofitted and HC structure present expected annual losses about half of those observed for the LC structure.

**Figure 15.** EALs (%) for the as-built and TRM-retrofitted mid-rise RC buildings for different levels of seismic hazards.



## 7 Analysis of combined seismic and energy retrofitting for twenty case study locations

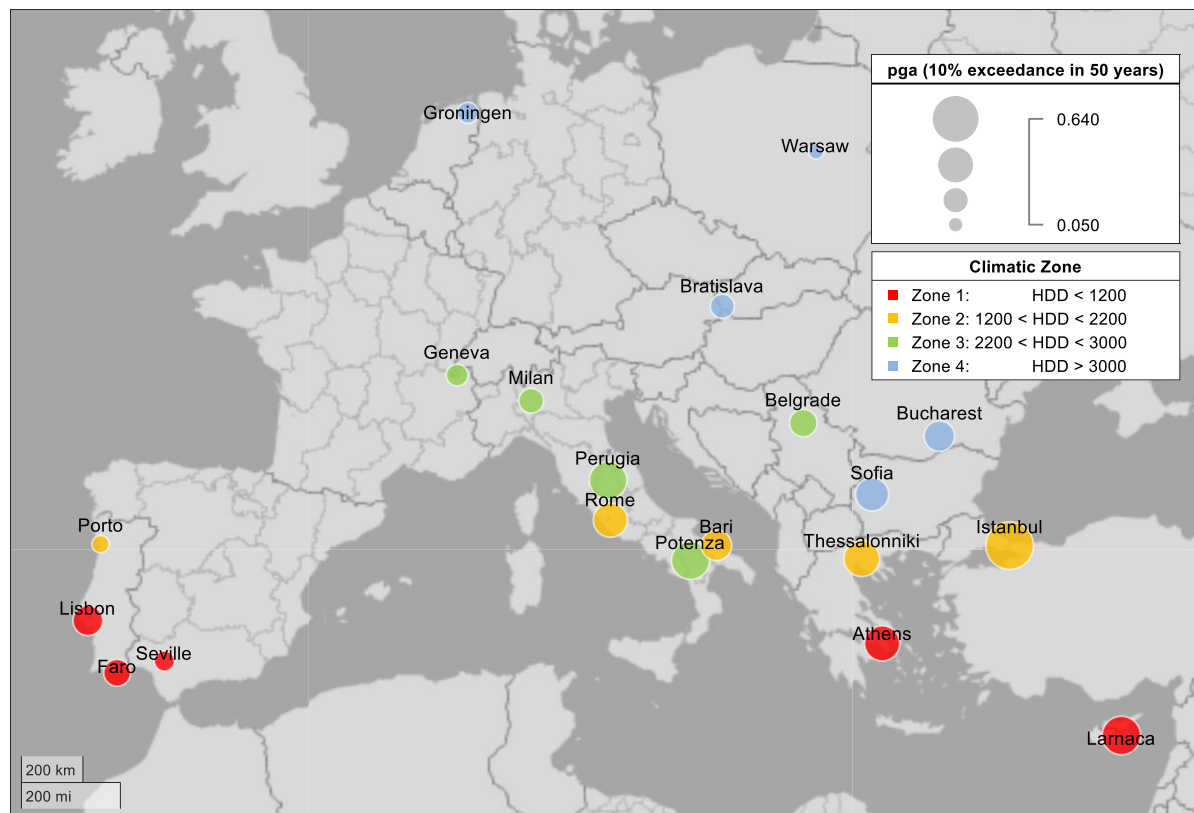
The current European building stock is ageing and requires significant renovation efforts to improve its energy performance and ensure structural safety. Renovation is needed to reduce the impact of the existing building stock on the environment, with buildings currently being responsible for a large CO<sub>2</sub> emission share in the EU (36%) and heating and cooling accounting for 50% of the EU final energy consumption (Heat Roadmap Europe, 2017; European Parliament and Council of the European Union, 2018).

As emphasised in Section 2, the ambitious plans of the European Green Deal, emphasise the need for the EU and its Member States to engage in a ‘renovation wave’ of public and private buildings (European Commission, 2019). Until recently, the renovation of existing buildings was focusing either on solving structural safety problems or on increasing the energy performance.

### 7.1 Case study locations

To assess whether energy efficiency and disaster-resilient practices could be integrated, a common approach for building performance assessment was proposed (Pohoryles et al., 2020). This approach was investigated by numerical modelling of the energy and seismic performance of different EU building typologies. Initially, 20 case study locations across Europe have been selected, as shown in Figure 16, to be representative of a range of seismic hazard levels and climatic conditions.

**Figure 16.** Map of case study locations categorised by seismic risk and climatic conditions.



The case study cities were grouped in four different climatic and five seismic zones as where the zonation is defined in Table 16.

Table 16. Definitions of seismic and climatic zones.

<b>Zone</b>	<b>Seismic</b>	<b>Climatic</b>
1	$\text{pga} < 0.125$	$\text{HDD} \leq 1200$
2	$0.125 \leq \text{pga} < 0.2$	$1200 < \text{HDD} \leq 2200$
3	$0.2 \leq \text{pga} < 0.3$	$2200 < \text{HDD} \leq 3000$
4	$0.3 \leq \text{pga} < 0.4$	$3000 < \text{HDD} \leq 4000$
5	$\text{pga} \geq 0.4$	/

Seismic hazard was defined in terms of peak ground acceleration (pga) for a return period of 475 years obtained from the GEM seismic hazard map (Pagani et al., 2018), while climatic conditions are based on heating degree days (HDD), calculated using the ASHRAE method (American Society of Heating, 2013) for the local weather files (U.S. Department of Energy, 2019). The values of HDD and pga for the 20 cities are shown in Table 17.

Table 17. HDD and pga values for the case study locations

<b>Location</b>	<b>HDD</b>	<b>Climatic zone</b>	<b>pga (g)</b>	<b>Seismic zone</b>
Faro	769.9	1	0.19	2
Larnaca	758.9	1	0.41	5
Lisbon	1086.7	1	0.24	3
Seville	916.0	1	0.10	1
Athens	1111.9	1	0.34	4
Porto	1491.3	2	0.07	1
Rome	1513.9	2	0.32	4
Bari	1414.5	2	0.25	3
Thessaloniki	1740.9	2	0.35	4
Istanbul	1885.8	2	0.64	5
Perugia	2235.0	3	0.39	4
Milan	2639.4	3	0.16	2
Potenza	2689.5	3	0.40	5
Belgrade	2795.3	3	0.20	3
Geneva	2964.5	3	0.12	1
Bucharest	3030.3	4	0.25	3
Sofia	3073.4	4	0.30	4
Bratislava	3036.8	4	0.15	2
Groningen <sup>1</sup>	3279.1	4	0.10	1
Warsaw	3615.8	4	0.05	1

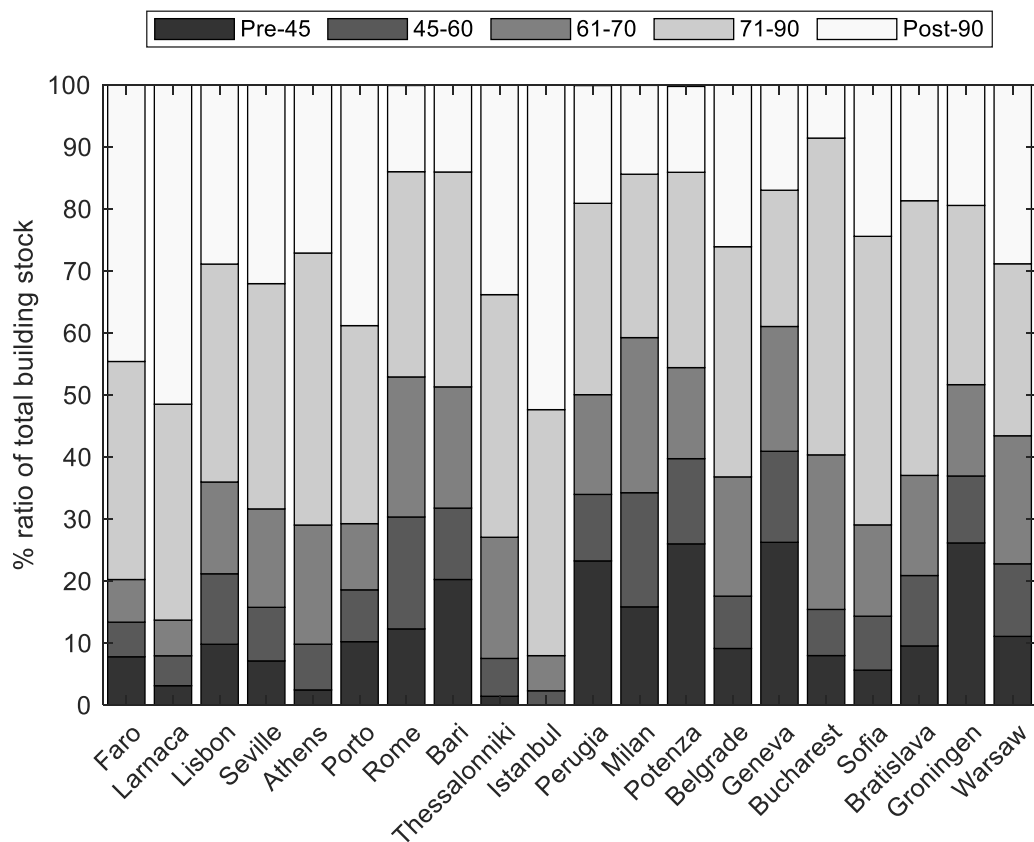
<sup>1</sup>Earthquakes induced by gas extraction in Groningen area were also considered by assigning a PGA value of 0.1 g (Dost, Ruigrok, and Spetzler, 2017)

## 7.2 Building stock

The assessment of the benefits of combined energy and seismic retrofitting was conducted at the building stock level, including a variety of EU residential building typologies. Representative existing buildings from five construction periods were selected and representative building typologies were defined. The construction period, the main structural system or material (e.g. RC or masonry) and the geometric dimensions (e.g. number of storeys) are key parameters for both the energy and the seismic performance of buildings. In terms of energy performance, the U-values of envelope elements varies with age (ECOFYS, 2007). For the seismic design of structures, typically a distinction of no-code, pre-code and modern-code is made, which again classifies the buildings into different age groups (e.g.: Kappos and Panagopoulos, 2010).

Data on the building stock for each case study location is obtained by two main sources. On the one hand the number of dwellings or average useful floor space constructed by decade is obtained from the respective Census data of 2011 (EUROSTAT, 2011; Statistical Office of the Republic of Serbia of Serbia, 2011; Turkish Statistical Institute (TurkStat), 2011). The building age from the Census data is shown Figure 17 for each case study location. It can be seen that some cities have a building stock dominated by more modern construction (e.g. Istanbul or Thessaloniki), while other cities, in particular Italian ones (e.g. Perugia, Potenza, but also Groningen or Geneva) have a large proportion between 20-30% of pre-1945 structures, classified as low and mid-rise masonry buildings.

**Figure 17.** Proportion of built floor area by period of construction in the selected locations.



Source: (Pohoryles et al., 2020) (CC BY 4.0); based on data from: (EUROSTAT, 2011; Statistical Office of the Republic of Serbia of Serbia, 2011; Turkish Statistical Institute (TurkStat), 2011)

On the other hand the proportion of construction type is taken from the NERA project (Ozcebe et al., 2014), from which data on building height was aggregated and allowed for a discretization of buildings into low to high-rise infilled RC buildings and low to mid-rise masonry buildings, respectively. As shown in Table 18, for the masonry buildings, low-rise and mid-rise buildings with stone and clay brick masonry as materials were defined in collaboration with the SPEctRUM project (Kouris et al., 2021). In the case of the RC buildings low (two storeys), mid (four storeys) and high-rise (eight storeys) structures were defined. The floor area of 8 x 18 m is chosen to be globally representative, as the selected buildings are theoretical in nature and their geometrical characteristics represent somewhat of an average of the building stock, similar to other large-scale studies on the building stock (e.g.: Stein, Loga, and Diefenbach, 2016; TABULA, 2012; Loga, Stein, and Diefenbach, 2016). Note that an opening percentage of 15% of wall area per storey is assumed. This corresponds to a 1.2 x 2.1 m door or two 0.9 x 1.45 m windows for two bays. Typical traditional masonry buildings do not have a constant storey-height along their height and respectively the size of openings decreases. Lower storeys tend to have a higher inter-storey height than typical RC structures. An average height of 4 m for the ground floor is assumed here and a window dimensions equal to 1.0 x 1.90 m, resulting in glazing 18.3% for low-rise and mid-rise masonry buildings.

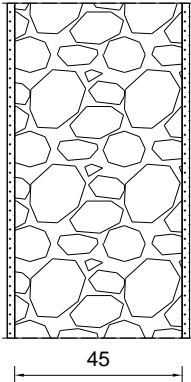
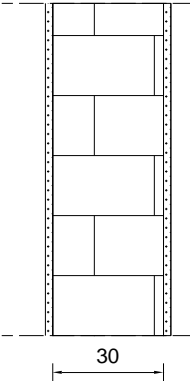
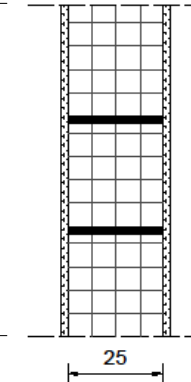
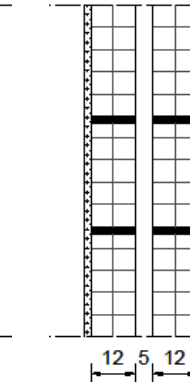
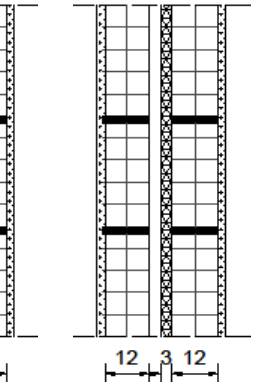
Table 18. Parameters of the case study buildings

<b>Structural material</b>	<b>Masonry</b>		<b>Reinforced Concrete</b>		
	Low-Rise stone or brick	Mid-Rise brick	Low-Rise	Mid-Rise	High-Rise
<b>Sketch</b>					
<b>Plan</b>	8m x 18m	8m x 18m	8m x 18m	8m x 18m	8m x 18m
<b>Tot. floor area</b>	m <sup>2</sup>	288	576	288	576
<b>No. of storeys</b>		2	4	2	4
<b>Storey height</b>	m	4 (first) / 3.30	4 (first) / 3.10	3	3
<b>Total height</b>	m	9.60	15.90	6	12
<b>Windows</b>	m <sup>2</sup>	66.10	124.20	40.60	86.42
<b>Exterior doors</b>	m <sup>2</sup>	5.80	11.60	5.04	5.04
<b>Glazing</b>	%	18.30	18.30	15	15

Source: (Pohoryles et al., 2020).

Among the building envelope components, the walls and windows typically represent the major share of the overall energy loss (Asdrubali, Baldassarri, and Fthenakis, 2013), so this study focused on these elements. Considering the extensive variations over the years and from country to country, five different typical external wall types were selected representing the different time periods, as illustrated in Table 19. A key parameter in terms of assessing the thermal performance of buildings is the thermal transmittance of its envelope elements (U-value in W/m<sup>2</sup>/K).

Table 19. Envelope characteristics for the different time periods

Period	Pre-1945	1945 -1959	1960-1969	1970 – 1989	Post-1989
Material	Stone or brick masonry	solid clay brick masonry	hollow clay brick masonry	hollow clay brick masonry	hollow clay brick masonry with thermal insulation
Detail	Multi-leaf wall	Multi-leaf wall	Single leaf wall	Cavity wall	Cavity wall
Sketch					
U (W/m <sup>2</sup> K)	1.30 - 2.25	1.77	0.97	0.79	0.35 – 0.75
EU-range	0.9 - 2.5	0.9 - 2.4	0.5 - 2.1	0.4 - 1.6	0.23 – 0.85

Source: (Pohoryles et al., 2020).

### 7.3 Retrofit targets

The iRESIST+ retrofit scheme combining thermal insulation and TRM for the building envelope is applied to reach the energy and structural performance targets after retrofitting. Targets for energy and seismic retrofitting were determined for the four characteristic climatic zones and five seismic zones, respectively.

#### 7.3.1 Energy retrofit target

To achieve an adequate energy performance in existing buildings, thermal insulation can be seen as the easiest and most cost-effective solution (ECOFYS, 2007). While energy renovation encompasses a variety of interventions (Filippín et al., 2017; Ma et al., 2012), including changes in HVAC system, adding renewable energy sources or shading devices, in this study, the renovation targets are defined in terms of the U-value of the envelope elements in order to reduce transmission heat losses.

National energy performance legislations typically recommend U-values for different envelope elements (exterior walls, windows, roofs) to be achieved by new-built or renovated structures. These values were collected in Table 20 for all case study locations and used to define U-value targets for the combined retrofit solution. In countries where U-value requirements for retrofitting of existing buildings are not available, the requirements for new built structures were taken, as illustrated in the last column of Table 20. As can be seen, in order to homogenize the energy performance of buildings placed in locations grouped in the same zone, a retrofit U-value target per zone for each envelope element was defined based on the values of the individual locations in the same zone.

Table 20. U-values target in each case-study location.

Zone	City	U-values [W/m <sup>2</sup> K]						New built / existing*	
		Walls		Roof		Floor on ground			
1	Larnaca	0.85	0.75	0.75	0.61	0.75	0.68	3.80	N+R N N N+R N
	Lisbon	0.80		0.70		0.70		2.80	
	Athens	0.50		0.45		0.45		3.00	
	Seville	0.82		0.45		0.82		3.10	
	Faro	0.80		0.70		0.70		2.80	
2	Bari	0.40	0.50	0.38	0.42	0.42	0.46	2.60	N N N N N+R
	Porto	0.70		0.60		0.50		2.40	
	Rome	0.36		0.32		0.36		2.40	
	Thessaloniki	0.45		0.40		0.40		2.80	
	Istanbul	0.60		0.40		0.60		2.40	
3	Perugia	0.34	0.40	0.30	0.33	0.33	0.39	2.20	N N N N+R -
	Milan	0.34		0.30		0.33		2.20	
	Potenza	0.36		0.32		0.36		2.40	
	Belgrade	0.40		0.40		0.40		1.50	
	Geneva	N/A		N/A		N/A		N/A	
4	Bucharest	0.56	0.35	0.20	0.22	0.22	0.30	1.30	N N+R N N N+R
	Groningen	0.20		0.20		0.29		1.65	
	Sofia	0.35		0.28		0.40		1.70	
	Bratislava	0.32		0.20		0.40		1.40	
	Warsaw	0.23		0.20		0.25		1.10	

Source: (Pohoryles et al., 2020); \*N - requirements for new buildings; N+R – same requirements for both new and retrofitted buildings.

In addition to changes in the U-value of exterior walls, the windows were improved by means of airtight frames and glass with low solar heat gain coefficient (SHGC) of 0.55. Replacing the existing windows has substantial effects on decreasing the infiltration heat losses by increasing the overall airtightness of the building. Therefore, the number of air changes was decreased from 1.0 to 0.60 h<sup>-1</sup> corresponding to moderate shielded buildings with medium airtightness (ISO, 2006).

### 7.3.2 Seismic retrofit target

In terms of the seismic retrofit component, the buildings selected in this study are grouped according to their ages and can hence be related to a certain level of seismic design of their time of construction. For the older unreinforced masonry (URM) and RC structures, (i) no seismic design is considered, an assumption valid for across all European cities. For the 1960-69 and 1970-89 structures, (ii) low and (iii) medium levels of seismic design code are assumed, respectively. For modern structures the assumption of a (iv) high-level of seismic design is taken. As a large and inhomogeneous building stock across multiple locations is hence addressed in this study, it is not possible to design a specific retrofit for reducing the vulnerability of all the different structures. Instead, a target performance to be achieved by the retrofitted structures is defined.

In the fragility assessment of mid-rise infilled RC buildings carried out in Section 6, it was shown that the proposed TRM-retrofit of a low-code structure ensured a behaviour comparable to a high-code building, corresponding to an improvement of two seismic design categories. Based on this, the assumption is made that this improvement can also be achieved for the other building typologies. The assumed performance improvement for all building typologies is summarised in Table 21. Therefore, RC buildings with no-seismic

design achieved a medium level of seismic design after retrofit (from (i) to (iii) and from (ii) to (iv), etc.). For the URM buildings the performance achieved after the TRM-retrofitting is assumed to be that of low (for stone walls) or medium-code (for brick walls) reinforced masonry (RBM) structures.

Table 21. Target seismic design level of the seismic retrofit scheme.

<b>Age</b>	<b>Pre-1945</b>	<b>Pre-1945</b>	<b>1945 - 1959</b>	<b>1960-1969</b>	<b>1970-1989</b>	<b>Post-1989</b>
<b>Material</b>	Stone	Brick	RC	RC	RC	RC
<b>Seismic design level</b>	URM (stone)	URM (brick)	No code	Low	Medium	High
<b>Target design level</b>	RBM (low)	RBM (medium)	Medium	High	High	N/A

## 7.4 Modelling

In order to model the energy performance and the seismic performance of the considered buildings, Building Energy Modelling (BEM) and seismic fragility analysis were carried out, respectively, for the twenty different cities. The modelling approaches are briefly described in the following sub-sections.

### 7.4.1 Building energy modelling

The buildings' energy demand and seismic safety before and after retrofitting are assessed for the different climatic and seismic scenarios. The energy performance of the case-study buildings was assessed by means of dynamic energy simulations in EnergyPlus (U.S. Department of Energy, 2018), namely by calculating the energy demand for space heating (HED) and cooling (CED) per conditioned floor area ( $\text{kWh}/\text{m}^2$ ) across the different locations. The details on the modelling assumptions, material parameters and occupancy schedule can be found in (Pohoryles et al., 2020).

The primary energy use and associated equivalent- $\text{CO}_2$  emissions were then calculated from heating and cooling demands using the respective total primary energy factors ( $f_{P_{tot}}$ ) and factors for equivalent operational  $\text{CO}_2$  emissions ( $k_{\text{CO}_2e}$  in  $\text{g}/\text{kWh}$ ). These are obtained by multiplying the factors for different energy sources from ISO 52000-1 (ISO, 2017) with the energy mix of the relevant countries from the 2015 residential profiles (Heat Roadmap Europe, 2017), which are shown in Table 22. Note that, for the future scenarios up to 2030 changes in energy mix are assumed to follow the scenario described in (European Commission, 2017).

Finally, the energy costs are evaluated by considering the energy prices from EUROSTAT (EUROSTAT, 2019b; EUROSTAT, 2019a) in Table 22. Using the building costs per  $\text{m}^2$  evaluated from (Numbeo, 2019), the estimated annual losses ( $EAL_E$ ) can be determined:

$$EAL_E = \frac{\text{annual heating + cooling cost}}{\text{total building value}} [\%] \quad (8)$$

The annual energy savings due to retrofitting are then expressed as the difference in  $EAL_E$  before and after retrofitting, again as a percentage of the total building value. Note that the building value would potentially increase as a consequence of retrofitting. As this is difficult to precisely quantify, it is conservatively ignored from the analysis.

Table 22. Data for energy factors and costs for each location

Location	$f_{Ptot}^*$	$k_{CO2e}^*$	2020	2020	2030	2030	Heat.	Cooling	Cost	Building
			$f_{Ptot}^1$	$k_{CO2e}^1$	$f_{Ptot}^1$	$k_{CO2e}^1$	cost <sup>2</sup>	cost <sup>2</sup>	index <sup>3</sup>	value <sup>4</sup>
		g/kWh		g/kWh		g/kWh	€/kWh	€/kWh		€/m <sup>2</sup>
Faro	1.45	212.0	1.41	191.9	1.41	175.4	0.0784	0.2293	50.33	1650.0
Larnaca	1.28	205.4	1.24	185.3	1.23	168.8	0.0784	0.2183	60.29	1050.0
Lisbon	1.45	212.0	1.41	191.9	1.41	175.4	0.0784	0.2293	50.33	2290.3
Seville	1.30	219.2	1.26	199.1	1.26	182.6	0.0875	0.2477	70.52	1366.6
Athens	1.43	239.2	1.39	219.1	1.39	202.6	0.0654	0.1646	63.46	1674.9
Porto	1.45	212.0	1.41	191.9	1.41	175.4	0.0784	0.2293	50.33	1493.5
Rome	1.27	205.2	1.23	185.1	1.23	168.6	0.0951	0.2161	93.63	2958.7
Bari	1.27	205.2	1.23	185.1	1.23	168.6	0.0951	0.2161	93.63	2180.0
Thessalon.	1.43	239.2	1.39	219.1	1.39	202.6	0.0654	0.1646	63.46	1262.0
Istanbul	1.43	239.2	1.39	219.1	1.39	202.6	0.0209	0.0857	68.00	691.1
Perugia	1.27	205.2	1.23	185.1	1.23	168.6	0.0951	0.2161	93.63	1246.0
Milan	1.27	205.2	1.23	185.1	1.23	168.6	0.0951	0.2161	93.63	3407.8
Potenza	1.27	205.2	1.23	185.1	1.23	168.6	0.0951	0.2161	93.63	1246.0
Belgrade	1.49	200.0	1.45	179.9	1.45	163.4	0.0342	0.0709	38.00	1291.9
Geneva	1.33	202.1	1.29	182.0	1.29	165.5	0.0951	0.2477	137.42	8426.9
Bucharest	1.19	141.2	1.15	121.0	1.14	104.5	0.0354	0.1317	46.40	1081.6
Sofia	1.49	200.0	1.45	179.9	1.45	163.4	0.0437	0.1005	48.69	981.7
Bratislava	1.36	257.4	1.32	237.3	1.32	220.8	0.0459	0.1462	51.68	2135.4
Groningen	1.19	220.2	1.15	200.0	1.14	183.5	0.0861	0.1707	82.00	2400.0
Warsaw	1.24	265.7	1.20	245.5	1.20	229.0	0.0450	0.1396	65.61	2010.6

Source: <sup>(1)</sup>ISO, 2017; <sup>(2)</sup> Heat Roadmap Europe, 2017; <sup>(3)</sup> EUROSTAT, 2019; <sup>(4)</sup> European Construction Costs, n.d.; <sup>(5)</sup> Numbeo, 2019).

Note: \*The cooling primary energy factor,  $f_{Ptot}$ , is 2.5 and the associated factor for equivalent operational CO<sub>2</sub> emissions ( $k_{CO2e}$  in g/kWh) proposed in ISO 52000-1 is 420 g/kWh.

#### 7.4.2 Seismic loss assessment

On the other hand, to determine seismic losses before and after retrofitting, i.e. the expected annual loss due to seismic events ( $EAL_s$ ), the PEER performance based earthquake engineering (PBEE) methodology was used (Porter, 2003). Rather than using a deterministic approach with specific mechanical characteristics of the building materials, a probabilistic approach is taken, i.e. in order to consider the typical spread of material characteristics for the different construction periods. The procedure used to define the  $EAL_s$  can be summarised as follows:

1. Fragility functions are used to determine the probability of reaching a certain level of damage (or damage state, DS) for a certain level of earthquake intensity, presented in terms of PGA to be compatible with the intensity of seismic hazard at each location
2. The damage levels are then associated with monetary loss as a fraction of the existing building value, by means of a damage-to-loss function specific for masonry and RC structures.
3. The fragility curves and damage-to-loss functions are then combined to give the vulnerability curve of the specific building type, i.e. the monetary loss (as a percentage of the building value) as a function of the selected intensity measure (PGA).
4. The hazard curve, i.e. the annual probability of exceedance (PE) of the seismic intensity, is then calculated using Eq. (7) as described in Section 6.5 for the seismic hazard at each location, defined in terms of the pga with a return period of 475 years from the GEM seismic hazard map (Pagani et al., 2018).
5. By combining the hazard curve (step 4) with the vulnerability curve (step 3), the annual probability of exceedance of loss (in % of building value) is calculated.
6. Finally, the expected annual seismic loss ( $EAL_s$ ) is the integral of the curve obtained in step 5.

For step 1, well documented fragility functions for different damage states ranging from 'no damage' to 'collapse' for the chosen infilled RC buildings (Kappos et al., 2003; Kappos et al., 2006; Kappos and Panagopoulos, 2010), as well as stone masonry (Ahmad, Crowley, and Pinho, 2010) and brick masonry (FEMA, 2003) buildings were selected. The age of the buildings was associated with the respective seismic design level of the construction period as: (pre-1959) no design, (1960-1969) low, (1970-1989) medium and (Post-1990) high level of seismic design. The vulnerability of the seismically retrofitted structures with TRM is defined according to the targeted performance, as defined in Table 21. The parameters to construct the fragility curves for the non-retrofitted and retrofitted buildings are shown in Table 23 and Table 24 for masonry and RC, respectively, together with the source of the parameters and the label of the building type from the source. The mean value  $\mu$  of the lognormal distribution functions are given per damage state (DS). Note that in accordance to the selected fragility curves for masonry from FEMA (2003), a constant standard deviation  $\sigma$  of 0.64 is applied to all building types. For the RC buildings, Kappos and Panagopoulos (2010) also suggest the use of a constant value (estimated between 0.6 and 0.7), hence 0.64 is also taken for RC buildings for consistency.

Table 23. Mean value  $\mu$  of the lognormal distribution functions per damage state (DS) of the fragility of masonry buildings (in terms of PGA).

<b>Description</b>	<b>Non-retrofitted</b>			<b>Retrofitted/reinforced</b>		
	Stone	Brick Low-rise	Brick Mid-rise	Stone	Brick Low-rise	Brick Mid-rise
<b>Source<sup>1</sup></b>	Ahmad	FEMA	FEMA	FEMA	FEMA	FEMA
<b>Label</b>	MUR/ST99 – 2 storeys	URML - pre code	URMM - pre code	RM1L - Low code	RM1L - Moderate code	RM1M - Moderate code
<b>DS1-Slight</b>	0.085	0.130	0.090	0.160	0.220	0.180
<b>DS2-Moderate</b>	0.107	0.170	0.130	0.200	0.300	0.260
<b>DS3-Extensive</b>	0.152	0.260	0.210	0.290	0.500	0.510
<b>DS4-Collapse</b>	0.179	0.370	0.380	0.540	0.850	1.030

<sup>1</sup>Ahmad = Ahmad et al., 2010; FEMA = FEMA, 2003.

Table 24. Mean value  $\mu$  of the lognormal distribution functions per damage state (DS) of the fragility of infilled RC buildings (in terms of PGA).

1945 -1959: no seismic design			1960-1969: low seismic design			1970-1989: medium seismic design			Post-1989: high seismic design			
DS	Low-rise	Mid-rise	High-rise	Low-rise	Mid-rise	High-rise	Low-rise	Mid-rise	High-rise	Low-rise	Mid-rise	High-rise
<b>Label</b>	C3.1LL	C3.1ML	C3.1HL	CR/LFINF LowRise LowCode	CR/LFINF MidRise LowCode	CR/LFINF HighRise LowCode	C3.1LM	C3.1MM	C3.1HM	CR/LFINF LowRise LowCode	CR/LFINF MidRise LowCode	CR/LFINF HighRise LowCode
<b>DS1</b>	0.021	0.005	0.013	0.119	0.034	0.078	0.090	0.008	0.017	0.146	0.120	0.114
<b>DS2</b>	0.101	0.055	0.097	0.241	0.181	0.230	0.123	0.078	0.109	0.359	0.248	0.319
<b>DS3</b>	0.201	0.190	0.210	0.300	0.251	0.309	0.298	0.201	0.419	0.923	0.484	0.978
<b>DS4</b>	0.257	0.216	0.296	0.393	0.290	0.439	0.730	0.422	0.923	2.137	1.041	1.884
<b>DS5</b>	0.343	0.254	0.548	0.540	0.346	1.505	1.391	0.853	3.471	2.793	2.066	5.504

Source: the values in this table are taken from the Openquake platform (<https://platform.openquake.org/vulnerability>), which digitized the curves, therefore their values may be different to those present in the original publications (Kappos et al., 2003; Kappos et al., 2006; Kappos and Panagopoulos, 2010).

For step 2, the values for the damage-to-loss functions from (Kappos et al., 2006) are shown in Table 25. Note that the four damage states are used for masonry buildings, while five exist for the RC buildings according to the selected fragility curves. The loss curves are evaluated based on the cost of repair for the specific damage states and are always less than or equal to the replacement cost, i.e. the value of the building. Other losses that can be associated with earthquakes, such as human losses and the social impact are however not considered, as the scope of this study focuses only on buildings and the assumption of repair costs alone renders more conservative results.

Table 25. Values for the damage-to-loss functions for masonry and RC buildings.

<b>DS</b>	<b>Loss (fraction of building value)</b>	
	Masonry	Infilled RC
<b>DS1</b>	0.020	0.005
<b>DS2</b>	0.120	0.050
<b>DS3</b>	0.350	0.200
<b>DS4</b>	0.750	0.450
<b>DS5</b>	/	0.800

Source: (Kappos et al., 2006)

The procedure for calculating  $EAL_s$  is repeated for all building typologies (i.e. material, age and building height) before and after retrofitting and for each location (i.e. for the individual seismic hazard of the site).

#### 7.4.3 Combined losses and retrofit costs

The combination of energy costs and seismic losses was then used to define a combined metric, namely the *combined expected annual loss*,  $EAL_c$  defined as in (Bournas, 2018b) as  $EAL_c = EAL_E + EAL_s$ . The reductions in losses due to retrofitting are then given as the difference of the initial annual losses ( $EAL_{c,i}$ ) and the losses after retrofit application ( $EAL_{c,r}$ ), as in Eq. (9):

$$\Delta EAL_c = EAL_{c,i} - EAL_{c,r} [\%] \quad (9)$$

It is worth noting that the cost estimations in this study are to be taken as preliminary in nature, and the values are not expected to reflect necessarily financial realities. Instead, the costs are taken indicatively in order to evaluate trends. Retrofit costs per  $m^2$  are defined for the energy retrofit and seismic retrofit based on averages obtained from multiple studies for various countries, including Greece and Italy (La Greca and Margani, 2018; Gkournelos, Bournas, and Triantafillou, 2019a; Gkournelos, Bournas, and Triantafillou, 2019b; Margani, 2019; Formisano, Vaiano, and Fabbrocino, 2019; Mora et al., 2018; Mastroberti et al., 2018; Calvi, 2013; Zavadskas, Raslanas, and Kaklauskas, 2008). The cost for energy retrofitting considers thermal insulation and the cost of replacing windows, and, like the cost of the seismic retrofit using glass-TRM (Koutas, Bousias, and Triantafillou, 2015), was assessed in a previous study (Bournas, 2018b). The cost of the combined intervention is estimated to be 25% cheaper than energy and the seismic retrofit applied separately (Gkournelos, Bournas, and Triantafillou, 2019b), due to the integration of seismic and energy retrofitting materials leading to reduced labour costs, scaffolding etc. Indicatively, the assumed retrofit costs used for Italy are taken to be 200 €/ $m^2$  for the energy retrofit alone, 160 €/ $m^2$  for the

seismic retrofit with TRM and 270 €/m<sup>2</sup> for the combined retrofit. To account for the geographic differences in retrofit costs, the broad assumption is made that the costs can be weighted for the different locations using the European Construction Costs Index (European Construction Costs).

Finally, as proposed in (Bournas, 2018b), the indicative payback period of the retrofitting interventions can be calculated as the ratio of the assumed costs of the retrofit (with respect to the non-retrofitted building) to the annual cost savings in Eq. (10):

$$t_{payback} = \frac{\text{Retrofit cost}_k/\text{building value}}{\Delta EAL_k} [\text{years}] \quad (10)$$

Where subscript  $k$  corresponds to the respective values of the energy, seismic or combined retrofit, depending on the evaluation.

## 7.5 Results

The results of the energy analyses and seismic analyses are presented first in this section, followed by a combined assessment of the integrated retrofitting, to evaluate in which locations combined retrofitting may offer benefits over energy retrofitting alone.

### 7.5.1 Energy performance evaluation

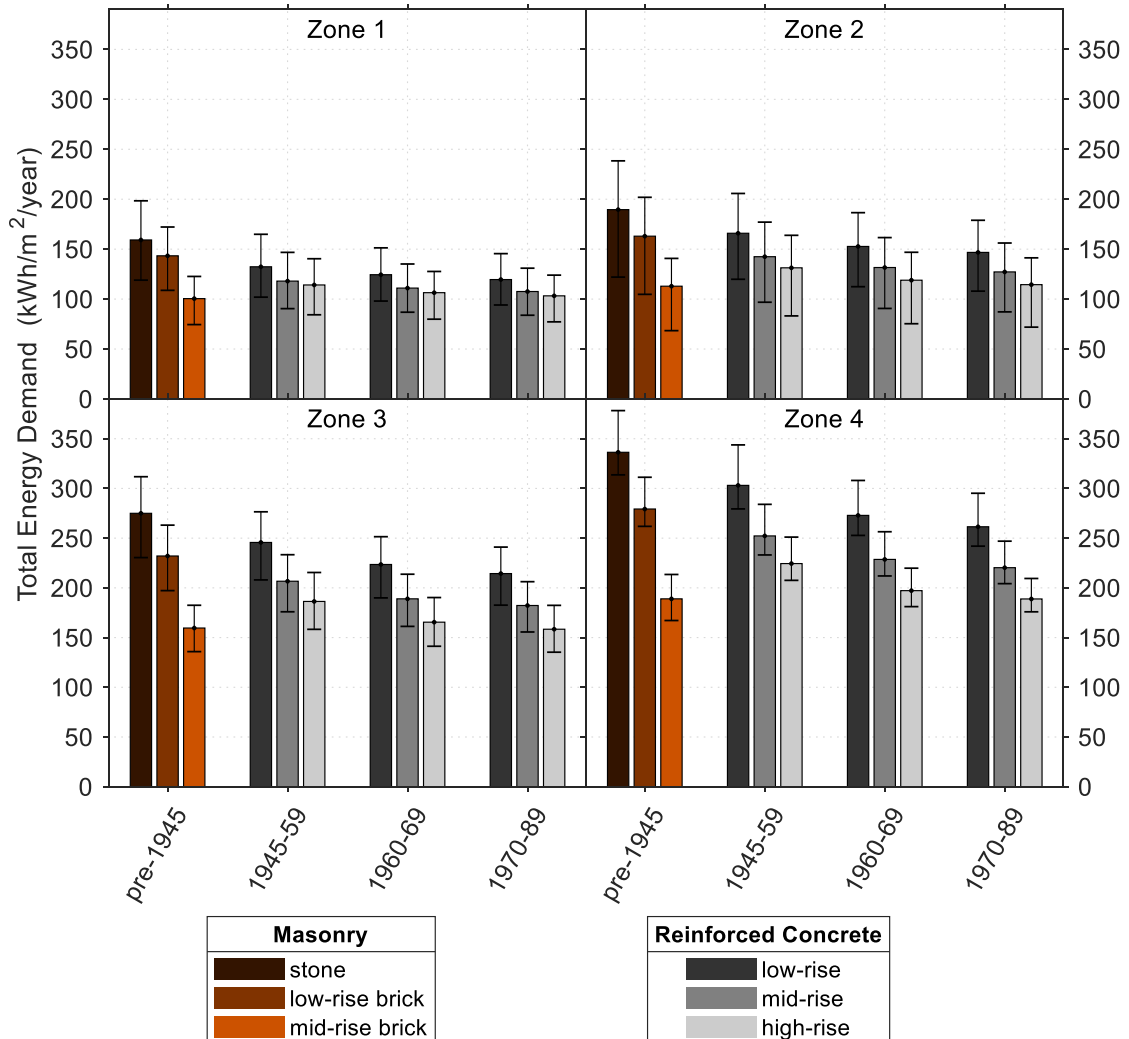
#### 7.5.1.1 Energy demand of existing and retrofitted buildings

The results in terms of total energy demands, hence the sum of heating and cooling demand for all building types across the four climatic zones are summarised in Figure 18. Some variation can be observed within each climatic zone, as the annual weather data varies, and this is indicated by the error bars in Figure 18.

It can be observed that the oldest structures (pre-1945), and the stone masonry buildings in particular, present the highest energy demand across all locations. Of the considered building typologies, the 1970-89 RC structures with improved U-values are the most energy efficient. As would be expected, the highest total energy demands can be observed in the colder regions (zone 4), with average energy demands doubled compared to the hotter zones for all the different building types. The obtained energy demands are reasonable compared to average annual energy demands in the EU-28 to be around 175 kWh/m<sup>2</sup> in 2014 (European Commission, 2016b), which contain a large number of post-1990's structures.

Moreover, higher energy demand per floor area is observed for low-rise structures compared to high-rise buildings, which is as expected due to different envelope area and floor area ratios, with high rise-building being more compact. In addition, mid-rise brick masonry buildings, consume less energy compared to their RC counterparts (Figure 18).

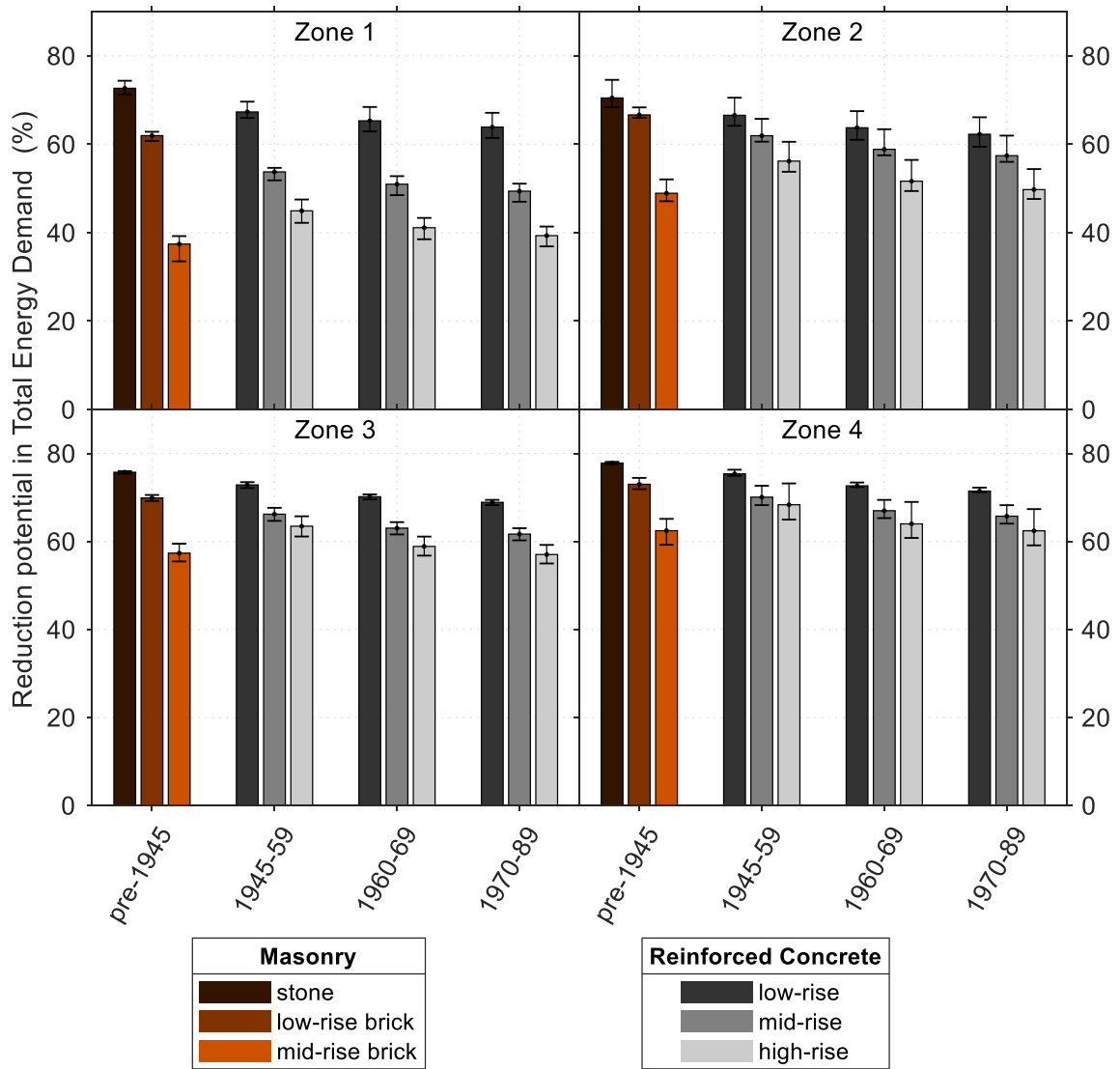
**Figure 18.** Average total annual energy demand per building type across all locations.



Source: (Pohoryles et al., 2020) (CC BY 4.0).

Looking at the effect of energy retrofitting solutions for the different zones, large decreases in total energy demand are observed for all building types, as shown in Figure 19. The highest reductions are obtained for older low-rise buildings (average 78%) and for the buildings of zone 4 (average improvements close to 75%), whereas for zone 1 the lowest reduction in total energy demands is observed. Mid-rise masonry and high-rise RC structures, present the lowest improvements in energy demand (between 37 and 45% for zone 1), compared to reductions close to 70% for low rise buildings. This difference is less pronounced in the colder zones.

**Figure 19.** Average reduction in total annual energy demand due to retrofit per building type in each zone.

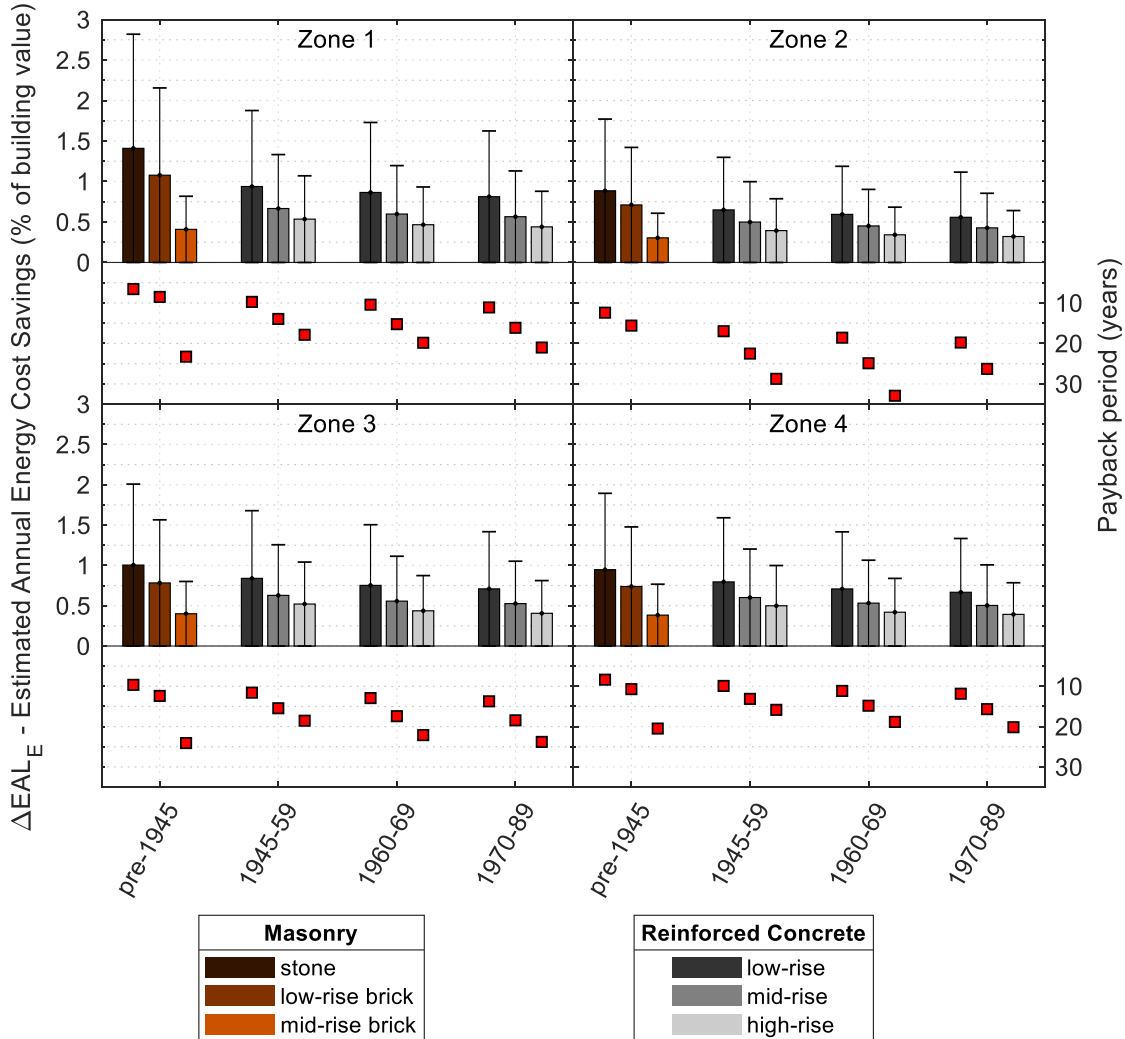


Source: (Pohoryles et al., 2020) (CC BY 4.0).

The obtained reductions in energy demand due to retrofitting were used to calculate energy cost savings. The estimated annual savings in energy costs normalised by the building value ( $\Delta EAL_E$ ) are shown in Figure 20. Together with the assumed costs of energy retrofitting in each case study location, the payback periods of the energy retrofit were also calculated. Note that energy costs in Europe do not vary in the same way as property and construction costs, which explain the large variations in  $\Delta EAL_E$  across within the same zones. In Energy Zone 1, while the savings in energy demand are the lowest, average savings are the highest, leading to very low payback periods between five years for older masonry structures and 25 years for high rise RC buildings. This is mainly attributable to the relatively high heating energy costs and electricity costs for cooling in the countries of Zone 1 (Cyprus, Greece, Spain and Portugal) together with lower real estate values compared to the EU-average. The ratio of savings to property value is hence very high in these locations. For Energy Zone 4, the highest reductions in energy consumption were calculated made, and with respect to Zones 2 and 3, larger cost savings are hence observed. Payback periods of around 10 - 20 years are obtained, while these are closer to

15 – 35 years in Zone 2 and 10 - 25 years in Zone 3. Lowest payback periods are observed in low-rise structures and older structures for which the highest energy savings are obtained. Compared to other studies for Italian low and mid-rise buildings, similar payback periods are calculated (Gkournelos, Bournas, and Triantafillou, 2019b; Calvi, Sousa, and Ruggeri, 2016). The effect of combined seismic and energy retrofitting on the payback periods is studied in section 7.5.3.

**Figure 20.** Estimated annual energy cost savings and payback periods per building type in each zone.



Note: the red squares indicate the payback period for the energy retrofit.

Source: (Pohoryles et al., 2020) (CC BY 4.0).

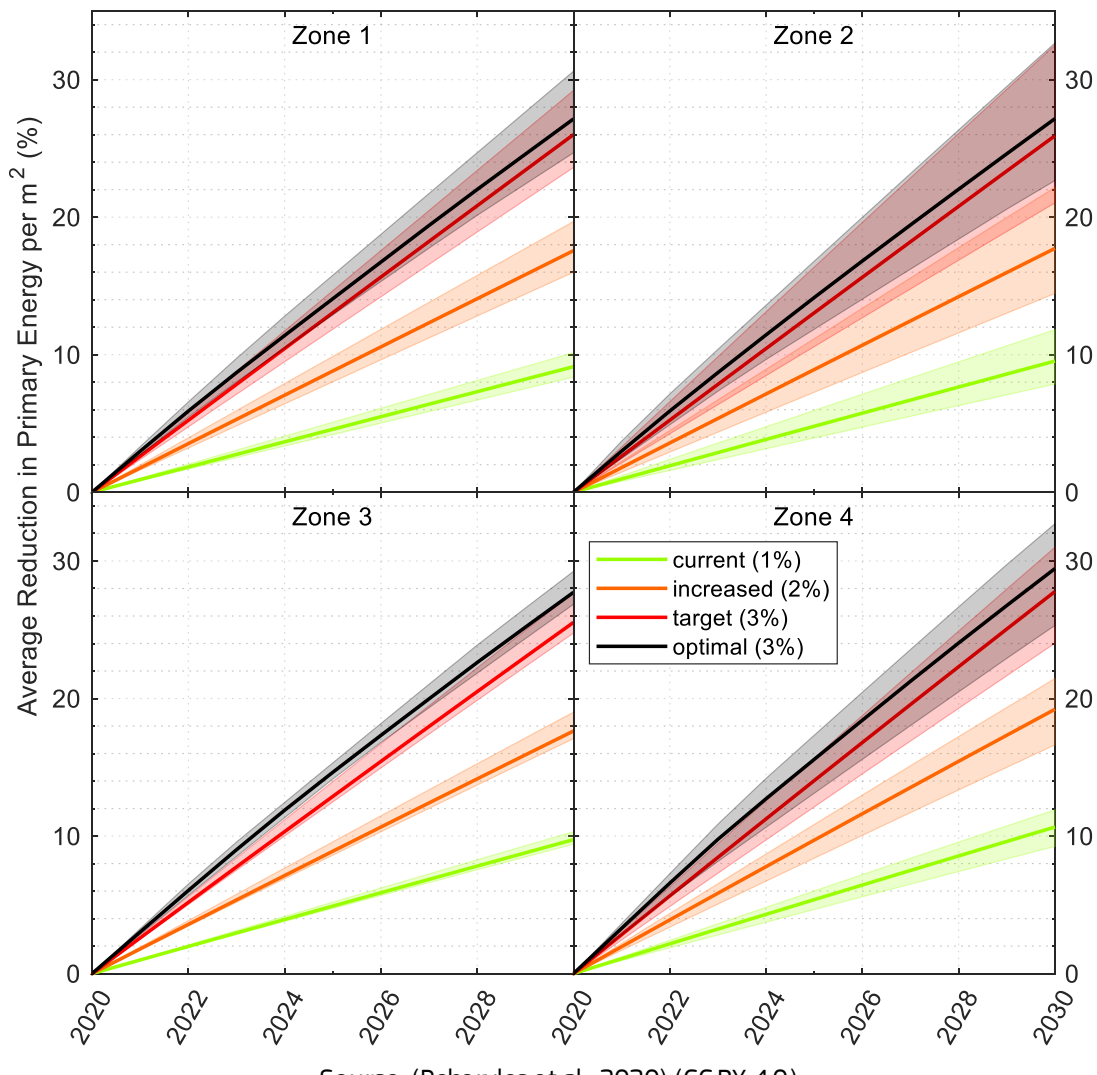
Looking at the overall results in terms of energy consumption and savings due to retrofitting, it is important to add that low and mid-rise buildings are the most common building typologies in Europe. Focussing energy retrofitting on the structures with the highest energy reduction potential could result in larger savings in overall energy use.

To assess this, the impact of various renovation strategies on the building stock level is studied in the next section up to the year 2030. This is done by combining the obtained energy demands for all building typologies and their relative distribution within the building stocks of the case study locations.

### 7.5.1.2 Foresight study on renovation impact

To evaluate the impact of building renovation, three scenarios were assumed: keeping the rate of renovation as it is (1% - 'current'), increasing it to 2% ('increased') or reaching the target 3% ('target'), i.e. the average rate recommended in the EPBD (European Parliament and Council of the European Union, 2018) and more recently by the EU Green Deal. A last scenario is added, looking at keeping the same 3% target renovation rate, but starting by renovating the oldest buildings first before moving to buildings from more recent times. This latter scenario will be referred to as 'optimal' scenario both in terms of reduction of energy demands and possible seismic damage, as the more deficient buildings are renovated first. The reduction in primary energy up to 2030 compared to the evaluation year 2020 is shown in Figure 21. The average reduction is shown by the solid line and the range across the five cities in each zone is shown by the respective shaded area.

**Figure 21.** Reduction in primary energy use for all zones (2020 – 2030) with four different renovation strategies.



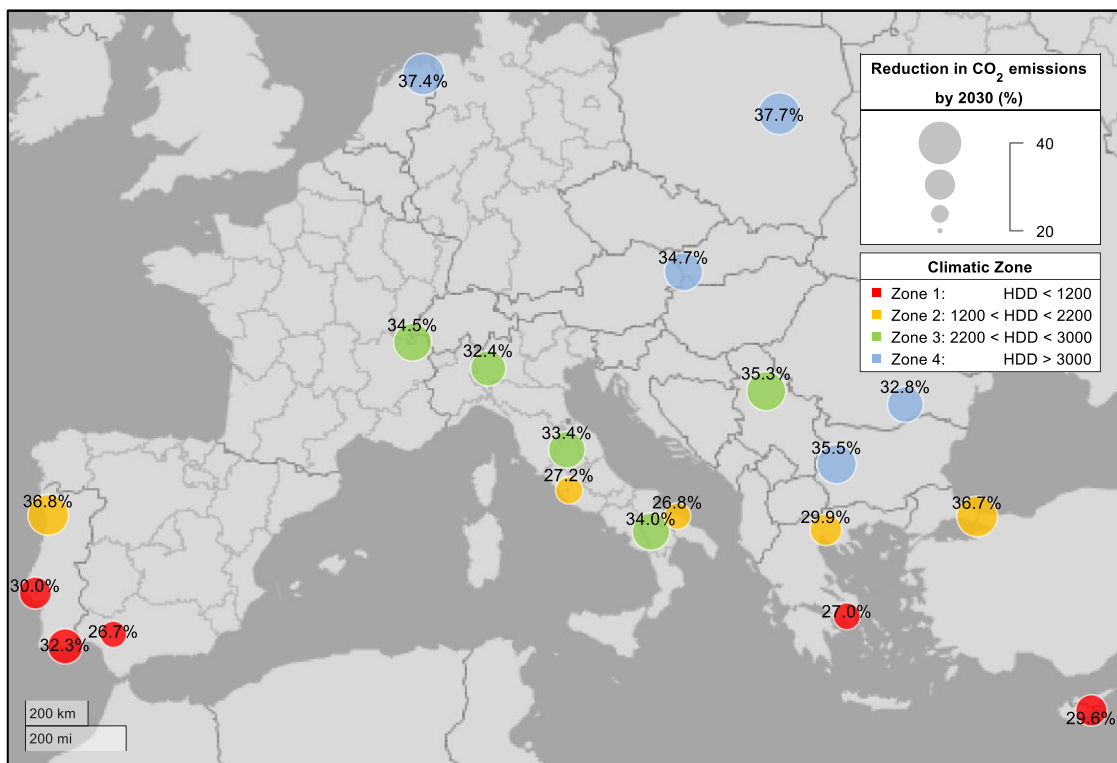
Source: (Pohoryles et al., 2020) (CC BY 4.0).

Large reduction in primary energy use of the building stock between 20 and 30% can be seen by 2030 across all zones for the target (3%) and optimal (3%) renovation strategies. If the current renovation rate is kept, the reduction is merely one third of these values. With the 2% increased rate, by 2030 a maximum reduction of 20% compared to 2020 is

obtained for the considered building stock, however the range of reduction can be as low as 14%.

To relate the obtained results with the EU Council's promoted target of cutting emissions by 30% by 2030 due to energy efficiency measures in the residential sector (European Commission, 2018), equivalent CO<sub>2</sub> emissions are calculated based on the obtained primary energy consumption. The reduction in equivalent CO<sub>2</sub> emissions by 2030 is mapped in Figure 22 for the optimal renovation strategy. It can be observed that the target for 2030 may indeed be reached in most locations-zones if the optimal renovation rate of 3% is implemented. Instead, with the current (1%) renovation rate, only 10-20% of CO<sub>2</sub> emission reduction can be obtained. It's worth noting that an additional reduction in CO<sub>2</sub> emissions is further expected (albeit not considered herein) due to seismic retrofitting, as repair and reconstruction works after seismic events are reduced.

**Figure 22.** Reduction in CO<sub>2</sub>-emissions by 2030 after implementation of an optimal renovation strategy.



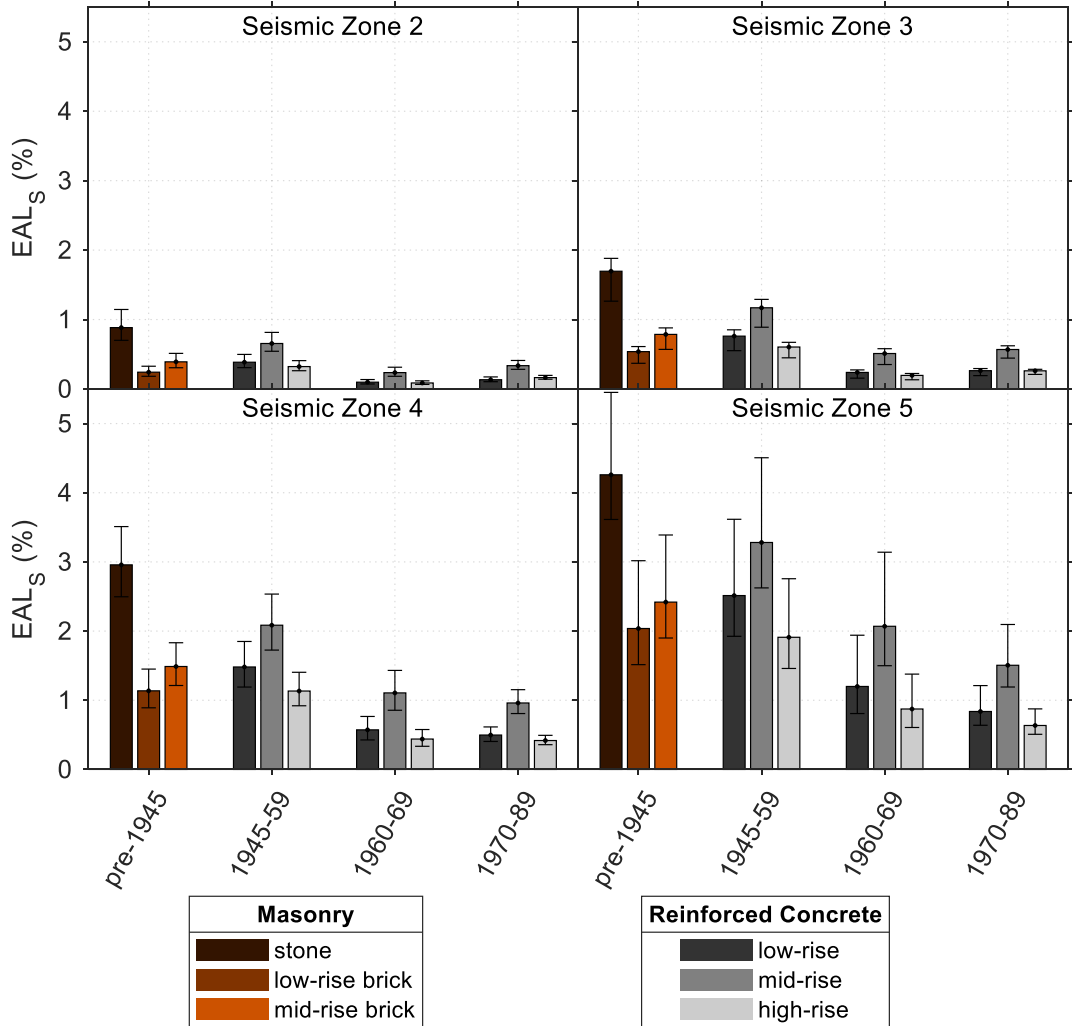
Source: (Pohoryles et al., 2020) (CC BY 4.0).

### 7.5.2 Seismic performance

In order to evaluate the seismic performance of the existing buildings, the expected annual losses as a fraction of the building costs were calculated using the procedure presented in Section 7.4.2. The resulting  $EAL_s$  for each building typology is shown for Seismic Zones 2 to 5 in Figure 23. The results obtained can be used to assess the most vulnerable building typologies and define which are most at risk in terms of seismic losses. As for the energy performance evaluation of the different building typologies, a broad observation can be made in terms of increasing losses with increasing seismic hazard, but also in terms of the oldest buildings presenting the highest  $EAL_s$  for all locations. It can be observed that stone masonry buildings present the highest losses across all zones. Mid-rise RC buildings present the highest losses of the RC typologies. The same is observed for the mid-rise brick

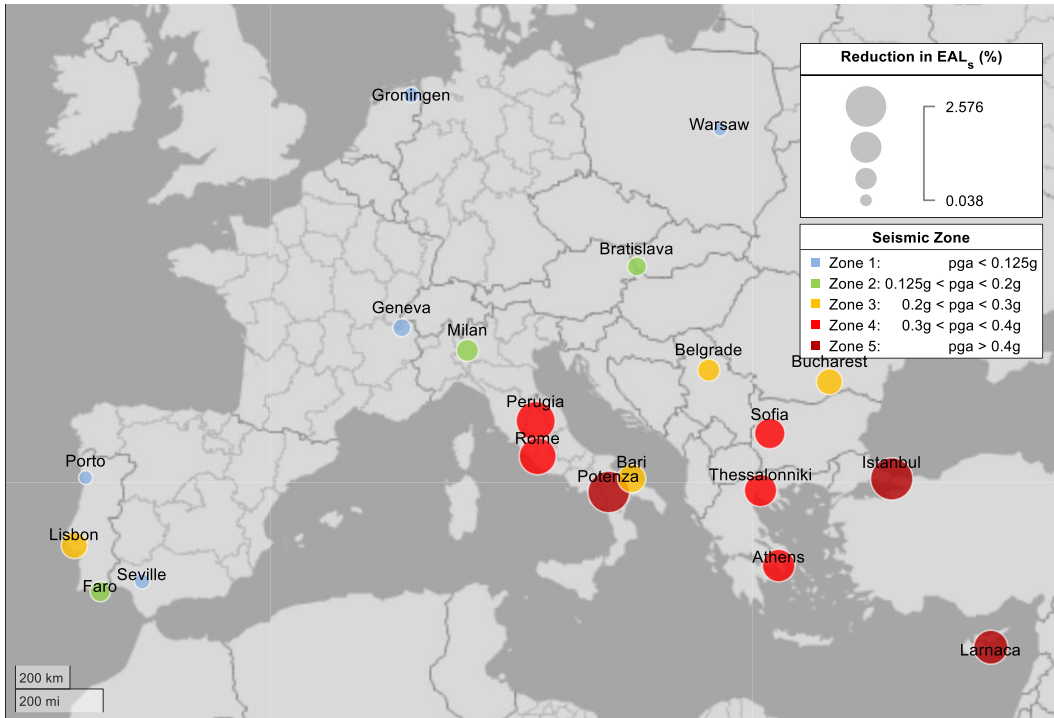
masonry buildings compared to the low-rise ones. With the selected fragility curves, the low-rise and high-rise RC buildings present the lowest losses.

**Figure 23.** Average  $EAL_S$  per building type across all locations for Seismic Zones 2 to 5.



With the results of the total energy demand results in mind, again the older masonry buildings and the 1945–1959 RC buildings are the structures which are most in need for retrofitting. Looking at the full building stock of the twenty locations, when applying the 3% optimised renovation strategy up to 2030, i.e. targeting the oldest structures first, the reductions in annual seismic losses are shown in Figure 24. The presented figure can be seen in analogy to the plot of reductions in equivalent CO<sub>2</sub> emissions by 2030 in Figure 22. It can be observed that reductions in average  $EAL_S$  up to 2.5% of the value of the building stock can be achieved by 2030 when 3% of the building stock is renovated annually. The values are highest for Seismic Zones 3 and 4, as one would expect, however also for moderate seismicity (Seismic Zone 3), reductions in annual losses around 1% of the building stock value can be observed.

**Figure 24.** Reduction in  $EAL_s$  (%) across the building stock of the twenty locations by 2030 after implementation of an optimal renovation strategy.

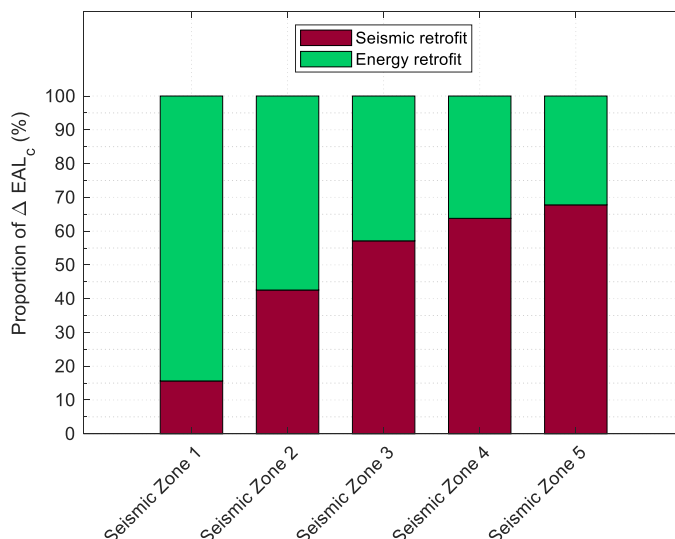


### 7.5.3 Combined assessment of integrated retrofitting

#### 7.5.3.1 Disaggregation of seismic and energy loss reductions

Based on the seismic and energy assessments of the different building typologies, a disaggregation of the potential savings in annual losses due to seismic and energy retrofitting can be found in Figure 25. It can be observed that even for low to moderate seismic hazard, i.e. Seismic Zone 2, the seismic loss reductions constitute about 40% of the average combined expected annual loss reductions ( $\Delta EAL_c$ ). This number increases to 54% for Seismic Zone 3 and reaches nearly 70% in the zone of highest seismic hazard. It has to be however noted, that the values of  $\Delta EAL_c$  are significantly lower for Seismic Zones 1 to 3, as will be shown in the next sub-section.

**Figure 25.** Disaggregation of  $EAL_c$  (%) in its seismic and energy components averaged for each Seismic Zone.



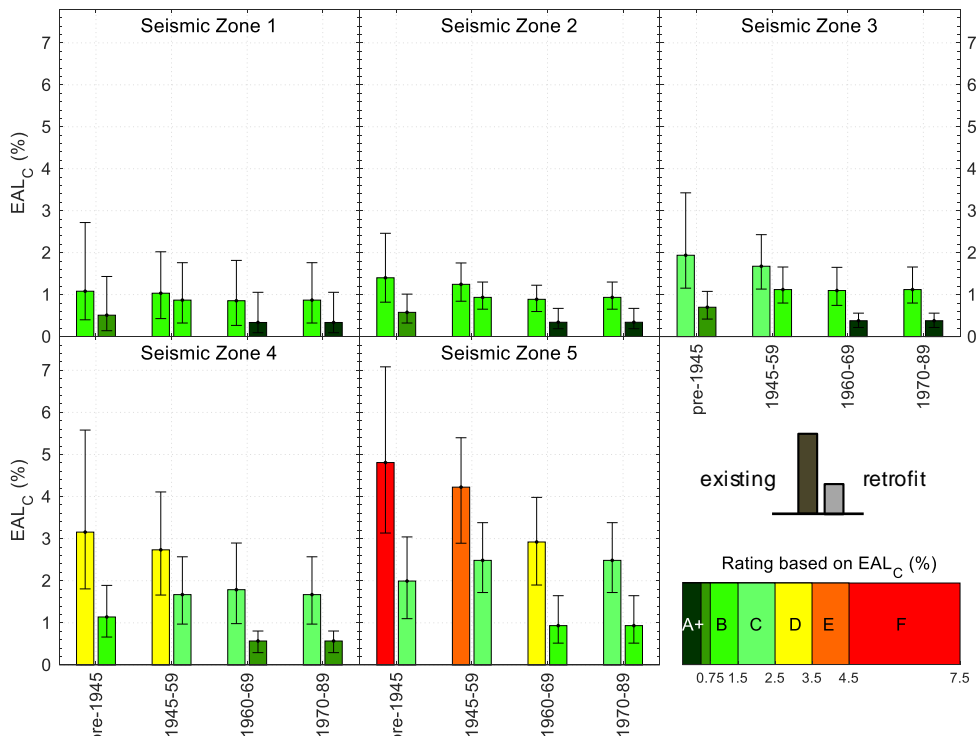
### 7.5.3.2 Combined seismic and energy classification

The combined seismic and energy performance of buildings is evaluated using as an index the sum of energy and seismic  $EAL$  classified in the performance levels proposed in (Calvi, Sousa, and Ruggeri, 2016) and applied also in (Bournas, 2018b; Gkournelos, Bournas, and Triantafillou, 2019b). The different building typologies are assessed in their existing and retrofitted states stocks in all case study locations in Figure 26. The classification from F to A+ is done in terms of combined expected annual losses  $EAL_c$  (in % of the building value) and allows an insight onto the effect of different seismic hazard and climatic conditions on the losses. Values of  $EAL_c$  above 4.5% correspond to a category F, while a value below 0.5% of annual losses corresponds to an A+ rating. The scale follows the categorisation from Calvi et al. (2016) and is shown in Figure 26.

As shown in Figure 26, the increase in seismic hazard (going from seismic zone 1 to 5), leads to an increase of the  $EAL$  due to the corresponding increase in the seismic  $EAL_s$ . The error bars show the variation in  $EAL_c$  related to the different climatic zones, but also the variation of seismic hazard within the seismic zones. The average for the three building heights is shown for each building typology. Note that the  $EAL_c$  of the retrofitted counterparts is always indicated on the right of the existing state.

In the low to moderate seismic zones, all buildings present on average a combined rating better than 'C'. However, it can be observed that the variation ranges up to a 'D' classification for the oldest structures even for Seismic Zone 1 due to the low energy efficiency. The proposed retrofit scheme achieves average improvements to A or A+ for most buildings in Seismic Zones 1 to 3. As expected, with increasing seismic hazard, the combined classification of the existing building deteriorates. Above Seismic Zone 4, where the seismic losses dominate, average ratings of the older structures are 'D' or worse, however retrofitting of the buildings can achieve improvements of at least one category, with improvements of 2 categories achieved for the older buildings.

**Figure 26.** Average combined classification of the different building typologies across all seismic zones.



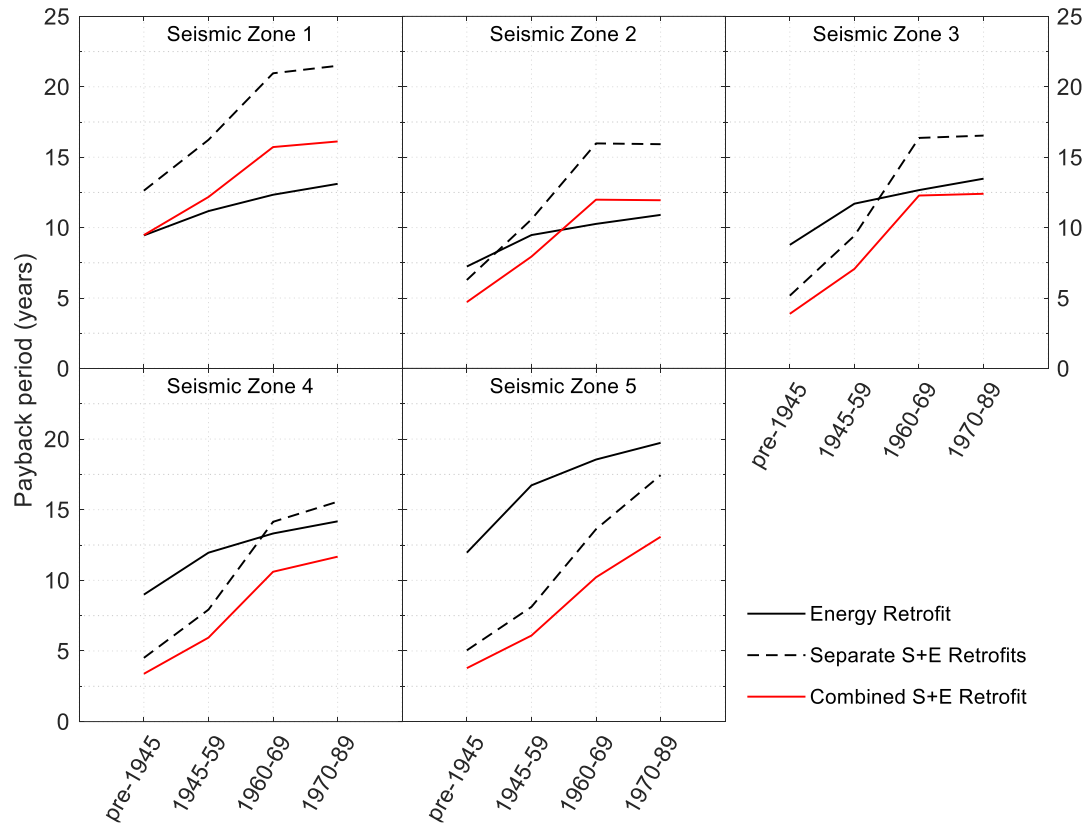
When looking at the highest seismic zone, the pre-1945 buildings have an average 'F' rating, as would be expected for very old structures in very high seismic zones. For these structures, retrofitting can lead to large reductions in seismic losses and energy costs, hence leading to an average 'C' rating, with lower variation, for the retrofitted counterparts.

### **7.5.3.3 Payback periods of combined energy retrofits**

Finally, the impact of the renovation strategy in terms of cost benefits for each seismic zone is evaluated by comparing the savings in terms of energy costs and seismic losses with the initial investment costs by means of assessing the payback periods, calculated using equation (10). The plots in Figure 27 allow to assess whether a combined retrofit is worthwhile compared to an energy retrofit alone for each building type and seismic zone. The average of the payback periods in the four cities (i.e. four climate zones) is calculated for each seismic zone. The payback periods of separate seismic and energy intervention are also indicated. Note that for seismic zone 5, there is no city in the coldest climatic zone, hence increasing the payback period for the energy retrofitting alone.

The exact values of payback periods should be considered rather preliminary in nature, as further analysis of the financial aspects is required, in particular with more detailed seismic loss modelling and cost estimations. Still, the results shown herein indicate important trends regarding the benefits of combined retrofit interventions. For locations of low seismicity (seismic zone 1,  $\text{pga} < 0.125\text{g}$ ), the effect of adding seismic retrofitting is generally not beneficial and the payback period is lower for energy retrofitting alone than the combined retrofitting scenario. However, when assessing locations in zones of medium to high seismicity (seismic zones 3 to 5, i.e.  $\text{pga} > 0.2\text{g}$ ), the benefits of providing simultaneously the seismic and energy retrofitting are shown, particularly for the older building groups. In these zones the importance of seismic loss reduction becomes more critical than the energy savings alone. The benefits are particularly important for older buildings, as losses due to energy costs and due to seismic events can be significantly reduced. Even for seismic zone 2, with low to moderate seismic hazard, the combined retrofit payback period is reduced for the oldest masonry and RC buildings, i.e. buildings designed without seismic guidelines. Importantly, for zones in which seismic retrofit are essential (i.e. above seismic zone 3) but combined seismic and energy retrofitting has lower payback periods for all building types than energy retrofitting alone. It is hence shown that combined retrofitting is recommendable in these cases. In all cases, doing the seismic intervention separately from the energy retrofit, will lead to longer payback periods.

**Figure 27.** Payback periods for all building ages (average taken over the four climate zones) for the energy retrofit compared to combined and separate seismic and energy retrofitting shown for each Seismic Zone.



In conclusion, when using a combined monetary metric, namely expected annual loss, for energy and seismic performance across the locations, significant improvements leading to average reductions of at least one category in terms of combined seismic and energy classes for the building stock were obtained. The implementation of an increased renovation rate was shown not only to achieve the emission reduction targets, but to also be economically efficient, as reduced losses from energy costs and seismic damage make the renovation strategies more viable. Looking at payback periods for the combined energy and seismic retrofit investment, already in low seismicity zones, integrated interventions started showing financial benefits over energy retrofitting alone. In zones in which seismic retrofitting is essential due to higher seismic activity, performing the combined retrofit at once instead of separate interventions, showed significant reduction in the intervention's payback period.

## **8 Conclusions**

As a consequence of the poor energy performance, as well as the vulnerability of older buildings to seismic hazards, a large proportion of the existing EU buildings require both structural and energy upgrading. The iRESIST+ project aimed to address this need by exploring a novel seismic-plus-energy retrofit for existing RC buildings and by assessing the impact of applying this combined retrofit approach on the EU building stock.

The research conducted in iRESIST+ is of high timeliness, given the launch of the Renovation Wave initiative under the EU Green Deal, which calls for an increase in building renovations across the EU MS in order to meet the ambitious energy saving targets for 2030 and beyond. While a target of at least doubling renovation rates was set-out, this is however associated with financial and technical limitations. Moreover, natural or man-made risks, such as fire or earthquakes may result in loss of investments in energy retrofitting, which has recently been recognised by the new EBPD.

A holistic view on building renovation, as was proposed in iRESIST+, is of high relevance for policies related to the energy efficiency of buildings, circular-economy principles, as well as resilience. This high relevance to policy making was highlighted by the reference to iRESIST+ and combined retrofitting in a number of policy documents related to the safeguarding of cultural heritage, including the European framework for action on cultural heritage and the Urban Agenda Action Plan.

A review of the experimental studies on TRM highlighted their potential for seismic strengthening, but also their suitability for combined seismic and energy retrofitting. To assess the effectiveness of the proposed solution, an experimental study on a full-scale prototype RC structure is planned at the JRC's ELSA laboratory. To complement the experimental campaign, but also extend and generalise its scope, a series of numerical studies were performed and presented in this report.

Based on the gathered scientific literature, a new macro-modelling approach for TRM-strengthened infilled RC buildings was developed and shown to sufficiently replicate experimental results. The model was used to assess the effect of different amounts of TRM-strengthening on the iRESIST+ prototype structure. The results highlight significant increases in base-shear capacity and a shift to higher displacements at maximum base-shear. To further extend the scope of the numerical study, the developed macro-model was used to develop seismic fragility curves of typical mid-rise RC structures with and without TRM retrofitting. The TRM-retrofitted low-code structure was shown to achieve a performance similar to that of a (non-retrofitted) modern high-code structure in terms of seismic losses from infills for different levels of seismic hazard.

Finally, the scope of combined retrofitting was extended to address its implications on the European building stock. Typical structures were defined to be representative of the existing European buildings in terms of their structural and thermal characteristics. Information on different building types and for the building stock composition of 20 case-study locations with different levels of seismic hazard and climatic conditions was collected. The building energy performance was evaluated by means of Building Energy Modelling and their seismic performance was modelled through fragility curves. The long-term effect up to 2030 of different building renovation rates was assessed in terms of energy consumption reduction, reductions in carbon emissions, as well as seismic losses.

For the current annual renovation rate of around 1%, the ambitious targets for energy reduction are not going to be achieved. If renovation rates are increased to 3%, in particular when starting with the oldest building typologies first, the energy use for heating and cooling may be reduced by up to 32.5%. This would lead to reductions of around 30% in CO<sub>2</sub> emissions across all cities to be achieved by 2030, with reductions ranging from 26.8 to 37.7%, due to a more homogenous energy performance of the building stock. In terms of seismic performance, the assessments of different building typologies showed particular potential in seismic loss reductions for older and mid-rise buildings. Applying the combined retrofitting scheme can hence lead to significant energy performance improvements, as well as reduced seismic losses. This was evaluated by using a combined monetary metric, namely expected annual loss, for energy and seismic performance across the twenty locations.

Disaggregating the potential savings from seismic and energy retrofitting, showed that combined retrofitting may be beneficial even for areas of moderate and high seismic hazard. Significant improvements leading to reductions of at least one category in terms of combined seismic and energy classes for the different building typologies were obtained, leading to cost effectiveness of the retrofit, as reduced losses from energy costs and seismic damage make the renovation strategies more viable. Looking at payback periods for the combined energy and seismic retrofit investment, already in moderate seismicity zones, combined interventions present financial benefits over energy retrofitting alone. Finally, in zones in which seismic retrofitting is essential due to higher seismic activity, performing the combined retrofit at once instead of separate interventions, showed significant reduction in the intervention's payback period.

Overall, the presented results in this report highlight the potential of combined retrofitting with TRM and thermal insulation for EU buildings. The proposed retrofit is cost-effective and lends itself to large-scale applications due to its easy application and reduced building down-time compared to traditional retrofitting. As a next step, the validity of the proposed approach will be evaluated on the iRESIST+ prototype structure by means of hybrid pseudo-dynamic testing at the European Laboratory for Structural Assessment (ELSA) at the European Commission's Joint Research Centre (JRC) in Ispra.

## 9 References

- Aditya, L., T.M.I. Mahlia, B. Rismanchi, H.M. Ng, M.H. Hasan, H.S.C. Metselaar, O. Muraza, and H.B. Aditiya, 'A Review on Insulation Materials for Energy Conservation in Buildings', *Renewable and Sustainable Energy Reviews*, Vol. 73, June 1, 2017, pp. 1352–1365, doi:10.1016/j.rser.2017.02.034.
- Ahmad, N., H. Crowley, and R. Pinho, *Analytical Fragility Functions for Reinforced Concrete and Masonry Buildings and Building Aggregates*, UPAV-internal report, Pavia, Italy, 2010.
- Akhoundi, F., G. Vasconcelos, P. Lourenço, L.M. Silva, F. Cunha, and R. Fanguero, 'In-Plane Behavior of Cavity Masonry Infills and Strengthening with Textile Reinforced Mortar', *Engineering Structures*, Vol. 156, February 1, 2018, pp. 145–160, doi:10.1016/j.engstruct.2017.11.002.
- Akhoundi, F., G. Vasconcelos, P. Lourenço, G. Vasconcelos, and P. Lourenço, 'In-Plane Behavior of Infills Using Glass Fiber Shear Connectors in Textile Reinforced Mortar (TRM) Technique', *International Journal of Structural Glass and Advanced Materials Research*, Vol. 2, No. 1, January 14, 2018, pp. 1–14, doi:10.3844/sgamrsp.2018.1.14.
- Almusallam, T.H., and Y.A. Al-Salloum, 'Behavior of FRP Strengthened Infill Walls under In-Plane Seismic Loading', *Journal of Composites for Construction*, Vol. 11, No. 3, June 1, 2007, pp. 308–318, doi:10.1061/(ASCE)1090-0268(2007)11:3(308).
- Altin, S., Ö. Anil, and M.E. Kara, 'Strengthening of RC Nonductile Frames with RC Infills: An Experimental Study', *Cement and Concrete Composites*, Vol. 30, 2008, p. 612 621.
- Altin, S., Ö. Anil, M.E. Kara, and M. Kaya, 'An Experimental Study on Strengthening of Masonry Infilled RC Frames Using Diagonal CFRP Strips', *Composites Part B: Engineering*, Vol. 39, No. 4, June 1, 2008, pp. 680–693, doi:10.1016/j.compositesb.2007.06.001.
- American Society of Heating, R. and A.-CE., *2013 ASHRAE Handbook: Fundamentals*., 2013, ISBN 978-1-62870-535-5.
- Asdrubali, F., C. Baldassarri, and V. Fthenakis, 'Life Cycle Analysis in the Construction Sector: Guiding the Optimization of Conventional Italian Buildings', *Energy and Buildings*, Vol. 64, September 1, 2013, pp. 73–89, doi:10.1016/j.enbuild.2013.04.018.
- Asteris, P.G., S.T. Antoniou, D.S. Sophianopoulos, and C.Z. Chrysostomou, 'Mathematical Macromodeling of Infilled Frames: State of the Art', *Journal of Structural Engineering*, Vol. 137, No. 12, December 2011, pp. 1508–1517, doi:10.1061/(ASCE)ST.1943-541X.0000384.
- Asteris, P.G., L. Cavalieri, F.D. Trapani, and V. Sarhosis, 'A Macro-Modelling Approach for the Analysis of Infilled Frame Structures Considering the Effects of Openings and Vertical Loads', *Structure and Infrastructure Engineering*, Vol. 12, No. 5, May 3, 2016, pp. 551–566, doi:10.1080/15732479.2015.1030761.
- Asteris, P.G., C.Z. Chrysostomou, I. Giannopoulos, and P. Ricci, 'Modeling of Infilled Framed Structures', in M. Papadakakis, M. Fragiadakis, and V. Plevris (eds.), *Computational Methods in Earthquake Engineering*, Vol. 30, Springer Netherlands, Dordrecht, 2013, pp. 197–224, ISBN 978-94-007-6572-6, doi:10.1007/978-94-007-6573-3\_10.
- Ayatar, M.E., E. Canbay, and B. Binici, 'Strengthening of Reinforced Concrete Frames with Engineered Cementitious Composite Panels', *Proceedings of the Institution of Civil Engineers - Structures and Buildings*, December 10, 2018, pp. 1–15, doi:10.1680/jstbu.18.00001.
- Baker, J.W., 'Efficient Analytical Fragility Function Fitting Using Dynamic Structural Analysis', *Earthquake Spectra*, Vol. 31, No. 1, February 1, 2015, pp. 579–599, doi:10.1193/021113EQS025M.
- Berardi, U., 'The Benefits of Using Aerogel-Enhanced Systems in Building Retrofits', *Energy Procedia*, Vol. 134, October 2017, pp. 626–635, doi:10.1016/j.egypro.2017.09.576.
- Borri, A., M. Corradi, R. Sisti, C. Buratti, E. Belloni, and E. Moretti, 'Masonry Wall Panels Retrofitted with Thermal-Insulating GFRP-Reinforced Jacketing', *Materials and Structures*, Vol. 49, No. 10, October 1, 2016, pp. 3957–3968, doi:10.1617/s11527-015-0766-4.
- Bournas, D.A., *Innovative Materials for Seismic and Energy Retrofitting of the Existing EU Buildings*, EUR 29184 EN, Publications Office of the European Union, Luxembourg, 2018a, ISBN 978-92-79-81995-7, doi:10.2760/091621, JRC109907.

Bournas, D.A., 'Concurrent Seismic and Energy Retrofitting of RC and Masonry Building Envelopes Using Inorganic Textile-Based Composites Combined with Insulation Materials: A New Concept', *Composites Part B: Engineering*, Vol. 148, September 2018b, pp. 166–179, doi:10.1016/j.compositesb.2018.04.002.

Bournas, D.A., P. Negro, and F.F. Taucer, 'Performance of Industrial Buildings during the Emilia Earthquakes in Northern Italy and Recommendations for Their Strengthening', *Bulletin of Earthquake Engineering*, Vol. 12, No. 5, October 2014, pp. 2383–2404, doi:10.1007/s10518-013-9466-z.

Breveglieri, M., G. Camata, and E. Spacone, 'Strengthened Infilled RC Frames: Continuum and Macro Modeling in Nonlinear Finite Element Analysis', *Composites Part B: Engineering*, Vol. 151, October 15, 2018, pp. 78–91, doi:10.1016/j.compositesb.2018.05.042.

Calvi, G.M., 'Choices and Criteria for Seismic Strengthening', *Journal of Earthquake Engineering*, Vol. 17, No. 6, August 18, 2013, pp. 769–802, doi:10.1080/13632469.2013.781556.

Calvi, G.M., L. Sousa, and C. Ruggeri, 'Energy Efficiency and Seismic Resilience: A Common Approach', in P. Gardoni and J.M. LaFave (eds.), *Multi-Hazard Approaches to Civil Infrastructure Engineering*, Springer International Publishing, Cham, 2016, pp. 165–208, ISBN 978-3-319-29711-8, doi:10.1007/978-3-319-29713-2\_9.

Cardone, D., G. Gesualdi, and G. Perrone, 'Cost-Benefit Analysis of Alternative Retrofit Strategies for RC Frame Buildings', *Journal of Earthquake Engineering*, Vol. 23, No. 2, February 7, 2019, pp. 208–241, doi:10.1080/13632469.2017.1323041.

Cardone, D., and G. Perrone, 'Damage and Loss Assessment of Pre-70 RC Frame Buildings with FEMA P-58', *Journal of Earthquake Engineering*, Vol. 21, No. 1, January 2, 2017, pp. 23–61, doi:10.1080/13632469.2016.1149893.

Cardone, D., and G. Perrone, 'Developing Fragility Curves and Loss Functions for Masonry Infill Walls', *Earthquakes and Structures*, Vol. 9, No. 1, 2015, pp. 257–279, doi:10.12989/eas.2015.9.1.257.

Cardone, D., M. Rossino, and G. Gesualdi, 'Estimating Fragility Curves of Pre-70 RC Frame Buildings Considering Different Performance Limit States', *Soil Dynamics and Earthquake Engineering*, Vol. 115, December 2018, pp. 868–881, doi:10.1016/j.soildyn.2017.11.015.

CEN, *BS EN 1996-1-1:2005 Eurocode 6. Design of Masonry Structures - Part 1-1: General Rules for Reinforced and Unreinforced Masonry Structures*, BSI, London, 2005.

CEN, 'BS EN 1998-1:2004 Eurocode 8. Design of Structures for Earthquake Resistance. General Rules, Seismic Actions and Rules for Buildings', BSI, 2004.

CEN, 'BS EN 1998-3:2005 - Eurocode 8. Design of Structures for Earthquake Resistance. Assessment and Retrofitting of Buildings', BSI, January 11, 2006.

Cerniauskas, G., Z. Tetta, D.A. Bournas, and L.A. Bisby, 'Concrete Confinement with TRM versus FRP Jackets at Elevated Temperatures', *Materials and Structures*, Vol. 53, No. 3, May 20, 2020, p. 58, doi:10.1617/s11527-020-01492-x.

Coppola, L., D. Coffetti, E. Crotti, A. Marini, C. Passoni, and T. Pastore, 'Lightweight Cement-Free Alkali-Activated Slag Plaster for the Structural Retrofit and Energy Upgrading of Poor Quality Masonry Walls', *Cement and Concrete Composites*, Vol. 104, November 2019, p. 103341, doi:10.1016/j.cemconcomp.2019.103341.

Corrado, V., and I. Ballarini, 'Refurbishment Trends of the Residential Building Stock: Analysis of a Regional Pilot Case in Italy', *Energy and Buildings*, Vol. 132, 2016, pp. 91–106.

Crisafulli, F.J., 'Seismic Behaviour of Reinforced Concrete Structures with Masonry Infills', PhD, University of Canterbury, 1997.

De Luca, F., G.M. Verderame, F. Gómez-Martínez, and A. Pérez-García, 'The Structural Role Played by Masonry Infills on RC Building Performances after the 2011 Lorca, Spain, Earthquake', *Bulletin of Earthquake Engineering*, Vol. 12, No. 5, October 1, 2014, pp. 1999–2026, doi:10.1007/s10518-013-9500-1.

Decanini, L.D., and G.E. Fantin, 'Modelos Simplificados de La Mampostería Incluida En Porticos', *Características de Stiffness y Resistencia Lateral En Estado Límite. Jornadas Argentinas de Ingeniería Estructural*, Vol. 2, 1986, pp. 817–836.

Dehghani, A., F. Nateghi-Alahi, and G. Fischer, 'Engineered Cementitious Composites for Strengthening Masonry Infilled Reinforced Concrete Frames', *Engineering Structures*, Vol. 105, December 15, 2015, pp. 197–208, doi:10.1016/j.engstruct.2015.10.013.

DG EAC, European Commission, *European Framework for Action on Cultural Heritage (SWD 2018/491)*, Publications Office of the European Union, Luxembourg, 2019, ISBN ISBN 978-92-76-03453-7.

Dost, B., E. Ruigrok, and J. Spetzler, 'Development of Seismicity and Probabilistic Hazard Assessment for the Groningen Gas Field', *Netherlands Journal of Geosciences*, Vol. 96, No. 5, December 2017, pp. s235–s245, doi:10.1017/njg.2017.20.

ECOFYS, *U-Values for Better Energy Performance of Buildings*, November 27, 2007.

Economidou, M., B. Atanasiu, C. Despret, J. Maio, I. Nolte, and O. Rapf, *Europe's Buildings under the Microscope. A Country-by-Country Review of the Energy Performance of Buildings*, Buildings Performance Institute Europe (BPIE), 2011.

Erol, G., and H.F. Karadogan, 'Seismic Strengthening of Infilled Reinforced Concrete Frames by CFRP', *Composites Part B: Engineering*, Vol 91, April 15, 2016, pp. 473–491, doi:10.1016/j.compositesb.2016.01.025.

European Commission, *Action Plan on the Sendai Framework for Disaster Risk Reduction 2015–2030. A Disaster Risk-Informed Approach for All EU Policies (SWD 2016/205 Final/2)*, Publications Office of the European Union, Brussels, 2016a.

European Commission, *COMMUNICATION FROM THE COMMISSION TO THE EUROPEAN PARLIAMENT, THE COUNCIL, THE EUROPEAN ECONOMIC AND SOCIAL COMMITTEE AND THE COMMITTEE OF THE REGIONS A New Circular Economy Action Plan For a Cleaner and More Competitive Europe*, Brussels, November 3, 2020a.

European Commission, *COMMUNICATION FROM THE COMMISSION TO THE EUROPEAN PARLIAMENT, THE COUNCIL, THE EUROPEAN ECONOMIC AND SOCIAL COMMITTEE AND THE COMMITTEE OF THE REGIONS A Renovation Wave for Europe - Greening Our Buildings, Creating Jobs, Improving Lives*, Brussels, October 14, 2020b.

European Commission, *CORDIS Results Pack on Deep Renovation*, Publications Office of the European Union., 2018, ISBN 978-92-78-41796-3.

European Commission, 'EU Building Stock Observatory', Database, *EU Buildings Database*, October 13, 2016b. <https://ec.europa.eu/energy/en/eu-buildings-database>.

European Commission, 'In Focus: Energy Efficiency in Buildings', February 17, 2020c.

European Commission, *Mapping and Analyses of the Current and Future (2020 - 2030) Heating/Cooling Fuel Deployment (Fossil/Renewables)*, February 2017.

European Commission, *The European Green Deal - Communication From The Commission To The European Parliament, The European Council, The Council, The European Economic And Social Committee And The Committee Of The Regions.*, European Commission, Brussels, November 12, 2019.

European Construction Costs, 'Cost Index', *European Construction Costs*, n.d. <http://constructioncosts.eu/cost-index/>.

European Parliament and Council of the European Union, Decision (EU) 2019/420 of the European Parliament and of the Council of 13 March 2019 Amending Decision No 1313/2013/EU on a Union Civil Protection Mechanism, *OJ L*, Vol. 077I, Vol. 077I, 20.3.2019.

European Parliament and Council of the European Union, Directive (EU) 2018/844 of the European Parliament and of the Council of 30 May 2018 Amending Directive 2010/31/EU on the Energy Performance of Buildings and Directive 2012/27/EU on Energy Efficiency (Text with EEA Relevance), *156*, Vol. OJ L, Vol. OJ L, 19.6.2018.

EUROSTAT, 'Census 2011', 2011. <https://ec.europa.eu/CensusHub2/>.

EUROSTAT, 'Electricity Prices for Household Consumers - Bi-Annual Data (from 2007 Onwards)', 2019a. [https://appsso.eurostat.ec.europa.eu/nui/show.do?dataset=nrg\\_pc\\_204&lang=en](https://appsso.eurostat.ec.europa.eu/nui/show.do?dataset=nrg_pc_204&lang=en).

EUROSTAT, 'Gas Prices for Household Consumers - Bi-Annual Data (from 2007 Onwards)', 2019b. [https://appsso.eurostat.ec.europa.eu/nui/show.do?dataset=nrg\\_pc\\_202&lang=en](https://appsso.eurostat.ec.europa.eu/nui/show.do?dataset=nrg_pc_202&lang=en).

FEMA, *HAZUS-MH 2.1 Technical Manual: Multi-Hazard Loss Estimation Methodology*, Technical manual, FEMA, USA, 2003.

Fikri, R., D. Dizhur, K. Walsh, and J. Ingham, 'Seismic Performance of Reinforced Concrete Frame with Masonry Infill Buildings in the 2010/2011 Canterbury, New Zealand Earthquakes', *Bulletin of Earthquake Engineering*, September 19, 2018, doi:10.1007/s10518-018-0476-8.

Filippín, C., F. Ricard, S. Flores Larsen, and M. Santamouris, 'Retrospective Analysis of the Energy Consumption of Single-Family Dwellings in Central Argentina. Retrofitting and Adaptation to the Climate Change', *Renewable Energy*, Vol. 101, February 1, 2017, pp. 1226–1241, doi:10.1016/j.renene.2016.09.064.

Formisano, A., G. Vaiano, and F. Fabbrocino, 'Seismic and Energetic Interventions on a Typical South Italy Residential Building: Cost Analysis and Tax Detraction', *Frontiers in Built Environment*, Vol. 5, 2019, doi:10.3389/fbuil.2019.00012.

Gkournelos, P.D., D.A. Bournas, and T.C. Triantafillou, *Combined Seismic and Energy Upgrading of Existing Buildings Using Advanced Materials: Case Studies on Reinforced Concrete Buildings in South Europe*, EUR 29172 EN, Publications Office of the European Union, Luxembourg, 2019a, ISBN ISBN 978-92-79-81824-0, doi:10.2760/17376, JRC111303.

Gkournelos, P.D., T.C. Triantafillou, and D.A. Bournas, 'Integrated Structural and Energy Retrofitting of Masonry Walls: Effect of In-Plane Damage on the Out-of-Plane Response', *Journal of Composites for Construction*, Vol. 24, No. 5, October 1, 2020, p. 04020049, doi:10.1061/(ASCE)CC.1943-5614.0001066.

Gkournelos, P.D., D.A. Bournas, and T.C. Triantafillou, 'Combined Seismic and Energy Upgrading of Existing Reinforced Concrete Buildings Using TRM Jacketing and Thermal Insulation', *Earthquakes and Structures*, Vol. 16, No. 5, May 25, 2019b, pp. 625–639, doi:10.12989/EAS.2019.16.5.625.

Güneyisi, E.M., and G. Altay, 'Seismic Fragility Assessment of Effectiveness of Viscous Dampers in R/C Buildings under Scenario Earthquakes', *Structural Safety*, Vol. 30, No. 5, September 1, 2008, pp. 461–480, doi:10.1016/j.strusafe.2007.06.001.

Heat Roadmap Europe, *Heating and Cooling Facts and Figures*, June 2017.

Iervolino, I., C. Galasso, and E. Cosenza, 'REXEL: Computer Aided Record Selection for Code-Based Seismic Structural Analysis', *Bulletin of Earthquake Engineering*, Vol. 8, No. 2, April 2010, pp. 339–362, doi:10.1007/s10518-009-9146-1.

Indirli, M., L.A.S. Kouris, A. Formisano, R.P. Borg, and F.M. Mazzolani, 'Seismic Damage Assessment of Unreinforced Masonry Structures After The Abruzzo 2009 Earthquake: The Case Study of the Historical Centers of L'Aquila and Castelvecchio Subequo', *International Journal of Architectural Heritage*, Vol. 7, No. 5, January 1, 2013, pp. 536–578, doi:10.1080/15583058.2011.654050.

Ismail, N., T. El-Maaddawy, and N. Khattak, 'Quasi-Static in-Plane Testing of FRCM Strengthened Non-Ductile Reinforced Concrete Frames with Masonry Infills', *Construction and Building Materials*, Vol. 186, October 20, 2018, pp. 1286–1298, doi:10.1016/j.conbuildmat.2018.07.230.

ISO, ed., *ISO 13790:2006 - Energy Performance of Buildings – Calculation of Energy Use for Space Heating and Cooling*, International Organization for Standardization, Geneva, Switzerland, 2006.

ISO, ed., *ISO 52000-1:2017 - Energy Performance of Buildings - Overarching EPB Assessment - Part 1: General Framework and Procedures*, International Organization for Standardization, Geneva, Switzerland, 2017.

Jelle, B.P., 'Traditional, State-of-the-Art and Future Thermal Building Insulation Materials and Solutions – Properties, Requirements and Possibilities', *Energy and Buildings*, Vol. 43, No. 10, October 1, 2011, pp. 2549–2563, doi:10.1016/j.enbuild.2011.05.015.

Kappos, A.J., C. Panagiotopoulos, G. Panagopoulos, and E.I. Papadopoulos, *WP4 Reinforce Concrete Buildings (Level 1 and Level 2 Analysis)*, 2003.

Kappos, A.J., G. Panagopoulos, C. Panagiotopoulos, and G. Penelis, 'A Hybrid Method for the Vulnerability Assessment of R/C and URM Buildings', *Bulletin of Earthquake Engineering*, Vol. 4, No. 4, 2006, pp. 391–413, doi:10.1007/s10518-006-9023-0.

Kappos, A.J., K.C. Stylianidis, and K. Pitilakis, 'Development of Seismic Risk Scenarios Based on a Hybrid Method of Vulnerability Assessment', *Natural Hazards*, Vol. 17, No. 2, March 1, 1998, pp. 177–192, doi:10.1023/A:1008083021022.

Kappos, A.J., and E.G. Dimitrakopoulos, 'Feasibility of Pre-Earthquake Strengthening of Buildings Based on Cost-Benefit and Life-Cycle Cost Analysis, with the Aid of Fragility Curves', *Natural Hazards*, Vol. 45, No. 1, April 2008, pp. 33–54, doi:10.1007/s11069-007-9155-9.

Kappos, A.J., and G. Panagopoulos, 'Fragility Curves for Reinforced Concrete Buildings in Greece', *Structure and Infrastructure Engineering*, Vol. 6, No. 1–2, February 2010, pp. 39–53, doi:10.1080/15732470802663771.

Kapsalis, P., M. El Kadi, J. Vervloet, M. De Munck, J. Wastiels, T. Triantafillou, and T. Tysmans, 'Thermomechanical Behavior of Textile Reinforced Cementitious Composites Subjected to Fire', *Applied Sciences*, Vol. 9, No. 4, February 21, 2019, p. 747, doi:10.3390/app9040747.

Kim, S., J. Seo, J. Cha, and S. Kim, 'Chemical Retreating for Gel-Typed Aerogel and Insulation Performance of Cement Containing Aerogel', *Construction and Building Materials*, Vol. 40, March 2013, pp. 501–505, doi:10.1016/j.conbuildmat.2012.11.046.

Korkmaz, S.Z., M. Kamanli, H.H. Korkmaz, M.S. Donduren, and M.T. Cogurcu, 'Experimental Study on the Behaviour of Nonductile Infilled RC Frames Strengthened with External Mesh Reinforcement and Plaster Composite', *Natural Hazards and Earth System Science*, Vol. 10, No. 11, November 18, 2010, pp. 2305–2316, doi:10.5194/nhess-10-2305-2010.

Kouris, L.A., R.P. Borg, and M. Indirli, 'The L'Aquila Earthquake, April 6th, 2009: A Review of Seismic Damage Mechanisms', *Proceedings of the Final Conference of COST Action C26, Urban Habitat Constructions Under Catastrophic Events*, Mazzolani, FM September, 2010, pp. 16–18.

Kouris, L.A., D.A. Bournas, D.A. Pohoryles, G. Valsamos, T. Savvas, and C. Maduta, *Seismic plus Energy Upgrading of Masonry Buildings Using Advanced Materials*, Publications Office of the European Union, Luxembourg, 2021, ISBN 978-92-76-28603-5, JRC123617.

Koutas, L., S. Bousias, and T. Triantafillou, 'Seismic Strengthening of Masonry-Infilled RC Frames with TRM: Experimental Study', *Journal of Composites for Construction*, Vol. 19, No. 2, 2015, p. 04014048, doi:10.1061/(ASCE)CC.1943-5614.0000507.

Koutas, L., T.C. Triantafillou, and S.N. Bousias, 'Analytical Modeling of Masonry-Infilled RC Frames Retrofitted with Textile-Reinforced Mortar', *Journal of Composites for Construction*, Vol. 19, No. 5, October 2015, p. 04014082, doi:10.1061/(ASCE)CC.1943-5614.0000553.

Koutas, L.N., and D.A. Bournas, 'Out-of-Plane Strengthening of Masonry-Infilled RC Frames with Textile-Reinforced Mortar Jackets', *Journal of Composites for Construction*, Vol. 23, No. 1, February 1, 2019, p. 04018079, doi:10.1061/(ASCE)CC.1943-5614.0000911.

Koutas, L.N., Z. Tetta, D.A. Bournas, and T.C. Triantafillou, 'Strengthening of Concrete Structures with Textile Reinforced Mortars: State-of-the-Art Review', *Journal of Composites for Construction*, Vol. 23, No. 1, February 2019, p. 03118001, doi:10.1061/(ASCE)CC.1943-5614.0000882.

Koutromanos, I., M. Kyriakides, A. Stavridis, S. Billington, and P.B. Shing, 'Shake-Table Tests of a 3-Story Masonry-Infilled RC Frame Retrofitted with Composite Materials', *Journal of Structural Engineering*, Vol. 139, No. 8, August 2013, pp. 1340–1351, doi:10.1061/(ASCE)ST.1943-541X.0000689.

Kyriakides, M.A., and S.L. Billington, 'Cyclic Response of Nonductile Reinforced Concrete Frames with Unreinforced Masonry Infills Retrofitted with Engineered Cementitious Composites', *Journal of Structural Engineering*, Vol. 140, No. 2, February 1, 2014, p. 04013046, doi:10.1061/(ASCE)ST.1943-541X.0000833.

La Greca, P., and G. Margani, 'Seismic and Energy Renovation Measures for Sustainable Cities: A Critical Analysis of the Italian Scenario', *Sustainability*, Vol. 10, No. 1, January 19, 2018, p. 254, doi:10.3390/su10010254.

Li, Y., J. Zhu, and Z. Wang, 'Investigation on Mechanical Properties of Masonry Infill Wall Strengthened with ECC', *KSCE Journal of Civil Engineering*, Vol. 23, No. 1, January 2019, pp. 295–306, doi:10.1007/s12205-018-5424-2.

Loga, T., B. Stein, and N. Diefenbach, 'TABULA Building Typologies in 20 European Countries—Making Energy-Related Features of Residential Building Stocks Comparable', *Energy and Buildings*, Vol. 132, November 15, 2016, pp. 4–12, doi:10.1016/j.enbuild.2016.06.094, *Towards an Energy Efficient European Housing Stock: Monitoring, Mapping and Modelling Retrofitting Processes*.

Longo, F., A. Cascardi, P. Lassandro, and M.A. Aiello, 'A New Fabric Reinforced Geopolymer Mortar (FRGM) with Mechanical and Energy Benefits', *Fibers*, Vol. 8, No. 8, August 2020, p. 49, doi:10.3390/fib8080049.

Longo, F., P. Lassandro, A. Moshiri, T. Phatak, MariaA. Aiello, and K.J. Krakowiak, 'Lightweight Geopolymer-Based Mortars for the Structural and Energy Retrofit of Buildings', *Energy and Buildings*, Vol. 225, October 15, 2020, p. 110352, doi:10.1016/j.enbuild.2020.110352.

Ma, Z., P. Cooper, D. Daly, and L. Ledo, 'Existing Building Retrofits: Methodology and State-of-the-Art', *Energy and Buildings*, Vol. 55, December 1, 2012, pp. 889–902, doi:10.1016/j.enbuild.2012.08.018, *Cool Roofs, Cool Pavements, Cool Cities, and Cool World*.

Mainstone, R.J., 'Supplementary Note on the Stiffness and Strength of Infilled Frames', *Current Paper CP13/74, Buildings Research Establishment, London*, 1974.

Maio, R., and G. Tsionis, *Seismic Fragility Curves for the European Building Stock: Review and Evaluation of Existing Fragility Curves*, EU Publications Office, Luxembourg, 2015, ISBN 978-92-79-54136-0, Vol. EUR 27635 EN of.

Mander, J.B., M.J. Priestley, and R. Park, 'Theoretical Stress-Strain Model for Confined Concrete', *Journal of Structural Engineering*, Vol. 114, No. 8, 1988, pp. 1804–1826.

Margani, Giuseppe, ed., *Energy and Seismic Renovation Strategies for Sustainable Cities*, MDPI, 2019, ISBN 978-3-03897-945-6, doi:10.3390/books978-3-03897-945-6.

Masi, A., and M. Vona, 'Vulnerability Assessment of Gravity-Load Designed RC Buildings: Evaluation of Seismic Capacity through Non-Linear Dynamic Analyses', *Engineering Structures*, Vol. 45, December 1, 2012, pp. 257–269, doi:10.1016/j.engstruct.2012.06.043.

Mastroberti, M., D. Bournas, M. Vona, B. Manganelli, and V. Palermo, 'Combined Seismic plus Energy Retrofitting for the Existing RC Buildings: Economic Feasibility', *Proceedings of the 16th European Conf. on Earthquake Engineering*, Thessaloniki, Greece, 2018.

Menegotto, M., and P.E. Pinto, 'Method of Analysis for Cyclically Loaded Reinforced Concrete Frames Including Changes in Geometry and Non-Elastic Behavior of Elements under Combined Normal Forces and Bending Moment', *IASBE Proceedings*, 1973.

Mora, T.D., M. Pinamonti, L. Teso, G. Boscato, F. Peron, and P. Romagnoni, 'Renovation of a School Building: Energy Retrofit and Seismic Upgrade in a School Building in Motta Di Livenza', *Sustainability*, Vol. 10, No. 4, March 26, 2018, p. 969, doi:10.3390/su10040969.

Numbeo, 'Europe: Prices by City of Price per Square Meter to Buy Apartment', 2019. [https://www.numbeo.com/cost-of-living/region\\_prices\\_by\\_city?itemId=100&region=150&displayCurrency=EUR](https://www.numbeo.com/cost-of-living/region_prices_by_city?itemId=100&region=150&displayCurrency=EUR)

O'Reilly, G.J., and T.J. Sullivan, 'Probabilistic Seismic Assessment and Retrofit Considerations for Italian RC Frame Buildings', *Bulletin of Earthquake Engineering*, Vol. 16, No. 3, March 2018, pp. 1447–1485, doi:10.1007/s10518-017-0257-9.

Ozcebe, S., H. Crowley, H. Baker, R. Spence, and R. Foulser-Piggott, *NERA D7.5 Census Data Collection and Harmonisation for Europe*, 2014.

Özel, A.E., and E.M. Güneyisi, 'Effects of Eccentric Steel Bracing Systems on Seismic Fragility Curves of Mid-Rise R/C Buildings: A Case Study', *Structural Safety*, Vol. 33, No. 1, January 1, 2011, pp. 82–95, doi:10.1016/j.strusafe.2010.09.001.

Ozkaynak, H., E. Yuksel, O. Buyukozturk, C. Yalcin, and A.A. Dindar, 'Quasi-Static and Pseudo-Dynamic Testing of Infilled RC Frames Retrofitted with CFRP Material', *Composites Part B: Engineering*, Vol. 42, No. 2, March 1, 2011, pp. 238–263, doi:10.1016/j.compositesb.2010.11.008.

Pagani, M., J. García-Pelaez, R. Gee, K. Johnson, V. Poggi, M. Simionato, R. Styron, et al., 'GEM Global Seismic Hazard Map v.2018.1', 2018, doi:10.13117/GEM-GLOBAL-SEISMIC-HAZARD-MAP-2018.1.

Papadopoulos, A.M., 'State of the Art in Thermal Insulation Materials and Aims for Future Developments', *Energy and Buildings*, Vol. 37, No. 1, January 1, 2005, pp. 77–86, doi:10.1016/j.enbuild.2004.05.006.

Pohoryles, D.A., and D.A. Bournas, 'A Unified Macro-Modelling Approach for Masonry-Infilled RC Frames Strengthened with Composite Materials', *Engineering Structures*, Vol. 223, November 15, 2020a, p. 111161, doi:10.1016/j.engstruct.2020.111161.

Pohoryles, D.A., and D.A. Bournas, 'Combined Seismic and Energy Retrofit of RC Buildings: In-Plane Strengthening of Masonry Infills Using Textile Reinforced Mortars', *Proc. 17th World Conference on Earthquake Engineering*, Sendai, Japan, 2020b, pp. 3b–0106.

Pohoryles, D.A., and D.A. Bournas, 'Seismic Retrofit of Infilled RC Frames with Textile Reinforced Mortars: State-of-the-Art Review and Analytical Modelling', *Composites Part B: Engineering*, Vol. 183, February 15, 2020c, p. 107702, doi:10.1016/j.compositesb.2019.107702.

Pohoryles, D.A., C. Maduta, D.A. Bournas, and L.A. Kouris, 'Energy Performance of Existing Residential Buildings in Europe: A Novel Approach Combining Energy with Seismic Retrofitting', *Energy and Buildings*, Vol. 223, September 15, 2020, p. 110024, doi:10.1016/j.enbuild.2020.110024.

Porter, K.A., 'An Overview of PEER's Performance-Based Earthquake Engineering Methodology', *Proceedings of Ninth International Conference on Applications of Statistics and Probability in Civil Engineering*, 2003.

da Porto, F., G. Guidi, M. Dalla Benetta, and N. Verlato, 'Combined In-Plane/out-of-Plane Experimental Behaviour of Reinforced and Strengthened Infill Masonry Walls', *12th Canadian Masonry Symposium, Vancouver, British Columbia*, 2013.

da Porto, F., G. Guidi, N. Verlato, and C. Modena, 'Effectiveness of Plasters and Textile Reinforced Mortars for Strengthening Clay Masonry Infill Walls Subjected to Combined In-Plane/out-of-Plane Actions / Wirksamkeit von Putz Und Textilbewehrtem Mörtel Bei Der Verstärkung von Ausfachungswänden Aus Ziegelmauerwerk, Die Kombinierter Scheiben- Und Plattenbeanspruchung Ausgesetzt Sind', *Mauerwerk*, Vol 19, No. 5, October 1, 2015, pp. 334–354, doi:10.1002/dama.201500673.

Raoof, S.M., and D.A. Bournas, 'Bond between TRM versus FRP Composites and Concrete at High Temperatures', *Composites Part B: Engineering*, Vol. 127, October 15, 2017a, pp. 150–165, doi:10.1016/j.compositesb.2017.05.064.

Raoof, S.M., and D.A. Bournas, 'TRM versus FRP in Flexural Strengthening of RC Beams: Behaviour at High Temperatures', *Construction and Building Materials*, Vol. 154, November 2017b, pp. 424–437, doi:10.1016/j.conbuildmat.2017.07.195.

Ricci, P., F. De Luca, and G.M. Verderame, '6th April 2009 L'Aquila Earthquake, Italy: Reinforced Concrete Building Performance', *Bulletin of Earthquake Engineering*, Vol. 9, No. 1, 2011, pp. 285–305.

Sagar, S.L., V. Singhal, and D.C. Rai, 'In-Plane and Out-of-Plane Behavior of Masonry-Infilled RC Frames Strengthened with Fabric-Reinforced Cementitious Matrix', *Journal of Composites for Construction*, Vol. 23, No. 1, February 2019, p. 04018073, doi:10.1061/(ASCE)CC.1943-5614.0000905.

Salvalai, G., M.M. Sesana, and G. Iannaccone, 'Deep Renovation of Multi-Storey Multi-Owner Existing Residential Buildings: A Pilot Case Study in Italy', *Energy and Buildings*, Vol. 148, 2017, pp. 23–36.

Schiavoni, S., F. D'Alessandro, F. Bianchi, and F. Asdrubali, 'Insulation Materials for the Building Sector: A Review and Comparative Analysis', *Renewable and Sustainable Energy Reviews*, Vol. 62, September 2016, pp. 988–1011, doi:10.1016/j.rser.2016.05.045.

Seismosoft Ltd, *SeismoStruct*, Seismosoft Ltd, Pavia (PV) - Italy, 2018.

Selim, M., C. Okten, M. Ozkan, and \_ Gencoglu, 'Behavior of RC Frames with Infill Walls Strengthened by Cement Based Composites', International Society of Offshore and Polar Engineers, 2015, ISBN 978-1-880653-89-0.

Statistical Office of the Republic of Serbia of Serbia, 'Census 2011', 2011. <http://data.stat.gov.rs/Home/Result/3102030601?languageCode=en-US>.

Stein, Britta, Tobias Loga, and Nikolaus Diefenbach, eds., *Scenario Analyses Concerning Energy Efficiency and Climate Protection in Local Residential Building Stocks: Examples from Eight European Countries*, Institut Wohnen und Umwelt GmbH, Darmstadt, 2016, ISBN 978-3-941140-52-3, Vol energy performance indicator tracking schemes for the continuous optimisation of refurbishment processes in European housing stocks : project duration: April 2013–March 2016 / co-funded by the Intelligent Energy Europe Programme of the European Union; coordinator: IWU Institut Wohnen und Umwelt, Darmstadt/Germany ; No. 2 of EPISCOPE Synthesis Report.

TABULA, *Application of Building Typologies for Modelling the Energy Balance of the Residential Building Stock*, IWU, Darmstadt, 2012, ISBN 978-3-941140-23-3.

Tetta, Z.C., and D.A. Bournas, 'TRM vs FRP Jacketing in Shear Strengthening of Concrete Members Subjected to High Temperatures', *Composites Part B: Engineering*, Vol. 106, December 2016, pp. 190–205, doi:10.1016/j.compositesb.2016.09.026.

Tetta, Z.C., L.N. Koutas, and D.A. Bouras, 'Shear Strengthening of Concrete Members with TRM Jackets: Effect of Shear Span-to-Depth Ratio, Material and Amount of External Reinforcement', *Composites Part B: Engineering*, Vol. 137, March 15, 2018, pp. 184–201, doi:10.1016/j.compositesb.2017.10.041.

Triantafillou, T.C., K. Karlos, P. Kapsalis, and L. Georgiou, 'Innovative Structural and Energy Retrofitting System for Masonry Walls Using Textile Reinforced Mortars Combined with Thermal Insulation: In-Plane Mechanical Behavior', *Journal of Composites for Construction*, Vol. 22, No. 5, October 1, 2018, p. 04018029, doi:10.1061/(ASCE)CC.1943-5614.0000869.

Triantafillou, T.C., K. Karlos, K. Kefalou, and E. Argyropoulou, 'An Innovative Structural and Energy Retrofitting System for URM Walls Using Textile Reinforced Mortars Combined with Thermal Insulation: Mechanical and Fire Behavior', *Construction and Building Materials*, Vol. 133, February 2017, pp. 1–13, doi:10.1016/j.conbuildmat.2016.12.032.

Turkish Statistical Institute (TurkStat), 'Census 2011', 2011. [http://www.turkstat.gov.tr/PreTabelo.do?alt\\_id=1047](http://www.turkstat.gov.tr/PreTabelo.do?alt_id=1047).

Urban Agenda for the EU, *Culture and Cultural Heritage - Orientation Paper*, Orientation Paper, October 2019.

U.S. Department of Energy, ed., *EnergyPlus™ Version 8.90 Documentation Engineering Reference*, U.S. Department of Energy, 2018.

U.S. Department of Energy, 'Weather Data', *Weather Data | EnergyPlus*, 2019. <https://energyplus.net/weather>.

USGS, 'Earthquake Hazards 201 - Technical Q&A', 2020. [https://www.usgs.gov/natural-hazards/earthquake-hazards/science/earthquake-hazards-201-technical-qa?qt-science\\_center\\_objects=0#qt-science\\_center\\_objects](https://www.usgs.gov/natural-hazards/earthquake-hazards/science/earthquake-hazards-201-technical-qa?qt-science_center_objects=0#qt-science_center_objects).

Vamvatsikos, D., and C.A. Cornell, 'Incremental Dynamic Analysis', *Earthquake Engineering & Structural Dynamics*, Vol. 31, No. 3, 2002, pp. 491–514, doi:10.1002/eqe.141.

Varum, H., 'Seismic Assessment, Strengthening and Repair of Existing Buildings', PhD Thesis, University of Aveiro, 2003.

Yaman, T.S., and E. Canbay, 'Seismic Strengthening of Masonry Infilled Reinforced Concrete Frames with Steel-Fibre-Reinforced Mortar', *Proceedings of the Institution of Civil Engineers - Structures and Buildings*, Vol. 167, No. 1, January 1, 2014, pp. 3–14, doi:10.1680/stbu.11.00076.

Yuksel, E., H. Ozkaynak, O. Buyukozturk, C. Yalcin, A.A. Dindar, M. Surmeli, and D. Tastan, 'Performance of Alternative CFRP Retrofitting Schemes Used in Infilled RC Frames', *Construction and Building Materials*, Vol. 24, No. 4, April 1, 2010, pp. 596–609, doi:10.1016/j.conbuildmat.2009.09.005.

Zavadskas, E., S. Raslanas, and A. Kaklauskas, 'The Selection of Effective Retrofit Scenarios for Panel Houses in Urban Neighborhoods Based on Expected Energy Savings and Increase in Market Value: The Vilnius Case', *Energy and Buildings*, Vol. 40, No. 4, January 1, 2008, pp. 573–587, doi:10.1016/j.enbuild.2007.04.015.

## **List of abbreviations and definitions**

BEM	Building Energy Modelling
CED	Cooling Energy Demand
DS	Damage State
EAL	Expected Annual Losses
ECC	Engineered Cementitious Composites
EPBD	Energy Performance of Buildings Directive
EU	European Union
EYCH	European Year of Cultural Heritage
FE	Finite Element
FEMA	Federal Emergency Management Agency (US)
FRP	Fibre Reinforced Polymer
GEM	Global Earthquake Model
HED	Heating Energy Demand
HDD	Heating Degree-Days
HVAC	Heating, ventilation, and air conditioning
ISO	International Organization for Standardization
LTRS	Long term renovation strategies
MS	Member State
NZEB	Nearly Zero-Energy Buildings
PBEE	Performance-based earthquake engineering
PEER	Pacific Earthquake Engineering Research Center (US)
PGA	Peak Ground Acceleration
RBM	Reinforced Brick Masonry
RC	Reinforced Concrete
TRM	Textile Reinforced Mortar
UCPM	Union Civil Protection Mechanism
URM	Unreinforced Masonry

## List of figures

Figure 1. (a) iRESIST+ combined retrofitting with TRM and thermal insulation. (b) Prototype structure at ELSA, Joint Research Centre (JRC), European Commission .....	4
Figure 2. Combined retrofitting at the nexus of relevant policy domains.....	5
Figure 3. (a) Carbon based textile (b) Application of textile with inorganic matrix on masonry infill walls. ....	8
Figure 4. Increase in secant stiffness against $\omega_{eff}$ for the experiments on composite strengthened frames ..	18
Figure 5. Normalised tie force against $\omega_{eff}$ for the experiments on composite strengthened frames.....	19
Figure 6. Ratio of calculated and experimental base shear for all specimens (including outliers). .....	19
Figure 7. Dimensions of building prototype in direction of loading and reinforcement detailing. Note: the modelled substructure is indicated in grey colour and dashed lines. .....	20
Figure 8. Dimensions of the physical structure for testing: plan view.....	21
Figure 9. Dimensions of the physical structure for testing: side view in X-direction.....	22
Figure 10. Dimensions of the physical structure for testing: side view in Y-direction.....	22
Figure 11. Full retrofit scheme of the iRESIST+ prototype building (thermal insulation in yellow). .....	23
Figure 12. Hysteresis curves from the cyclic analysis for the control and retrofitted buildings.....	25
Figure 13. Target and mean spectra for the selected ground motion records, normalised by pga.....	29
Figure 14. Fragility curves for the different mid-rise RC buildings: (a) Low Code; (b) Mid Code; (c) High Code; (d) TRM-Retrofit. .....	32
Figure 15. EALs (%) for the as-built and TRM-retrofitted mid-rise RC buildings for different levels of seismic hazards.....	33
Figure 16. Map of case study locations categorised by seismic risk and climatic conditions. .....	34
Figure 17. Proportion of built floor area by period of construction in the selected locations. .....	36
Figure 18. Average total annual energy demand per building type across all locations. .....	46
Figure 19. Average reduction in total annual energy demand due to retrofit per building type in each zone.	47
Figure 20. Estimated annual energy cost savings and payback periods per building type in each zone. ....	48
Figure 21. Reduction in primary energy use for all zones (2020 – 2030) with four different renovation strategies.....	49
Figure 22. Reduction in CO <sub>2</sub> -emissions by 2030 after implementation of an optimal renovation strategy ...	50
Figure 23. Average EAL <sub>s</sub> per building type across all locations for Seismic Zones 2 to 5.....	51
Figure 24. Reduction in EAL <sub>s</sub> (%) across the building stock of the twenty locations by 2030 after implementation of an optimal renovation strategy.....	52
Figure 25. Disaggregation of EAL <sub>C</sub> (%) in its seismic and energy components averaged for each Seismic Zone. ....	52
Figure 26. Average combined classification of the different building typologies across all seismic zones....	53
Figure 27. Payback periods for all building ages (average taken over the four climate zones) for the energy retrofit compared to combined and separate seismic and energy retrofitting shown for each Seismic Zone.	55

## List of tables

Table 1. Summary of composite retrofit applications in the literature.....	9
Table 2. Typical TRM properties from the literature.....	10
Table 3. Thermal insulation performance of different insulation products.....	15
Table 4. Material properties.....	23
Table 5. Modelling parameters for the compressive strut.....	24
Table 6. Modelling parameters for the tensile tie.....	25
Table 7. Peak response parameters for the four specimens under cyclic loading.....	26
Table 8. Materials and reinforcement details for the different design levels.....	27
Table 9. TRM material properties used for the retrofit of the LC building.....	28
Table 10. Eurocode 8 target displacements in m (and roof drifts in %) for the buildings for reference pgas of 0.24 and 0.36 g.....	29
Table 11. List of selected earthquake records for the incremental dynamic analysis.....	30
Table 12. Median inter-storey drift values for the four damage states for infilled frames with openings ...	30
Table 13. Full-face orthogonal TRM-strengthened infilled RC frame specimens tested in the literature .....	31
Table 14. Mean pga (standard deviation) for the fragility curves of the as-built and retrofitted buildings...	32
Table 15. Damage-to-loss function for infilled RC buildings.....	33
Table 16. Definitions of seismic and climatic zones.....	35
Table 17. HDD and pga values for the case study locations.....	35
Table 18. Parameters of the case study buildings .....	37
Table 19. Envelope characteristics for the different time periods .....	38
Table 20. U-values target in each case-study location.....	39
Table 21. Target seismic design level of the seismic retrofit scheme.....	40
Table 22. Data for energy factors and costs for each location.....	41
Table 23. Mean value $\mu$ of the lognormal distribution functions per damage state (DS) of the fragility of masonry buildings (in terms of PGA). ....	42
Table 24. Mean value $\mu$ of the lognormal distribution functions per damage state (DS) of the fragility of infilled RC buildings (in terms of PGA). ....	43
Table 25. Values for the damage-to-loss functions for masonry and RC buildings.....	44

## **GETTING IN TOUCH WITH THE EU**

### **In person**

All over the European Union there are hundreds of Europe Direct information centres. You can find the address of the centre nearest you at: [https://europa.eu/european-union/contact\\_en](https://europa.eu/european-union/contact_en)

### **On the phone or by email**

Europe Direct is a service that answers your questions about the European Union. You can contact this service:

- by free phone: 00 800 6 7 8 9 10 11 (certain operators may charge for these calls),
- at the following standard number: +32 22999696, or
- by electronic mail via: [https://europa.eu/european-union/contact\\_en](https://europa.eu/european-union/contact_en)

## **FINDING INFORMATION ABOUT THE EU**

### **Online**

Information about the European Union in all the official languages of the EU is available on the Europa website at: [https://europa.eu/european-union/index\\_en](https://europa.eu/european-union/index_en)

### **EU publications**

You can download or order free and priced EU publications from EU Bookshop at: <https://publications.europa.eu/en/publications>. Multiple copies of free publications may be obtained by contacting Europe Direct or your local information centre (see [https://europa.eu/european-union/contact\\_en](https://europa.eu/european-union/contact_en)).

**The European Commission's  
science and knowledge service**  
Joint Research Centre

**JRC Mission**

As the science and knowledge service of the European Commission, the Joint Research Centre's mission is to support EU policies with independent evidence throughout the whole policy cycle.



**EU Science Hub**  
[ec.europa.eu/jrc](http://ec.europa.eu/jrc)



@EU\_ScienceHub



EU Science Hub - Joint Research Centre



EU Science, Research and Innovation



EU Science Hub



Publications Office  
of the European Union

doi:10.2760/768985

ISBN 9 78-92-76-29687-4